EXPERIMENTAL INVESTIGATION OF THE SAND REMOVAL IN WATER-SOLUBLE SAND MOULDS USING WATERJETS

EXPERIMENTAL INVESTIGATION OF SAND REMOVAL IN WATER-SOLUBLE SAND MOULDS USING WATERJETS

By AYKUT DURSUN, B.Sc.

A Thesis Submitted to the School of Graduate Studies in Partial Fulfillment of the Requirements for the Degree Master of Applied Science in Engineering

McMaster University

McMaster University MASTER OF APPLIED SCIENCE IN ENGINEERING (2015)
Hamilton, Ontario

TITLE: Experimental Investigation of Sand Removal In Water-Soluble Sand Moulds Using Waterjets

AUTHOR: Aykut Dursun, B.Sc. (Dogus University)

SUPERVISOR: Dr. Mohamed Hamed

NUMBER OF PAGES: viii, 95

Abstract

Due to the strong competition in the automotive industry, automakers must find innovative ways to manufacture car parts out of low-density materials in order to provide weight reduction and consequently fuel economy for vehicles. The recently invented Ablation Casting technique presents great potential for vehicle light weighting and hence it is gaining momentum in commercial operations. In this technique, a spraying system is used to increase the solidification rate of the casting. The spraying system removes the water-soluble sand mould away and produces extremely high cooling rates by using waterjets directly impinging on the solidifying metal surface. The high cooling rates result in small grain size in the microstructure and consequently enhances the mechanical properties of the casting. Although the spraying system has a profound effect on the process, the effect of waterjet parameters on the removal of the sand mould has never been studied.

The objective of this study is to investigate the use of waterjets in the removal process of water-soluble sand moulds. This study aims to develop a predictive model of the rate of sand removal for a given set of operating conditions of the spraying system. The effect of waterjet parameters on the rate of sand removal is investigated qualitatively within the appropriate range of operating conditions in order to establish an empirical model. These parameters include: standoff distance, waterjet momentum and overlapping percentage of multijets. This model can be implemented and used for different sand and water-soluble binder systems and the time of sand mould removal for given mould thickness can be estimated. Additionally some aspects of the removal mechanism have been discussed.

The results of this study provide an understanding of the interaction between the waterjet parameters and their effect on the rate of sand removal. It was shown that the developed model in this study is able to predict the time of sand removal correctly in casting applications.

Acknowledgements

I would like to acknowledge the Automotive Partnership Canada, Fiat Chrysler Automotive Group, Nemak, Haley Industries and Canmet Materials for the funding and the technical support received.

I gratefully acknowledge my supervisor, Dr. Mohamed Hamed for his support and guidance.

I would also like to thank the members of my defense committee, Dr. Kumar Sadayappan and Dr. Sumanth Shankar for taking their time to review my thesis.

Special thanks to Dr. Kifah Takrouri, and Hino Pringnitz for their help and suggestions in conducting the experiments.

Finally I really have to thank my family for their continuous unwavering support and endless love.

Table of Contents

List of Figures

List of Tables

Nomenclature

Symbol	Unit	Description
A	m^2	Area of the Nozzle Orifice
h	m	Standoff Distance
$\dot{m}$	kg/s	Mass Flow Rate
P	Pa	Waterjet Pressure
ρ	kg/m^3	Density
$\dot{Q}$	m^3/s	Volumetric Flow Rate
t	sec	Time
u	m^3/J	Specific Energy Requirement of the Material
V	m/s	Waterjet Velocity

Abbreviations

Abbreviation	Meaning
AFS	American Foundry Society
AWJ	Abrasive Waterjet Cutting
HPDC	High Pressure Die Casting
MRR	Material Removal Rate
MT	Mould Thickness
OEM	Original Equipment Manufacturer
OP	Overlapping Percentage of Multijets
PWJ	Plain Waterjet Machining
SDAS	Secondary Dendrite Arm Spacing
SOD	Standoff Distance
SRR	Sand Removal Rate
UTS	Ultimate Tensile Strength
WJM	Waterjet Momentum
YS	Yield Strength

CHAPTER 1 : Introduction and Literature Review

1.1 INTRODUCTION

Over the last few decades the major automotive companies in the United States (Chrysler, Ford, GM) invested in high-risk, high payoff research and development projects with the potential to reduce fuel consumption of vehicles for more environmentally sustainable transportation sector. 95 percent of the United States' transportation energy needs are met with petroleum; this creates a big dependence, as it is two-thirds of all the petroleum used in the United States [1]. Lowering this dependence is crucial for both economic and environmental reasons and as oil prices continue to increase, it will become even more important. Research conducted with this aim includes new engine concepts, lightweight materials, alternate non-petroleum based fuels and hybrid propulsion [1]. Reducing weight of components used in motor vehicles to increase the fuel economy has been one of the major research areas.

Iron and steel casting designs have been largely replaced despite their property advantages whereas the use of low-density materials to produce lightweight automotive castings has gained wide acceptance by auto and truck original equipment manufacturers (OEMs) [2]. The trend in the industry has been to replace iron and steel with low-density materials. Especially in the past decade a lot of research activities and development projects have been carried out cooperatively between the automotive industry, government and academia working on the development of innovative techniques to produce castings of aluminum and magnesium.

Increased fuel economy is the most significant benefit of light weighting. Studies have shown that the fuel economy increases 6-8%, with every 10% drop in weight [3]. In addition to that for every kilogram reduced in the weight of a vehicle, there is about 20 kg of carbon dioxide emission reduction [4]. The level of global competition among the

automotive industry forces engineers and designers to take full advantage of the light weighting technology in manufacturing today's vehicles. Using lightweight components also improves vehicle performance by enhancing acceleration and deceleration. Weight reduction in the front allows the center of gravity to be moved rearward, which leads to improving the response of steering and cornering [5].

Other than the obvious fuel economy and performance advantages, using low-density materials provides better manufacturing value. Aluminum and magnesium components are cost efficient compared to steel and iron due to their higher machinability, less manufacturing cycle periods, less dimensional tolerances, ability to cast thin and thick walls, easier casting to near net shape and reduction in number of assemblies. These advantages allow the finishing, melting and metal-forming costs to decrease [4]. Moreover, magnesium has unique features over aluminum and steel. Magnesium is known as the lightest structural metal on Earth. It provides 75% weight saving over steel parts, which makes it attractive to build light and strong structures. Its lower specific heat and latent heat provides faster solidification times. Thus more components can be cast per unit time compared to aluminum, steel and iron [5].

The potential of aluminum and magnesium castings to aid the automotive industry in achieving weight reduction objectives has been demonstrated and continues to expand. Non-structural or semi-structural parts (such as brackets, covers, instrument panels and steering systems) [6] in today's vehicles are substituted with aluminum, magnesium, composites, foams and plastics. This implementation resulted in great mass reduction with comparable performance to iron-steel components. These rapid advancements led today's cars to be safer and more fuel-efficient than those of only a few years ago. Therefore, achieving weight reduction is getting more and more difficult, as non and semi-structural components are limited, which means that there is a need to develop innovative techniques to manufacture structural components from lightweight materials.

Over the last 15 years, the automotive industry has embraced the High Pressure Die Casting (HPDC) technique as a lightweight solution. In HPDC, molten metal is injected at very high speeds (greater than 10 m/s) into the mould cavity [5]. Typically in other casting methods, the cooling rates are slower compared to HPDC. This is detrimental for the component as it promotes a large grain size in the microstructure. Considering that the small grain size is the reflection of the high mechanical properties, faster cooling rates have to be achieved to enhance the properties such as ultimate tensile strength (UTS) and yield strength (YS). This is exactly why HPDC technique has been used in automotive applications to overcome the lack of strength of low-density materials. The drawback of this approach is the extremely high tooling cost that is required to create the desired cavity in the metal mould depending on the component that needs to be cast. Additionally the metal mould has a long lead-time and its use time is limited to certain number of shots for a HPDC application [7]. Despite the cost disadvantages of this technique, it became the method of choice in the industry, as the process is able to meet the requirements of mass production (dimensional accuracy, ability to fill thin sections, consistent metal quality throughout the casting) [8].

Nowadays the R&D efforts focus on the casting of structural components out of low-density materials to provide further weight reduction. The main technical challenge that needs to be overcome is to obtain lightweight components with reliable and adequate properties while keeping the cost at minimum. The recently invented casting technique "Ablation Casting" [9] is considered a cost competitive alternative of HPDC. In this technique, the molten metal is poured into a sand mould that is prepared using water-soluble binding agent and while the metal is in a semi-solid state, the mould is subjected to water. The water disintegrates the sand and reaches the metal providing rapid cooling by directly impinging on its surface. This significant heat extraction results in extremely high cooling rates, which leads to a refined microstructure and consequently high mechanical properties. Moreover, parts free of porosity can be cast using this technique. This provides extreme integral quality for the part [7]. Additionally, the sand can be reclaimed and the water can be reused in this process.

Thus the ablation casting technique has enormous cost advantages. An additional benefit of ablation casting is that the filling of sand mould castings is less turbulent and can be better controlled compared to HPDC [10]. The most significant impact of this technique was found in its ability to cast AZ91 and AM60 magnesium alloys (known as extremely difficult to cast and handle) without any problems [11].

This emerging new casting technology is slowly gaining momentum in commercial operation. Although the benefits of using water in the process are obvious, the available information of the effect of jet characteristics on the process is insufficient. It is clear that in order to provide the maximum grain refinement for the casting, the waterjet must go through the sand mould and reach the molten metal within the minimum delay time possible. Thus the momentum of the jet while going through the sand mould has to be high. However, if the waterjet starts impinging on the solidifying metal surface with high momentum, the surface will be defected. Therefore, a precise control of the waterjet momentum and time has to take place upon completion of sand removal. In order to predict the time and the required waterjet momentum, a model based on waterjet parameters must be developed. Considering that each alloy system has unique cooling characteristics, the delay times in each alloy systems are different. Additionally, the required impingement pressure to cool the part without any defects differs based on the alloy system. Thus, a study that correlates the jet parameters to sand removal and predicts the time of removal for a given sand mould thickness is required in order to employ ablation casting technology in industrial applications efficiently. This will expand the application of this casting technique immensely.

Thesis Outline

In the following section of this thesis, the relevant literature including ablation casting studies and waterjet machining has been reviewed and the necessary background information is provided. Chapter two presents the description of the experimental setup and the procedure to run the tests including data processing and process parameters. In

the third chapter, the results and discussion of the sand removal process are provided. The forth chapter presents the application of the knowledge obtained in real casting tests. The fifth chapter provides the summary and the conclusion of this study along with the future work.

1.2 Background and Literature Review

This section is divided into two subsections: In the first subsection, the background information and literature review on ablation casting studies is provided. Due to the recent invention of ablation casting, the technique is considered relatively new and a limited number of publications exists, moreover in each published study little information is provided regarding the spraying systems used.

In the second subsection, background information and literature review on waterjet machining studies is presented which provides information on how material removal is achieved by using waterjets. Most of the literature is focused on the mechanism of the material removal including some literature with proposed models to predict the penetration depth of the waterjet.

1.2.1 Ablation Casting

1.2.1.1 Background Information

The use of water-soluble sand binder systems in mould making enables a cleaner, environmentally friendly and economically advantageous casting process for both ferrous and non-ferrous near net shape components [12]. There have been several efforts in the development of water-soluble sand binder systems since the middle of the twentieth century. Until about the last decade of the twentieth century, such binder systems were used in the post solidification stages of the casting process wherein the cast component could be expeditiously and efficiently removed from the sand mould by

dissolution in water and circumvent the lengthy and expensive process of thermal sand removal.

During the last two decades there has been renewed interest in casting non-ferrous light metals with rapid solidification using waterjets to cut through sand moulds containing water-soluble binder systems to enhance heat extraction during solidification of the liquid metal in the mould cavity [7]. One such casting process is the ablation casting technology [9], wherein, aluminum alloys have been cast into net shaped components. The process uses a water spraying system that erodes the water-soluble sand mould and impinges on the solidifying aluminum metal inside the mould.

The ablation casting technology has received widespread attention from the automobile industry as a manufacturing option, and in the course of the past few years, several researchers have published studies related to this subject. A review of these studies is presented on the following pages.

1.2.1.2 Literature Review

Alotech Ltd. LLC patented an Ablation Casting Process in 2006 [9]. The apparatus for sand removal used in this process contains a working table that can move horizontally through a set of static nozzles fixed at prescribed locations. The mold is tilted about 20° to provide better filling after pouring the molten metal. Once the filling is completed the mold is returned back to its original position and then is moved towards the set of nozzles by the working table. The pressured set of waterjets washes the sand away and impinges on the metal surface to accelerate the solidification rate. The sand and water are reclaimed from collecting tank. Some details of the technique concerning the spraying system were reported. In the first example of the application, aluminum-6061 alloy was cast. The pouring temperature was 730° C and the nozzles were turned on 10 seconds after pouring. Water was used as the coolant and its temperature was kept at 20° C. In the second example, where the casting of an automotive knuckle took place out of aluminum A356 alloy, three banks of water spray nozzles were used.

Approximately 10-psi water was fed into the spraying system. The water temperature was kept at 40° C. In the third example, water pressure was kept at 15-psi. It was mentioned that the volumetric flow rate varied based on the nozzles. It was reported that this process provides uniform cooling for castings. Although the volumetric flow rate, pressure and temperature of coolant were listed as the important parameters to remove the sand away, no information was provided about the rate of sand removal or the achieved cooling rate.

J. Grassi et al. [7] discussed the advantages of the ablation casting technique with respect to other conventional sand casting techniques. In conventional casting, the solidifying metal contracts away from the cavity as it changes its state from liquid to solid, which leads to an air gap forming between the metal and the sand. This was considered as the main problem with conventional sand casting as the cooling rate becomes extremely low and the heat flow is less effective due to the air gap. In ablation casting, the coolant first removes the water-soluble sand mould, eliminating the formation of the air gap. The only parameter about the waterjet given by Grassi et al. [7] is the temperature of 65 °C of the water used. The overhead water spray system was applied from the coolest end of the casting to increase the solidification rate. Aluminum A356 alloy was used in this study and the casting part was an automotive steering knuckle. After heat treatment and aging processes, significantly improved mechanical properties compared to conventional sand casting and permanent mould casting were reported including comparable results to competitive casting processes (Squeeze Casting and Pressure Counter Pressure Casting). Furthermore, it has been reported that casting of aluminum 206 series alloys (known as difficult to cast) was straightforward with ablation casting. Moreover, aluminum 6000 and 7000 series wrought alloys were found to be castable. This technique was adapted to cast the rear swing arm for Buell motorcycles [13]. Aluminum B206 alloy was used in this casting application and a wall thickness of 2 mm was achieved with no porosity and hot tears.

J. Grassi et al. [14-15] updated their previous publication and reported that the high cooling rates achieved by the spraying system resulted into evenly distributed refined microstructure throughout the casting, including thin and thick sections. It was reported that combinations of both thin and thick wall castings (from 2 mm up to 100 mm) were cast successfully. Furthermore, some issues regarding the surface quality of castings and distortion as the metal solidifies were mentioned as the obstacles that have been successfully overcome.

Weiss et al [16-17-18] investigated the effect of ablation casting on hybrid metal matrix composites. Conventional sand casting and ablation experiments were conducted with 8 in wide by 16 in long plate shaped pattern that had thickness variation from 1.5 in to 2.5 inches. In this study, moulds were prepared out of an inorganic soluble binder. A solvent was used as the coolant and its temperature was kept at ambient conditions. The details of this solvent were not reported. The solvent jets were sequentially turned on from the thinnest section towards the thickest section of the casting, resulting in unidirectional solidification of the part. The increased solidification rate achieved by the process resulted in 35% decrease in the solidification time. More uniform microstructure was obtained including 20% reduction in the dendrite arm spacing. The yield strength of the ablated parts was up to 20% greater than conventionally cast parts. Furthermore, in this study, high levels of porosity were observed in castings of both processes. Typically in ablation process, creating unidirectional solidification from the coolest end of the casting towards the risers provides significant reduction in porosity content. It was mentioned that the gating design and pouring technique of this study was not optimized for ablation process and this contributed to high levels of porosity. They did not provide any details about the sand removal rate, flow rate, jet velocity or cooling rate.

Zindel [19] reported that the ability of ablation casting to cast complex shapes with enhanced mechanical properties has been proven over conventional casting processes in low volume experimental studies in AMD 405 (Improved Automotive Suspension

Components Cast with B206 Alloy) and AMD 601 (High Integrity Magnesium Automotive Components) projects. Ablation casting was successfully implemented for high volume production of Mercury marine transom bracket, which is the structural component that connects the engine to the boat. Details regarding the spraying system of the conducted experimental studies were not revealed. It was reported that sand reclamation opportunities made it possible to reuse the inorganic media and environmental friendly nature of the process was considered as an extra benefit.

M. Tiryakioglu [20] studied fatigue life of parts produced using ablation-casting process and compared it with forging and conventional casting. The wrought Aluminum 6061 alloy was used to cast a military handle. Casting dimensions were not mentioned. It was reported that the yield strength of the ablated castings was lower than forged castings. Furthermore, it was reported that the fatigue life of aluminum 6061 ablated castings was higher than conventionally cast aluminum A356 castings but lower than forged aluminum 6061 castings. No information was provided about the spraying system used in this study.

Bohlooli et al. [21] conducted an ablation-casting study where the solidification behaviour, porosity content and microstructure along with the feedability of aluminum A356 alloy were investigated and compared with conventional casting. The sand moulds were prepared with 2 wt. % Bentonite and 15 wt. % Clay and L-shape casting parts were cast. The spray system was positioned near the far end of the sand mould (the coolest end). The spraying system was turned on after the solid shell with sufficient thickness was obtained. This was determined by looking at the thermocouple that was placed at the jet's impact region, and when temperature reached 580 °C the process started. The effect of having feeders was also investigated and found that it weakened the cooling effect of ablation process by maintaining the temperature around the feeder area. Results showed that using the ablation casting process led to significant reduction in the porosity content of the castings. In addition to that, the process helped to obtain finer silicon phases, in other words more homogenous properties. They also quantified

the effect of the ablation process on A356 alloy and according to the reported results, 35% reduction in the secondary dendrite arm spacing (SDAS) was achieved.

Thomas et al. [22] conducted a feasibility study of the ablation casting process for steel castings and compared the process with conventional sand casting. Silica sand and phenolic urethane no-bake binder system were used to make the moulds. This sand/binder mix was non water-soluble and the cope of the castings was removed manually in order to provide cooling by the sprayer during the process. A 40-inch long, 2-inch square cross section bar with a riser was cast both conventionally and ablation. A low-pressure shower garden hose was used as the sprayer and it was turned on at 165 seconds after pouring to provide cooling from the end of the casting opposite of the riser. Translating of the water along the length was determined by the thermocouple readings. When the thermocouple near the end of the bar read 1400 °C, the sprayer was moved towards the direction of the riser and this was repeated along the length of the bar. The large temperature gradients created by the spray resulted in improved feeding during solidification and shortened the solidification time drastically. Additionally, compared to conventionally cast parts, the visible centerline porosity was successfully avoided by the ablation process. However, in this study, the effect of the ablation process on mechanical properties was unclear and inconsistent. Due to the complex cooling phases of steel, the feasibility of the process is not straightforward as in aluminum and magnesium castings. Furthermore, a sodium silicate binder was investigated as an alternative water-soluble binder agent. Sodium silica is known as water-soluble only at the early stages of curing. The use of this binder created another problem due to the high pouring temperatures of the casting. As soon as the molten metal filled the mould cavity, high temperatures accelerated the curing of the sodium-silica binder which resulted in the formation of a non water soluble mould shell, which diminished the cooling ability if the ablation casting process. It was reported that using sodium silicate, as a water-soluble binding agent may not be suitable in ablation casting processes. No details regarding the operating conditions of the waterjet parameters were provided.

Dudek et al. [23] investigated the sand removal behaviour of waterjets in ablation casting. A new apparatus was developed to conduct series of tests. The sand mold placed on a working table and after the pouring, this table was introduced into the experimentation chamber by circular and vertical motion of the working table. Then it was lowered to the area of nozzles' operation. Removal of the sand mold took place and followed by the rapid cooling of the solidifying metal. Upon completion of the process, the working table was controlled to move the part out of chamber. A high-pressure pump (12-MPa/1740-psi) was used to feed the nozzle system, which provided a flow rate of 6.5 L/min. This new testing apparatus resulted into large temperature gradients that helped to eliminate porosity, especially in big cross-sections. The apparatus used in this study was filed to the Patent Office of the Republic of Poland and was assigned the number "P.404518". The circular motion of the working table allowed the removal of the sand from all sections of the casting as it solidified. Sand removal was tested without having castings in the cavity while varying the rotational and vertical speeds of the working table. It was reported that in order to avoid any surface deformation in the castings, the shape of the casting and gating design must be selected carefully. This study was a good effort to bring a new perspective to the ablation casting process. However the developed apparatus may not be suitable for thick sand mold castings as the movement of the working table increases the complexity of the process.

Prescenzi [24] utilized the ablation-casting technique to manufacture six different body node castings for the 2016 Acura NSX. He was able to achieve high mechanical properties sufficient to meet the requirements of energy absorption, namely: 190 MPa Yield Strength, 287 MPa Tensile Strength and 16.1% of elongation were achieved using A356 aluminum alloy. The addition of strontium to the alloy composition resulted into a more refined eutectic microstructure, which led to an elongation percentage higher than the targeted value of 12. Prescenzi reported that ablation casting in light weighting applications is able to provide a nominal wall thickness of 4 mm instead of 5-6 mm when using the traditional gravity die-casting technique. Sand cores were used to create

complex hollow internal sections to achieve further light weighting. No information regarding the spraying system used in this study was provided. Prescenzi indicated that the use of ablation casting to obtain high mechanical properties and to produce hollow shapes is ideal for lightweight space frame structures.

1.2.1.3 Summary

According to the studies listed above, the effect of using a spraying system to accelerate the solidification rate and obtain refined microstructure is clear. However none of the conducted studies provides meaningful information about the interaction between the sand mould removal and jet parameters. Test conditions for some parameters were reported in some studies without presenting the reasoning behind. The little published information available in literature creates confusion in defining test conditions for jet parameters. The jet parameters play a vital role in this process and its characteristics must be studied in details. Therefore based on each individual casting scenario the right jet impingement setup can be decided. The requirements of a spraying system depend upon the type of the sand binder system, moulding conditions and thickness of sand mould, the solid-fraction of the alloy at the time of impingement and the dynamic pressure that the casting can withstand. The objective is to determine the operating conditions of the spraying system to obtain the maximum benefit on microstructure without causing any distortions on the casting. The next section will highlight the fundamental aspects of material removal using waterjets. This will help to derive a relationship between jet parameters and sand removal.

1.2.2 Waterjet Cutting

1.2.2.1 Background Information

Waterjets have been used for centuries for cutting of various materials. Early attempts of using waterjet cutting traces back to the nineteenth century, where high-pressured water was used mostly for mining purposes. The most basic application was developed to wash over a blasted rock face carrying loose coal and rock. Over the decades a lot of redevelopments occurred and waterjet cutting has taken different forms for rock

excavation applications. The use of waterjets as a drilling technique helped considerably in the growth of the mining industry in the post war era [25]. Early waterjet cutting systems were able to easily cut soft materials, but they were not as effective in cutting hard metallic materials. The addition of abrasive particles enhanced the cutting ability of waterjets immensely. In 1930s, the waterjet cutting technology provided fast cutting systems for a wide range of materials including steel, titanium, stone and glass with great precision [26].

In a waterjet cutting system, the cutting is initially achieved by micro erosion, which takes place on the surface of the material that is being cut. The required impact force to cut a material is provided by feeding a large volumetric flow through a nozzle with a small orifice size, typically 0.07mm to 0.51mm. The amount of water travelling through this small cross sectional area exits the orifice at high velocities up to 915 m/s. The stream leaving the nozzle impinges on the material surface and eventually causes a small crack on the workpiece. This crack gets bombarded by the constant stream of pressurized water (up to 415 MPa) and propagates until the cut is through. Water pressure, nozzle orifice diameter, water flow rate and the standoff distance (the distance between the nozzle and the workpiece) are considered as the key parameters of the waterjet cutting process [27].

The mechanism of material removal is basically the impinging pressure of the water exceeding the compressive strength of the work piece [27]. This limits the application of the waterjet to relatively soft materials only. Abrasive water cutting technology was developed to overcome this limitation. Abrasives such as garnet, silica, silicon carbide and aluminum oxide are fed to a mixing chamber, which is typically located on the downstream side of the waterjet orifice. A schematic diagram of an abrasive waterjet is shown in Figure 1.1.

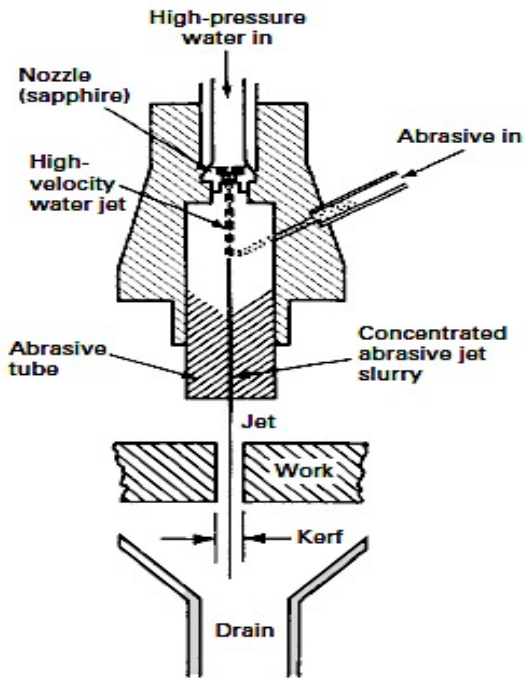

Figure 1.1: Waterjet with side feeding of abrasives into a mixing chamber [27]

High-pressure water is used to intensify the cutting abilities of the waterjet. This pressurized water leaves the sapphire nozzle orifice at extremely high velocities. In the mixing chamber, the momentum of water is gradually transferred to abrasive particles to enhance the cutting capabilities. The particles discharged from nozzle orifice along with the water directly imping on workpiece surface and the cutting occurs. A full range of materials including metals, plastics, rubber, glass, ceramics and composites can be cut using this technique with the right configuration of the abrasive waterjet pressure (207 MPa - 345 MPa), abrasive flow rate and abrasive nozzle orifice diameter (0.25mm - 5.6mm). The cutting through capabilities of the technique demonstrates itself up to 20.3cm workpiece material thickness. Additional key parameter in abrasive waterjet cutting is the type and the shape of the abrasive material; depending on the density and hardness of the abrasive materials the impact magnitude of impingement varies [27].

Waterjet cutting also known as plain waterjet machining (PWJ) and is considered as one of the most cost effective non-traditional machining processes. The material removal rate (MRR) is the most significant quantity in machining processes. MRR in waterjet

machining applications is directly proportional to the kinetic energy of the waterjet and inversely proportional to power input (or specific energy) required to machine the material [28]. The specific energy of a workpiece is calculated experimentally in order to determine how much power input is required to machine the desired amount of material. The value of the specific energy for the same workpiece material varies depending on the machining application (band saw, grinding, turning, milling, etc.) because of the forces that trigger the material removal from the workpiece surface are different in each application. Therefore, the power input requirement to machine the same amount of material differs.

As mentioned previously, there are two types of waterjets including plain waterjet and abrasive waterjet. In this study plain waterjets (PWJ) were utilized to remove the water-soluble sand moulds. However due to the limited cutting abilities of PWJ most of the available literature focuses on abrasive waterjet machining (AWJ). In the next section, the material removal mechanism of AWJ is reviewed thoroughly. Reviewed studies include the AWJ of ductile and brittle materials with proposed models as well as the erosion phenomena associated with the material removal.

1.2.2.1 Literature Review

In both machining process PWJ and AWJ, the understanding of the material removal is based on the effort of Finnie [29]. Finnie investigated the impact wear phenomena occurring on the material surface as a result of the excessive impact of solid particles and developed an analytical erosion model for the material removal. This erosive wear model relates the kinetic energy of the particles impacting on the material surface to the rate of wear. Finnie's equation proposes that the strength of the material determines the energy absorption during cutting, which means that the material removal only occurs when the kinetic energy of the impacting particles is greater than the strength of the material. As a result, only the part of the total energy exceeding this threshold can be used for the erosion action. Finnie reported that in brittle materials, elastic deformation occurs on the surface that is under heavy impact of the particles and ductile materials

can deform both elastically and plastically, which means there is not only one type of removal mechanism that can apply to all materials. The mechanism of the removal depends on the type of the material being cut, brittle or ductile. In ductile materials, material removal presents itself through plastic deformation in which micro cutting provided by the impact particles result in erosion [29]. On the other hand, in brittle materials, impact particles contribute to the initiation of multiple cracks on the material surface and material removal takes place when these cracks intersect with each other.

According to Finnie, the wear of a surface by the impact of solid particles depends on the motion and the impact angle of the particles as well as the hardness of the surface. At shallow angles of impact (less than 30°), the impact of the solid particles is not sufficient to remove the same amount of material as the particles impacting at near orthogonal angles. Finnie reported that predicting the impacting angle and particle velocity to obtain the maximum erosion is possible in ductile materials using his proposed model for erosion. However, the model did not seem valid for predicting the particle velocity and angle for brittle materials.

Bitter [30-31] studied the erosion phenomena thoroughly and developed an expression for erosion as a function of mass and velocity of the impinging particles, impingement angle, and mechanical and physical properties of erosive particles and eroded body. The proposed expression for the impact wear assumes the material removal in ductile materials due to plastic deformation. The theory derived by Bitter calculates the deformation wear depth at the regions where abrasive particles impacted. Bitter reported that there is a threshold velocity in abrasive waterjet machining below which no material removal is possible. Bitter discussed the dependence of erosion on particle velocity. When a rigid particle impinges on a steel surface at velocities around 100 m/s, the depth of penetration is only a fraction of the particle diameter. Plastic deformation takes place on the surface and indentation happens the size of which is the same as particle. This only occurs in conditions where the impinging particle is harder than the surface that it is impinging. In case of disintegration, the particle penetrates less. At

impinging velocities higher than 200 m/s, quite different erosion behaviour is observed. The depth of the penetration created by the impact of these high velocity particles is several times greater than the diameter of the particle. Heavy erosion occurs on the surface due to massive impingement forces, resulting in two types of wear; deformation wear and cutting wear [30]. Bitter showed that depending on the characteristics of the work material and impingement conditions, cutting wear or deformation wear or both might trigger the material removal. Deformation wear mode takes place due to the repetition of collisions, which results in cracking of the target surface, and the component of the normal force to the target surface is responsible for the cracking. The deformation wear typically present itself with brittle materials. In ductile materials, material removal is driven by the excessive plastic deformation at the large angles of impact. The cutting wear mode prevails as a result of the cutting action of the moving particles, which generates plastic deformation. In ductile materials, the cutting wear mainly occurs at shallow angles of impact. In practise these two types of wear typically take place simultaneously where the impact angle varies.

Hashish [32] carried out an experimental study based on Finnie's erosion model. Later this study was expanded [33] and presented an analytical model to predict the depth of cut in AWJ cutting for different metals. Hashish tried to visualize the cutting process in order to develop a kinematic model. His kinematic jet solid penetration model can predict the depths of cut based on the different modes of erosion along the kerf [33]. However, he assumed the width of the kerf to be constant along the depth of cut. Parallel findings as in his previous work [35] were observed in the analysis of the depth of cut. At the shallow angles of impact, cutting wear mode prevails while at the large angles of impact cutting occurs predominantly due to the deformation wear mode. Hashish utilized Bitter's model to predict the depth of the cut obtained in deformation wear mode. Hashish described two material properties including the dynamic flow stress and the threshold velocity of abrasive particle. The flow stress is defined as the required load stress to plastically deform the material and keep the metal removal flowing. This stress is found to be proportional to the elastic modulus of the material

that is being cut. The flow strength required to cut a material is equal to 14 times of its elastic modulus. Hashish also obtained the critical particle velocity for 17 different metals through this experimental work and listed the threshold velocities to achieve penetration.

Paul et al. [34] investigated the mechanism of material removal in AWJ of ductile materials and developed an analytical model including a generalized cutting kerf shape of aluminum and steel. As opposed to Hashish's work mentioned above, they considered the variation in the width of the cutting kerf along its depth including the transition zone between the wear modes (micro-cutting zone and plastic deformation zone). This consideration improved the accuracy of the model drastically in predicting the depth of cut. The width of the cutting kerf is proportional to nozzle insert diameter. The width progressively decreases and reaches its minimum value. Additionally, this study proposes that the depth of cut is determined by specific energy of the material that is being cut rather than its elastic modulus. The required threshold velocity for penetration was reported as a complex function of waterjet parameters and abrasive material.

Hashish [35] conducted a study to visualize the abrasive-waterjet cutting process where penetration of waterjet was recorded by using a high-speed camera. Transparent materials including Lexan, glass and Lucite were used as workpiece material, which represent both ductile and brittle behaviour. The visualization study revealed two types of cutting modes depending on the impact angle. This finding was in agreement with the study conducted by Bitter [31]. The cutting wear mode, which occurs, at shallow angles of impact results in a steady state jet solid interface at the top of the kerf. The deformation wear mode occurs at large angles of impact results in an unsteady penetration zone down the kerf. Hashish indicated that the two cutting modes repeat itself in a cyclic nature and the conditions of the operation dictate which of these modes contribute the most. Additionally, Hashish reported similar penetration patterns in abrasive machining of a ductile material (Lexan) and a brittle material (glass). In other

words the penetration of abrasive waterjet machining process does not depend on the type of material. The dynamics of the interaction between the abrasive particle and material was reported as the only difference. Hashish also investigated the effect of particle size, impact angle, abrasive flow rate and jet pressure on the depth of penetration. Increasing particle size was not favourable for the steady state penetration as it decreases the depth of cut. To obtain the maximum depth of cut, the right cutting angle must be used. Working with shallower or larger angles results in insufficient penetration depths. The depth of cut obtained by the cutting wear mode found to be more sensitive to the changes in the abrasive flow rate than the cut obtained by the deformation wear mode. Jet pressure played a big role in the penetration depth of the deformation wear mode.

Kovacevic [36] experimentally studied the depth of abrasive waterjet penetration and established an empirical relationship between the depth of cut and jet parameters including size of the nozzle orifice, abrasive flow rate, stand-off distance, traverse speed and waterjet pressure. Due to the complex nature of the abrasive waterjet milling operation, monitoring the depth of cut is impractical. Kovacevic conducted experiments and measured the depth of penetration achieved under different conditions of AWJ parameters. Through multiple regression analysis correlations between depth cut and waterjet parameters was established. Kovacevic reported that increasing the waterjet pressure, abrasive flow rate and nozzle orifice size will result in greater depth of cut. Additionally, any increase in jet traverse speed and standoff distance will decrease the depth of penetration. Mild steel was used as the workpiece in this study. Kovacevic added that for the machining of different materials the normal force of that specific material must be calculated. According to the normal force the abrasive waterjet parameters can be configured and the model can still be valid.

Momber et al. [37] experimentally investigated the removal mechanism of high-energy jets in different type of concretes and observed the crack propagation closely. In order to create a multiphase brittle material aggregate grains were added to concrete mix in

one sample group and plain portland cement (PZ 35 F, DIN 1164) concrete was used as the other sample group and they compared the fracture patterns of these two samples during cutting with pressurized water. The pressure of the waterjet was reported as the cause of the micro crack growth on surface, which leads to the failure and eventually the destruction of the material. Addition of aggregate grains weakens the fracture toughness of the material and waterjet can penetrate with less energy compared to the plain concrete. Therefore the required threshold energy to penetrate the material is reduced and the destruction of the sample can be done with lower level of energy input. They reported that depending on the mechanical properties of the material that is being cut, the required pressure to initiate a crack on material surface changes. Each material has different mechanisms for energy absorption and a penetration can only happen when waterjet overcomes the threshold energy. As a result of that different fracture patterns along the penetration occurs.

Zeng et al. [38] experimentally investigated the erosion behaviour in abrasive waterjet cutting of polycrystalline ceramics and derived a model for material removal. They reported that a several different crack patterns including conical, radial and lateral crack systems were observed on material surface as a result of the impact created by the abrasive particles. This study focused on the material removal occurrence due to crack networking (intergranular cracking) and related removal to the fracture energy provided by the waterjet. Typically in brittle materials, removal takes place as a result of lateral cracking. Their study showed that lateral type of cracking is mostly observed with 90° impacts of abrasive particles. Erosion at this angle occurs as a result of the waterjet aimed at workpiece and particles erode the surface continuously and form the cutting kerf. The width of this cutting kerf decreases along the way due to the energy dissipation of waterjet. As a result of this sudden curvature changes occur and cutting kerf forms steps along the lower section of cutting front [38]. They reported that deflected jet stream contributes to material removal as well as the direct jet stream. This creates significant difference in the impingement force and results in sudden curvature changes especially behind the directly impacted zones [38]. They concluded that

material removal in brittle materials occurs due to network cracking. Fractures created on the surface by the impinging force of the waterjet are the main contributor of this networking. Developed model suggests that the fracture energy of target materials is strongly correlated with the erosion rate.

Paul et al. [39] also derived a model of material removal for polycrystalline materials. This study distinguishes itself from Zeng's study mentioned above by considering the abrasive particle shape and size in the model. Removal mechanism is reported as follows; at the shallow angles of impact, removal mechanism is due to microcutting and intergranular fractures and as the impact angle gets near orthogonal, removal mechanism turns into plastic deformation and intergranular cracking. Developed model in this study does not account for any variation in the width of cut and it is reported that this could lead to an error up to 20% in predicting the depth of cut. Threshold velocity to initiate the penetration is reported to be proportional to the specific energy of workpiece.

Fan et al. [40] used dimensional analysis technique to develop a model of the material removal in micro abrasive air jet machining of glasses. Air was used as the fluid in this study instead of water. The transfer of the potential energy of compressed air to the kinetic energy of blasting abrasive particles provided the material removal by creating brittle fractures on the target surface. A predictive model of the removal rate was derived as a function of common jet parameters (air pressure, abrasive mass flow rate, standoff distance, traverse speed, nozzle diameter) and target material properties (elastic modulus, vickers hardness, fracture toughness, density). According to the developed model, material removal is directly proportional to air pressure, standoff distance and nozzle diameter and inversely proportional to abrasive mass flow rate [40]. Although the proposed model for the rate of removal includes material properties such as elastic modulus and fracture toughness, the interaction between the jet parameters and these properties was not discussed. Nevertheless this study recognizes

importance of fracture toughness and elastic modulus on the penetration and the removal rate of the material.

Wu et al. [41] experimentally investigated the aspects of material removal mechanism of plain waterjet application for coating removal. Target material was chosen as aluminum 6061-T6 and waterjet process parameters including pressure (140-345Mpa), orifice size (0.152-0.381mm), standoff distance (6.35-127mm) and traverse speed were varied. They reported that the increase in pressure provides more material removal as expected. Although the width of the kerf does not change with different pressures, it was reported that the width of cut achieved by a jet at orthogonal angle to workpiece is larger compared to inclining angles to workpiece, consequently more material removal is provided at 90° angle. Also it was reported that the different jet types such as continuous jet, mixed jet and impact jet result in different force loadings on target material, providing different removal behaviours. Continuous jet provides static loading whereas impact jet provides dynamic loading and the mixed jet results in combined static and dynamic loading. The interaction between the standoff distance and pressure comes to play to obtain the maximum material removal. Varying the standoff distance while keeping the pressure unchanged, result in constant static load however the dynamic portion of the stagnation force increases rapidly with an increase in standoff distance [41]. This means that the material removal is optimum at a certain standoff distance. One would expect that the material removal to reach its maximum at low standoff distances due to more continuous, less pulsated nature of the flow stream. However the velocity of the water that is deflecting from material surface at the bottom of the kerf is 2-10 times greater than the impact jet velocity and as a result of this occurrence the jet cannot cut any deeper because the deflecting droplets cancelling out the main stream of the flow as the depth gets greater. Nonetheless, in this circumstance the jet typically creates enough energy to damage the target through crack initiation and propagation [41]. The impact of waterjet causes extremely intense local stress concentrations and when the internal stresses exceed the fracture strength of material, the crack is initiated.

1.2.2.3 Summary

The literature reviewed in the previous section clearly indicate that the removal mechanism in ductile materials is due to plastic deformation and fractures whereas removal occurs due to intersection of cracks in brittle materials. In terms of different wear modes, at smaller angles of impact the material is removed by cutting wear in ductile materials and at higher impact angles by deformation wear in both brittle and ductile materials.

The importance of the threshold energy for initiating penetration and subsequent material removal was emphasized heavily. A certain amount of energy must be provided by the waterjet to create a crack on the target surface. From fracture mechanics, this energy is known as the fracture toughness of the material and also referred as the fracture threshold, the threshold pressure, the threshold or the critical velocity in the literature. The threshold energy is the initial condition for a material removal to take place and if the jet energy is less than the threshold energy, no material removal is possible.

There are different ways in determining the required energy to achieve the desired depth of cut in the workpiece. Hashish [33] mentioned that the elastic modulus of the material plays a role whereas Paul [34] reported that the specific energy of the material determines the depth of cut. However in terms of predicting the removal rate rather than the depth of cut, the calculation of the required energy to remove a desired amount of material is straightforward and it can be assumed proportional to the kinetic energy of the waterjet [28].

The efficiency of the material removal is greatly dependent on the waterjet parameters. The waterjet pressure, nozzle orifice size, flow rate of water and the waterjet velocity were listed as the common process parameters and their effects on material removal were investigated in each study. These reported findings were taken into consideration in conducting experiments, correlating parameters and establishing empirical models.

The general effect of waterjets on material removal is well understood. However, the literature survey shows that there has not been any study conducted on sand removal of water-soluble sand moulds using waterjets. Nonetheless, the survey provides insightful information regarding the material removal process that is driven by the mechanical forces of the waterjet. The sand removal process of water-soluble sand mould however is rather complex as dissolution comes to play. In order to exploit the potential of The Ablation Casting Technique for applications of industrial interest, the sand removal rate of water-soluble sand moulds has to become well understood and better predictable.

1.3 THE MAIN OBJECTIVES OF THE CURRENT STUDY

The main objective of this study is to address the problem of lack of technical information of the removal process of water-soluble sand moulds. It is clear that the ablation casting technique is consisted of two separate stages; rapid sand removal stage followed by accelerated cooling stage. These two stages have contradicting objectives for the waterjet system. In order to maximize the benefit of the waterjet cooling on the microstructure of the casting, the sand removal stage must be performed rapidly. However, performing the accelerated cooling stage with the same momentum may result in a surface defect. Therefore, as opposed to the sand removal stage, the cooling must be provided with a lower waterjet momentum. This requires an instantaneous shift in the momentum of the waterjet upon completion of the sand removal. Hence, there is a need for a model that correlates the waterjet parameters to the sand removal rate. With the aid of this model, the exact time of the sudden drop required in the momentum of the waterjet can be predicted and the accelerated cooling stage can be done effectively. This study focuses on the relationship between waterjet parameters and sand removal; namely the interaction between each waterjet parameter (momentum of the jet, standoff distance, overlapping of multijets) and sand removal rate of the water-soluble sand mould. Also this study developed for the first time an

empirical model of sand removal that can predict the time of sand removal for given mould thickness. Additionally, the aspects of the removal mechanism of the water-soluble sand mould have been investigated. The identification of the maximum allowable waterjet momentum to successfully cool the casting without any surface defects have been investigated for aluminum 6061 and 7050 wrought alloys along with some microstructure analyses of 7050 alloy.

CHAPTER 2 : Experimental Setup and Experimental Procedure

This chapter is divided into three sections. In the first section, the details of the experimental setup are presented and the design considerations including the selection and orientation of the nozzles are explained with justification. In the second section, the experimental procedure is described. This section includes the preparation of the water-soluble sand moulds and the methodology and data processing of the sand removal rate experiments. The third section presents the process parameters and the range of each parameter.

2.1 EXPERIMENTAL SETUP

The waterjet impingement tests to analyze the sand removal rate (SRR) were conducted at The Thermal Processing Laboratory (TPL) at McMaster University. The waterjet system consists of a multi-stage centrifugal pump attached to a hosing system along with a rotameter, a solenoid valve and a pressure transducer. A schematic of the experimental setup is shown in Figure 2.1. An image of the experimental setup is shown in Figure 2.2.

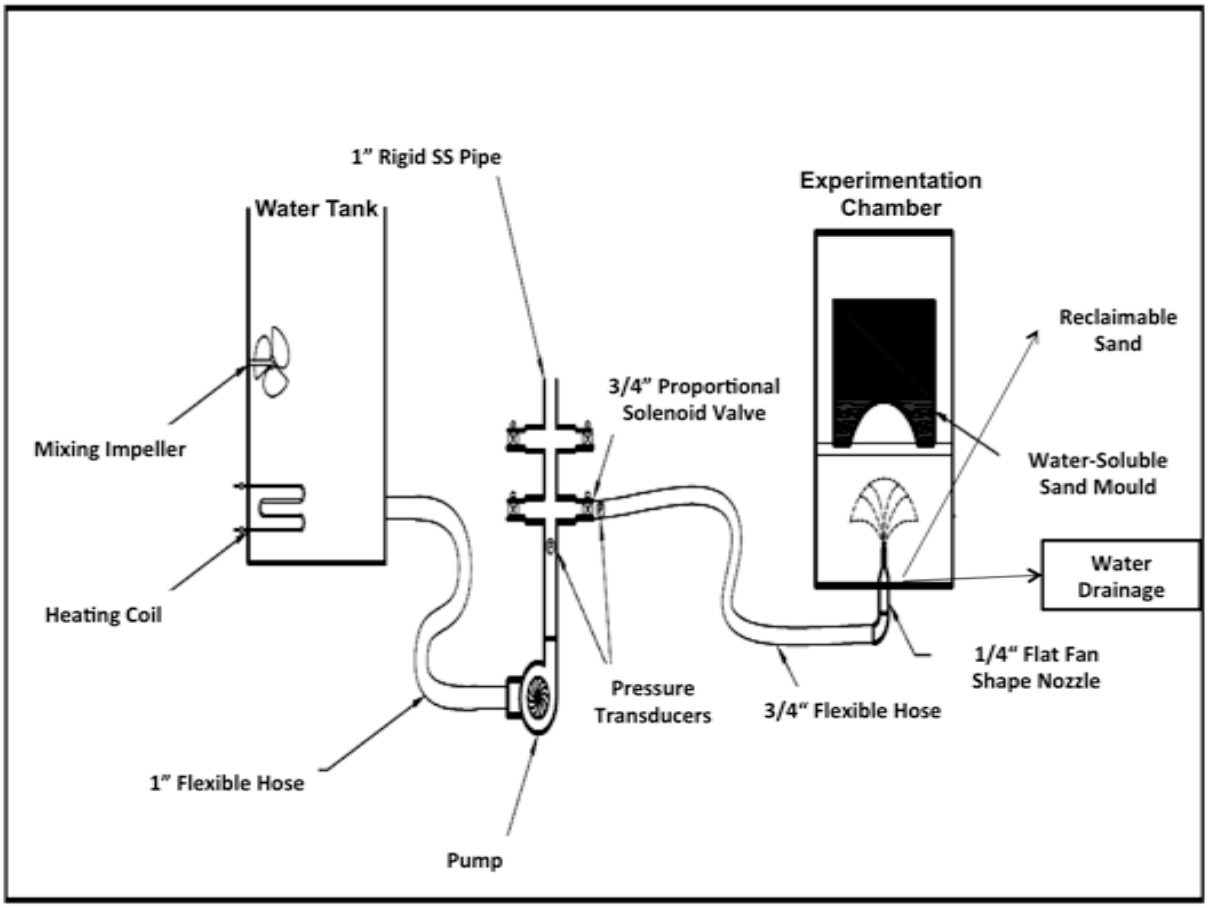

Figure 2.1: The schematic of the experimental setup

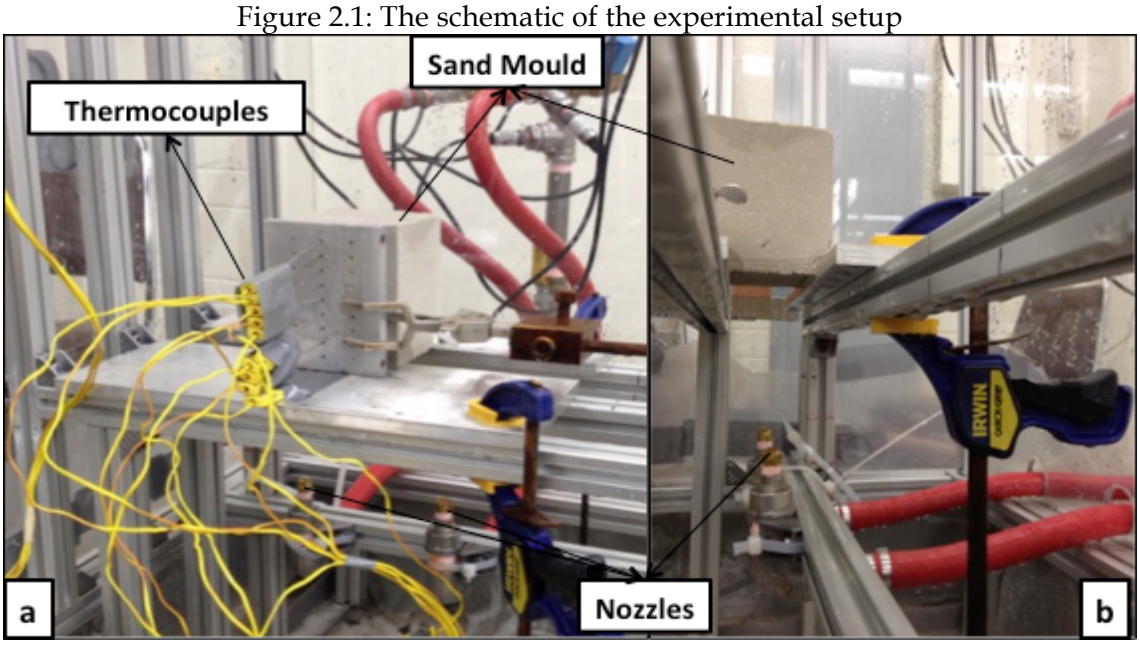

Figure 2.2: a. The water-soluble sand mould with thermocouples embedded
b. Bottom view of the setup

The sand mould was placed inside a plexiglass experimentation chamber where hosing system fed water through a flat fan nozzle or nozzles depending on the nature of the experiment. The orientation of the nozzle was orthogonal to the sand mould. The pressure of the waterjet was controlled using a solenoid valve and was kept constant during the sand removal stage and it was lowered to a pre-set value during the intensive cooling stage of the process. Pressure transducers were placed before the manifold and after the manifold on every branch of the hosing system. Each hose between the manifold and the nozzle holder (elbow) was one meter in length. An aluminum plate was employed to avoid sagging of the thermocouples and keep them at the desired locations. Table 2.1 presents the main components of the experimental setup with details.

Table 2.1: Main components of the experimental setup

Equipment	**Specifications**	**Manufacturer**
Pump	2 HP Multi-Stage Centrifugal Pump	Gould Pumps
Data acquisition system	Max. Sampling Rate: 500kSample/s	National Instruments
Rotameter	Max. Flow Rate: 5.5×10^{-4} m^3/s	Kobold
Thermocouples	Range: -270 °C to 1372 °C Error 1.1 °C or 0.4%	Omega
Nozzles	50° Flat fan-shaped spray pattern	Bex Spray Nozzles
Solenoid Valve	Flow Range: 1.39×10^{-4} m^3/s 3.53×10^{-3} m^3/s	Danfoss
Pressure Transducer	Pressure Range: 0 – 1035 kPa Error: ±2%	Omega
Computer	Prodesk, 4 GB RAM, 3.40 GHz Intel I3 Processor	HP

Flat fan nozzles were selected over tubular nozzles in order to provide gradual and continuous sand removal. Tubular nozzles were tested in preliminary experiments and found not suitable. Their extremely high impinging energy creates cracks resulting in a

sudden collapse of the sand mould. The spray pattern of a flat fan nozzle is illustrated in Figure 2.3. The spray angle of flat fan nozzles varies from 15° to 145°. In this study 50° nozzles were chosen as they create almost a 1:1 ratio between the standoff distance and the spray coverage. The standoff distance is the distance between the nozzle and the surface of the sand mould.

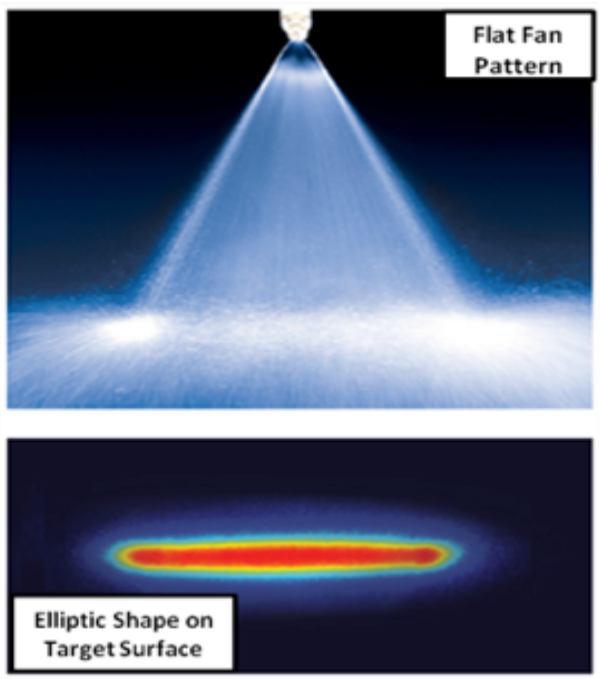

Figure 2.3: Spray pattern of flat fan nozzle [42]

In this type of nozzles, the shaped orifice breaks the fluid into a fan spray pattern and heavy concentration of fluid in an elliptic shape acts on the target surface, which makes them suitable for large area coverage. Detailed specifications of the nozzles used in this study are presented in Table 2.2. The pressure values are the maximum values that the existing pump can deliver.

Table 2.2: Specifications of the nozzles used in this study

Nozzle Type	Max. Pressure (kPa)	Spray Angle (°)	Diameter (mm)	Max. Flow Rate (m^3/s)	Orifice Area (m^2)	Max. Velocity (m/s)	Max. Momentum ($kg.m/s^2$)
F5005	586.1	56	1.422	4.61E-05	1.59E-06	28.998	1.336
F5006	551.6	56	1.549	5.36E-05	1.89E-06	28.457	1.526
F5008	551.6	56	1.803	7.13E-05	2.55E-06	27.924	1.991
F5010	551.6	55	2.007	8.90E-05	3.16E-06	28.144	2.504
F5015	586.1	55	2.464	1.38E-04	4.77E-06	28.995	4.006
F5020	586.1	55	2.845	1.86E-04	6.35E-06	29.296	5.452
F5030	586.1	54	3.378	2.73E-04	8.96E-06	30.494	8.33
F5040	517.1	54	3.886	3.45E-04	1.19E-05	29.056	10.009
F5050	517.1	53	4.369	4.32E-04	1.50E-05	28.802	12.429
F5060	482.7	53	4.775	5.02E-04	1.79E-05	28.02	14.054
F5070	482.7	53	5.156	5.86E-04	2.09E-05	28.083	16.46

As opposed to the ablation studies reported in the literature, in the present study the spraying system was positioned underneath the sand mol. Positioning the nozzles underneath the sand mould rather than using an overhead spraying system prevented water accumulation on the sand mould. Karwa et al. [43] studied the effect of coolant accumulation in jet impingement quenching and found that even having a thin layer of liquid accumulated on the part drastically diminished the cooling efficiency.

2.2 Experimental Procedure

The information regarding the water-soluble binding agent was obtained from the patent of Goetz et al. [44]. Sand molds were prepared with the following recipe; Silica sand of AFS 70 fineness was bonded with the water-soluble binding agents: 1.2% wt. sodium dihydrogen phosphate and 3% wt. borax. In order to provide green strength to the sand mold, 3% wt. plaster of paris and 6% wt. calcium bentonite and 4% wt. water were added. The ingredients were mixed for 10 minutes using a commercial KitchenAid mixer. Upon completion of packing the sand/binder mix into the aluminum mould boxes, the sand moulds were baked at 200°C in an industrial furnace. The dimension of the sand mould was 10.16cm x 10.16cm x 12.7cm.

In order to measure the sand removal rate, K-type thermocouples were placed in the centerline of the sand mould with 1.27cm increments. Figure 2.4 illustrates the schematic of the sand mould with embedded thermocouples.

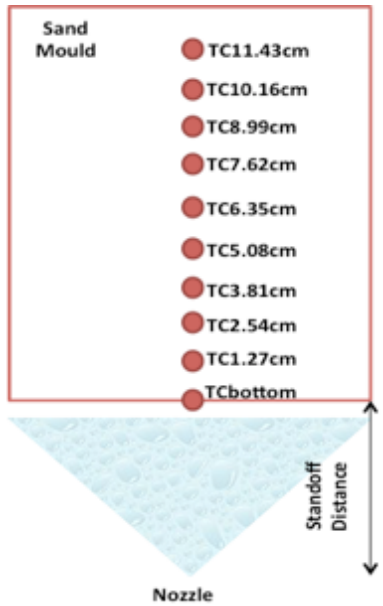

Figure 2.4: Schematic of the Sand Mould with embedded thermocouples

These thermocouples were connected to a data acquisition system. Temperatures were recorded at a sampling rate of 100 samples per second. The sand mould was placed above the waterjet in a position such that water leaving the nozzle can contact the tip of the thermocouples. After turning on the pump and establishing the water flow, temperatures were recorded indicating when the contact of water with the tip of each thermocouple was established. The inflection points in the thermal data recording are shown in Figure 2.5. One thermocouple was placed right underneath the sand mould (TC_{bottom}) to identify the exact time when the penetration started.

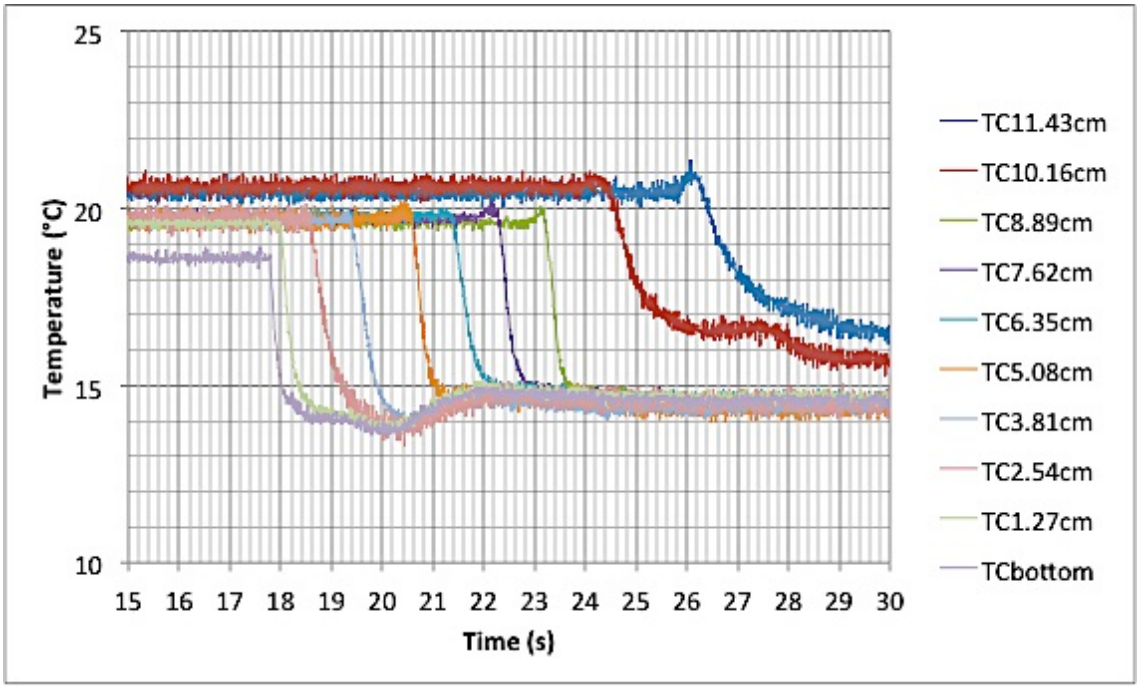

Figure 2.5: Typical thermal data recordings;
all thermocouple locations are measured from the bottom of the sand mould

These temperature measurements were used to determine the exact time when water contacted the tip of each thermocouple. Knowing the exact location of the thermocouples, the speed of water travelled through the sand mould was determined. Table 2.3 shows the recorded time of inflections and thermocouple locations.

Table 2.3: Time of sudden drop of various thermocouple readings
(**Δt** indicates the adjusted time based on TC_{bottom})

Thermo couple	Time (s)	Δt (s)	Distance (m)
TCbottom	17.801	0	0
TC1.27cm	18.020	0.219	0.0127
TC2.54cm	18.594	0.794	0.0254
TC3.81cm	19.415	1.615	0.0381
TC5.08cm	20.592	2.792	0.0508
TC6.35cm	21.441	3.640	0.0635
TC7.62cm	22.344	4.543	0.0762
TC8.89cm	23.220	5.419	0.0889
TC10.16cm	24.177	6.377	0.1016
TC11.43cm	25.874	8.074	0.1143

This data was used to determine the relationship between distance and time shown in Figure 2.6. The linear slope of the curve shown in Figure 2.6 was taken as the sand removal rate.

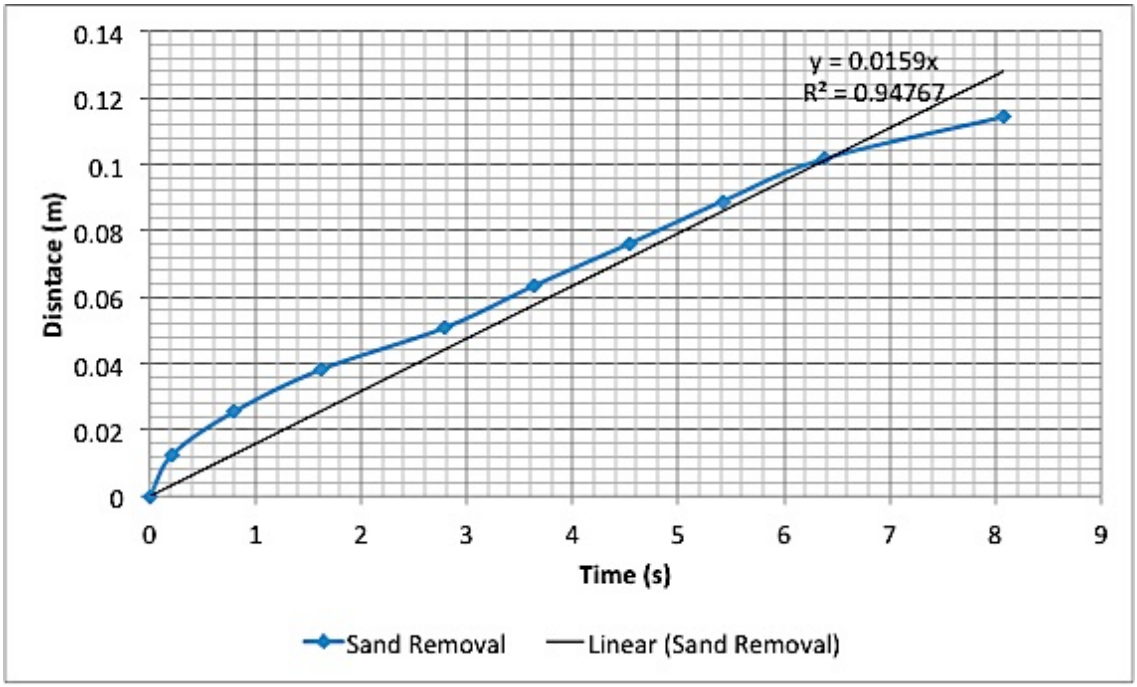

Figure 2.6: Relation between distance and time obtained using thermocouple measurements during a sand removal test

Using the procedure explained above, the sand removal rate was determined as a function of three major process parameters. The details of which are provided next.

2.3 Process Parameters

In order to investigate the influence of the main waterjet parameters on the rate of sand removal, three parameters were chosen: the momentum of the waterjet, the standoff distance and the overlapping percentage in the case of using multijets. Typically, the waterjet pressure, nozzle orifice size, velocity and flow rate are investigated in this type of removal processes. However, in this study the momentum of the waterjet was selected as a parameter that combines the interaction between the waterjet pressure and

nozzle size and between velocity and flow rate. The pressure of the waterjet determines the jet velocity, the force produced by the jet on the surface, Reynolds number and consequently the characteristic of the flow. The nozzle orifice size on the other hand, dictates the maximum velocity that the waterjet can reach at a given pressure. The flow rate increases with wider nozzle orifice sizes while the pressure is constant and the velocity naturally decreases in this case. In short, a large number of variables are involved and virtually these variables affect the rate of sand removal. However, no matter what the pressure, nozzle size, velocity and flow rate are, what matters is the momentum that corresponds to these parameters. So instead of worrying about the interaction of these four individual parameters, the effect of waterjet momentum on sand removal process was investigated. The momentum values were obtained by increasing the orifice size of the nozzle while keeping the waterjet pressure in a range from 482.7 kPa to 586.1 kPa. This resulted in a velocity range of 27.9 m/s to 30.5 m/s and according to Table 2.2; waterjet momentum was ranged from 1.336 kg.m/s^2 to 16.460 kg.m/s^2 including 11 data points. Only a single jet was used to investigate the effect of waterjet momentum on sand removal, the water temperature was at ambient conditions and the standoff distance was fixed at 13.97cm. Experiments repeatability was examined by repeating each test.

The standoff distance was chosen as the second important process parameter as it determines the impact magnitude of the waterjet. The droplets discharged from the nozzle orifice lose its energy as they get exposed to atmospheric air. This reduces the energy of the water and thus affects the maximum sand removal rate that can be achieved. The sand removal rate was investigated while the standoff distance was varied from 7.62cm to 31.75cm including 13.97cm and 22.86cm. One jet was used in the investigation of the standoff distance effect on the sand removal rate. The waterjet momentum was kept constant at 5.452 kg.m/s^2 and the temperature of the water was kept at ambient conditions. Each standoff distance test was repeated for three times.

In flat fan shaped nozzles, the intensity of the waterjet tapers off toward the outside of the spray pattern. This creates a gradual reduction in velocity towards the edges. This difference can be compensated with the addition of another jet. The overlapping of spray patterns is shown in Figure 2.7.

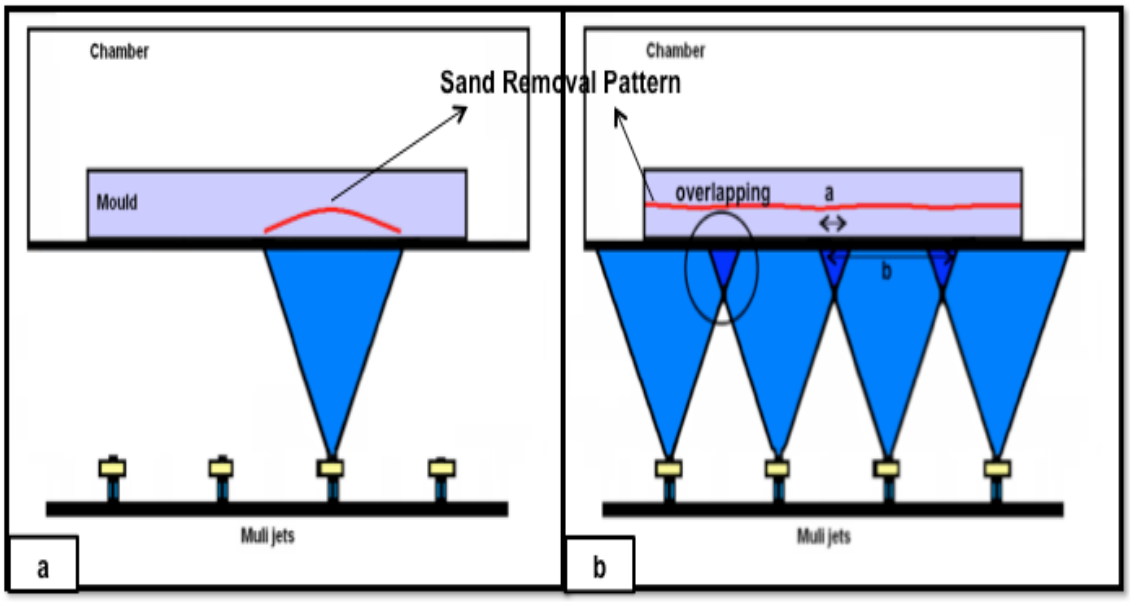

Figure 2.7: a. Spray pattern of a single jet b. Uniform removal along the mould by overlapping of multijets

A constant sand removal along the mould can be achieved by employing multijets. In order to attain a uniform sand removal, the optimum overlapping percentage must be identified. A set of experiments using two overlapping nozzles was carried out. The overlapping percentage was defined as the ratio of the overlapped area and the total coverage of a single nozzle, which is a/b in Figure 2.7.

Two identical nozzles were utilized for these experiments. Each nozzle provided 5.018 kg.m/s^2 waterjet momentum to remove the mold thickness of 12.7cm. The standoff distance was fixed at 13.97cm and water was at ambient temperature. The overlapping was varied from 0% to 30%, with 5% increments resulting in seven data points. Each overlapping test was repeated three times.

In order to investigate the influence of water temperature and two other parameters discussed above on sand removal process, a Taguchi orthogonal array was used to design a set of experiments. A L4, 3 Factors, 2 Levels Taguchi Experimental Matrix was established. Table 2.4 shows the details of the experimental matrix.

Table 2.4: L4, 3Factors, 2 Levels Taguchi Experimental Matrix

Experiment #	**WJM ($kg.m/s^2$)**	**SOD (m)**	**Water Temp. (°C)**
1	4.304	0.075	30
2	4.304	0.145	60
3	5.905	0.075	60
4	5.905	0.145	30

Three groups were considered in the experimental design, first one for waterjet momentum, second one for standoff distance and the third one for water temperature. Waterjet momentum is essential for sand removal to take place therefore its factors were chosen rather close to each other in order to see the influence of standoff distance and water temperature clearly. In this experiments an overhead nozzle provided downward removal and olivine sand was used as the sand type. The same water-soluble binding agent along with the other ingredients explained in Section 2.2 were added and the sand/binder mix was prepared with same procedure. Although the nozzle orientation and sand type were different than the rest of the conducted experiments in this study, these tests provided a good understanding regarding the influence of each parameter on the sand removal rate and their interaction with the water-soluble binder. Each experiment was repeated four times. This data was processed using statistical software Minitab. The percentage contribution of each process parameter in order to achieve the minimum sand removal time was analyzed. The effect of water temperature on sand removal process was found to be negligible due to the dominancy of the mechanical sand removal over the chemical (dissolution) component.

CHAPTER 3 : Results and Discussion

In this chapter the waterjet parameters that effect the sand removal are explored using the experimental setup and procedure described previously in Chapter 2. The effect of water temperature is addressed within the section where percentage contribution of waterjet parameters is presented, followed by a forced diffusion study to analyze the influence of dissolution on sand removal. In order to develop a predictive empirical model, the effects of the standoff distance, the waterjet momentum and the overlapping of multijets are investigated qualitatively. This predictive model only takes into account waterjet penetration in the vertical direction and the rate of sand removal calculated here is one-dimensional. Another model of the volume of sand removal has been also developed using the waterjet machining approach and the specific energy.

3.1 Sand Mould Properties

The sand moulds used in this study are extremely brittle and having low tension and high compression. The density and green hardness of the sand moulds were measured as 1432 kg/m^3 ± 45 and 94.1 ± 3.8 (B Scale), respectively. As it was mentioned in the waterjet machining literature section, the energy of the waterjet must overcome the fracture toughness of the material for initial penetration. However in the removal of a water-soluble sand mould establishing such initial condition is more complex. The waterjet weakens the mould by wetting it even if the penetration is not possible and this changes the entire dynamic of this initial condition. For this reason, the interaction between fracture toughness and the energy of the waterjet was not included in this study.

3.2 Percentage Contribution of Waterjet Parameters on Sand Removal Rate

In order to effectively remove the sand, first it is necessary to attain an understanding of the influence of each waterjet parameter has on the removal process. Sets of experiments presented in Table 2.4 were conducted to analyze the effect of waterjet momentum, standoff distance and water temperature on sand removal rate. It is obvious that the waterjet momentum is indispensable for this process and it cannot be neglected. Because of this reasoning in order not to interfere with the contribution analysis too much, relatively close momentum values 4.304 kg.m/s^2 and 5.905 kg.m/s^2 were chosen. As far as the standoff distance is concerned, it is clear that the lower standoff distance will result in higher impinging energy and provide faster sand removal. Standoff distances of 7.5cm and 14.5cm were selected. In a real ablation-casting scenario where the waterjet impinges on solidifying metal surface, water at ambient conditions would provide more effective cooling than water at relatively higher temperatures. On the other hand one could argue that water at high temperatures may result in faster sand removal due to the accelerated dissolution. Moreover, ablation casting studies in the literature reported different water temperatures of 20°C, 40°C and 65°C. Water temperatures of 30°C and 60°C were chosen to explore its effect on sand removal. The results of the experiments are shown in Table 3.1 including every repetition. Figure 8 illustrates the percentage contribution of these parameters on the sand maximum removal rate (minimum sand removal time).

Table 3.1: L4 Taguchi experimental design and result of each repetition

Experiment #	WJM (kg.m/s^2)	SOD (m)	Water Temp. (°C)	SRR R1 (m/s)	SRR R2 (m/s)	SRR R3 (m/s)	SRR R4 (m/s)
1	4.304	0.075	30	0.0463	0.0527	0.0633	0.0499
2	4.304	0.145	60	0.0157	0.0201	0.0209	0.0146
3	5.905	0.075	60	0.0672	0.0476	0.0543	0.1009
4	5.905	0.145	30	0.0305	0.0462	0.0296	0.034

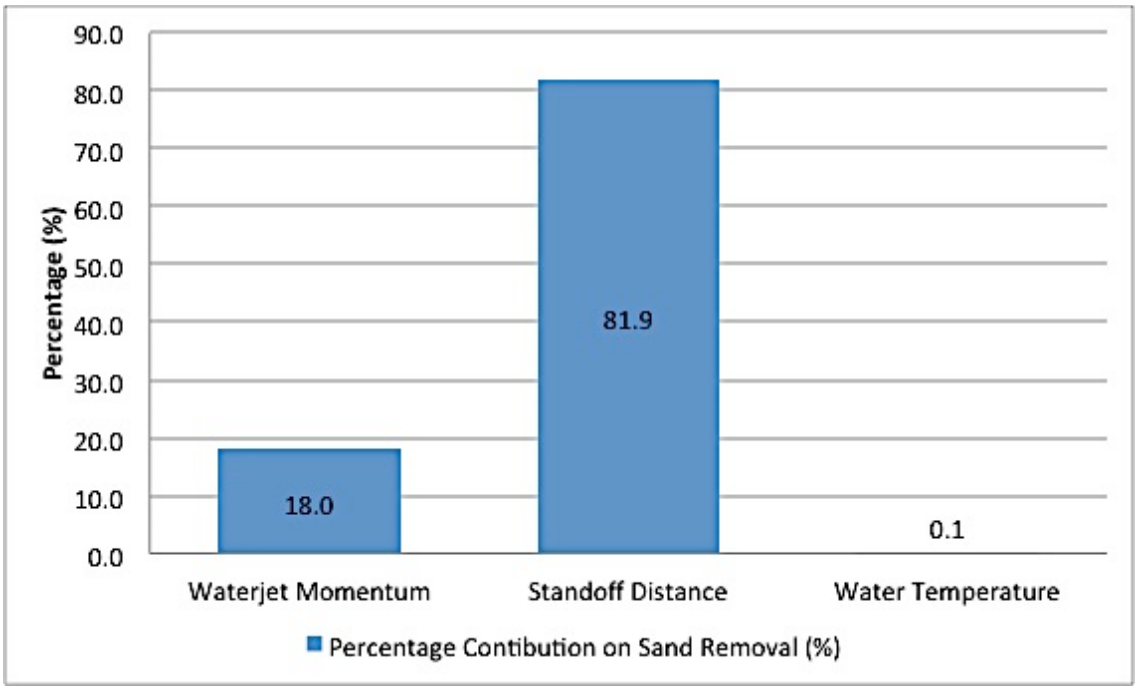

Figure 3.1: Influence of Process Parameters on Sand Removal Time

Figure 3.1 suggests that the standoff distance is the most dominant parameter affecting the sand removal rate. The role of standoff distance is at unattainable levels for the other parameters. Considering how much influence standoff distance has on the impact power of the waterjet, this result makes sense.

According to Figure 3.1, waterjet momentum contributes less than 20% to the rate of sand removal. Typically in this type of analysis any parameter that results in fewer than 20% can be neglected. However as mentioned before, if a wider range of waterjet momentum values was selected, the influence of waterjet momentum on the process would have been more significant.

It is clear from Figure 3.1 that the effect of water temperature on sand removal rate is negligible. Normally, one would expect faster removal under high water temperatures, however, higher temperatures of water do not accelerate the sand removal. This could have been possible if the sand removal was done in minutes rather than in few seconds. According to this finding, throughout this study water temperature was kept constant

at ambient conditions. Furthermore, the result suggests that the influence of the mechanical mode of the removal process dominates over the chemical mode (dissolution). In the next section the effect of dissolution is discussed.

3.3 Effect of Dissolution on Sand Removal

There are two modes that affect the rate of sand removal: the mechanical mode and the chemical mode. The mechanical mode occurs due to the impinging power of the waterjet whereas the chemical mode takes place as a result of the interaction between the water and the water-soluble binding agent. Considering the operating conditions of the waterjet, the removal process happens fairly quickly and the removal of a 12.7cm thick sand mold is usually done within few seconds. Therefore, it is not expected for the chemical mode to have a significant effect on the process.

A set of experiments was conducted with the purpose of understanding the impact of the dissolution of the water-soluble binder on the rate of sand removal. Two types of sand moulds were prepared; the first one included the regular sand binder mixture used in this study and the second one had all the ingredients but the water-soluble binder. Both sand moulds were prepared following the same mixing and baking procedure. Hardness values of 85 and 94 were recorded for the moulds without binder and with binder, respectively. Water at ambient conditions was used and a single nozzle (F5020) provided a waterjet momentum of 5.454 $kg.m/s^2$ from a 15.24cm standoff distance. The sand removal time for both cases is plotted in Figure 3.2.

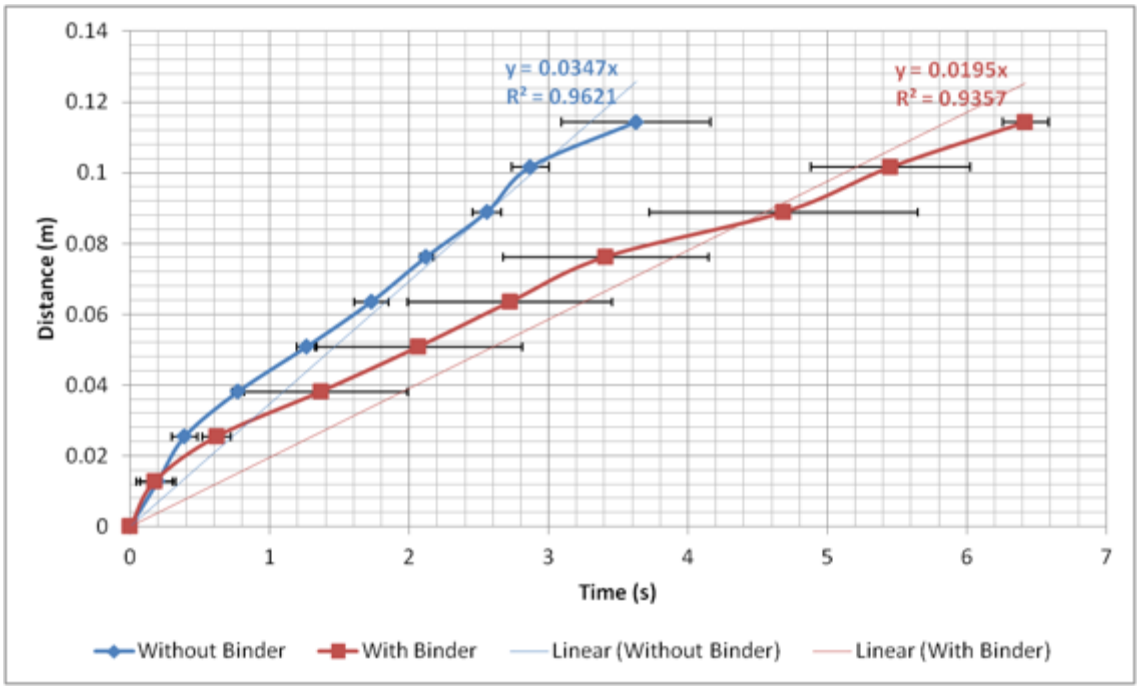

Figure 3.2: Effect of the water-soluble binder on sand removal time

According to Figure 3.2 the sand removal rate of the mould without binder is 56% faster. This could mean that without the binding agent the strength of the mould is not at the same level and the binding agent not only makes the mould water-soluble but also provides some sort of a structural integrity. Nonetheless the time taken for the removal of the mould with binder was longer despite the dissolution effect. The results created confusion in terms of understanding the impact of water-soluble binder as the mechanical mode interfered with the process. In order to investigate this impact clearly, the mechanical mode must be taken out of the process. Additionally, it can be noticed that although the time taken in three repetitions of the sand mould with binder resulted in 6.42s ± 0.17, the variation between the data points is quite large (up to 45%). According to this result, it was observed that even though the waterjet results in the same penetration time, there is not one typical removal pattern within the sand mould.

A forced diffusion test was conducted to investigate the effect of dissolution alone. A bucket was filled with 25-liter water at room temperature. The sand mould was placed

inside the bucket. The sand mould was taken out and the weight of it was measured at 1-minute intervals. The change in weight over time is plotted in Figure 3.3.

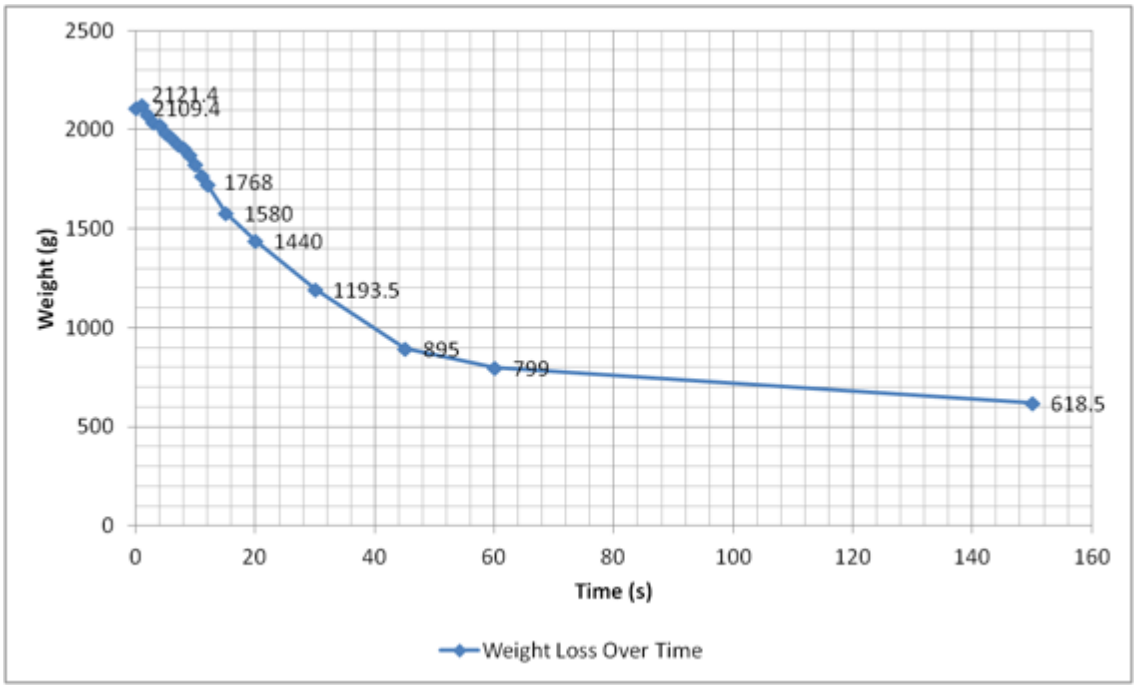

Figure 3.3: Change in sand mould weight over time during the diffusion test

According to Figure 3.3, the diffusion of 18 grams takes over a minute. The removal of the same amount can be achieved with 1.336kg.m/s^2 waterjet momentum in one second. This basically means that even using an extremely low waterjet momentum results in more than 60 times faster removal. The waterjet momentum of 16.46kg.m/s^2 can remove 277 grams per second. It takes about 10 minutes to remove the same amount of material during the forced diffusion test. Additionally, if the sand mould was not taken out every minute and kept for longer time intervals, the rate of sand removal have been less. Based on these two comparisons, the impact of the mechanical mode of removal is up to 600 times greater than the chemical mode and it can be even greater by lowering the standoff distance. Therefore, the impact of dissolution on sand removal process is definitely insignificant and negligible. The condition of the sand mold at different times of the test is shown in Figure 3.4.

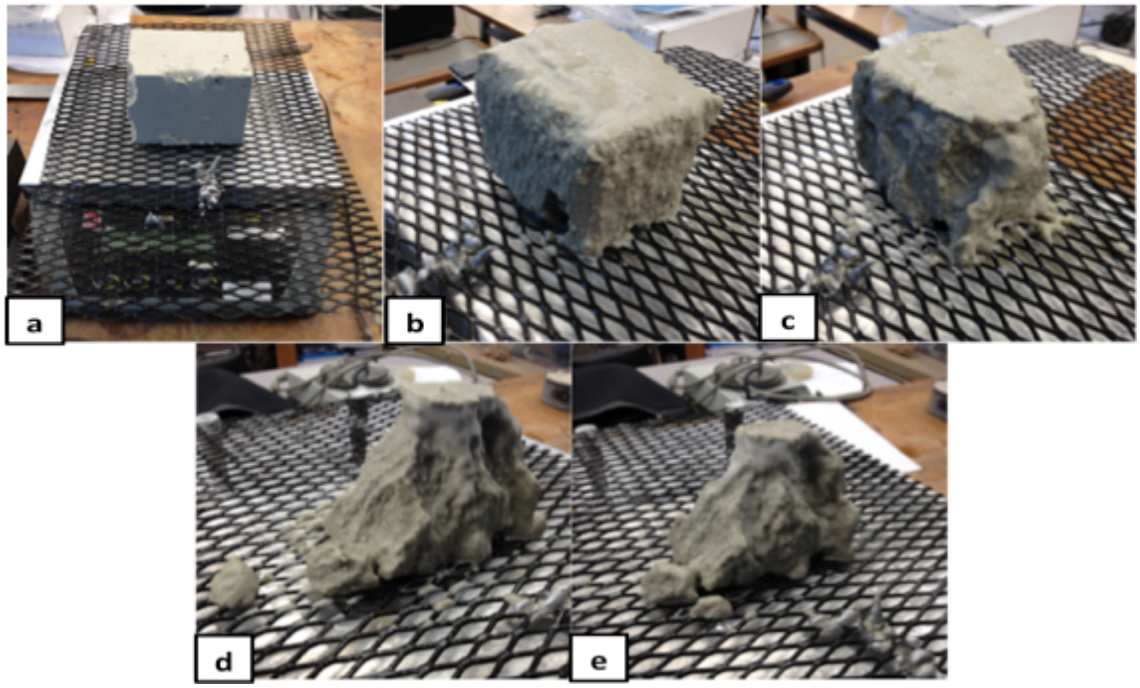

Figure 3.4: Sand Mould in Forced Diffusion Test a. Initial condition b.8th Minute c. 20th Minute d. 45th Minute e. 60th Minute

3.4 Effect of the Standoff Distance

It is common knowledge that an increase in standoff distance will reduce the kinetic energy of the droplets due to the effect of the atmospheric air on the flow. In order to investigate the relationship between the standoff distance and the sand removal rate tests were carried out using standoff distances of 0.0762m, 0.1397m, 0.1524 m, 0.2286m, and 0.3175m. A single nozzle (F5020) provided a waterjet momentum of 5.452 kg.m/s^2. The temperature of the water was kept at ambient conditions. Each test was repeated at least three times and the average of the best three repetitions was taken. Figure 3.5 illustrates the distance travelled by the waterjet through the sand over time for above-mentioned standoff distances.

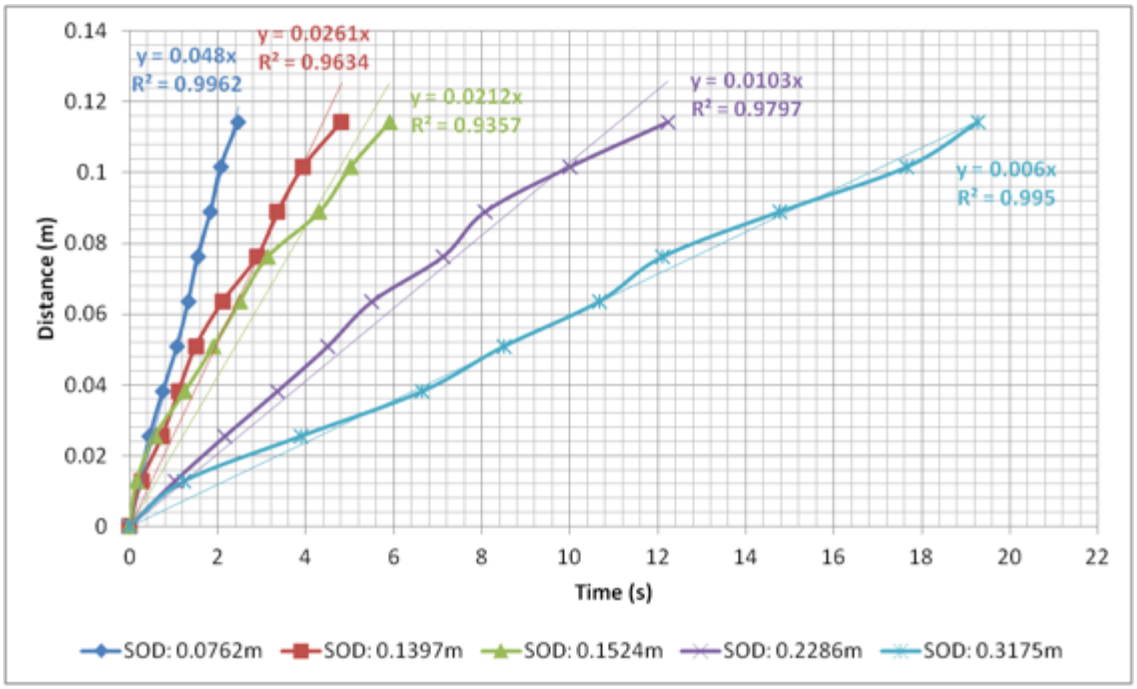

Figure 3.5: Effect of SOD on sand removal time

It is apparent from Figure 3.5 that the standoff distance has a significant impact on the time. The removal rate at 0.0762m standoff distance is 8 times greater than the removal rate at 0.3175m. Roughly speaking, a standoff distance that is 4 times lower results in 8 times faster rate. The sand removal rate calculated from these five standoff distance tests is plotted in Figure 3.6.

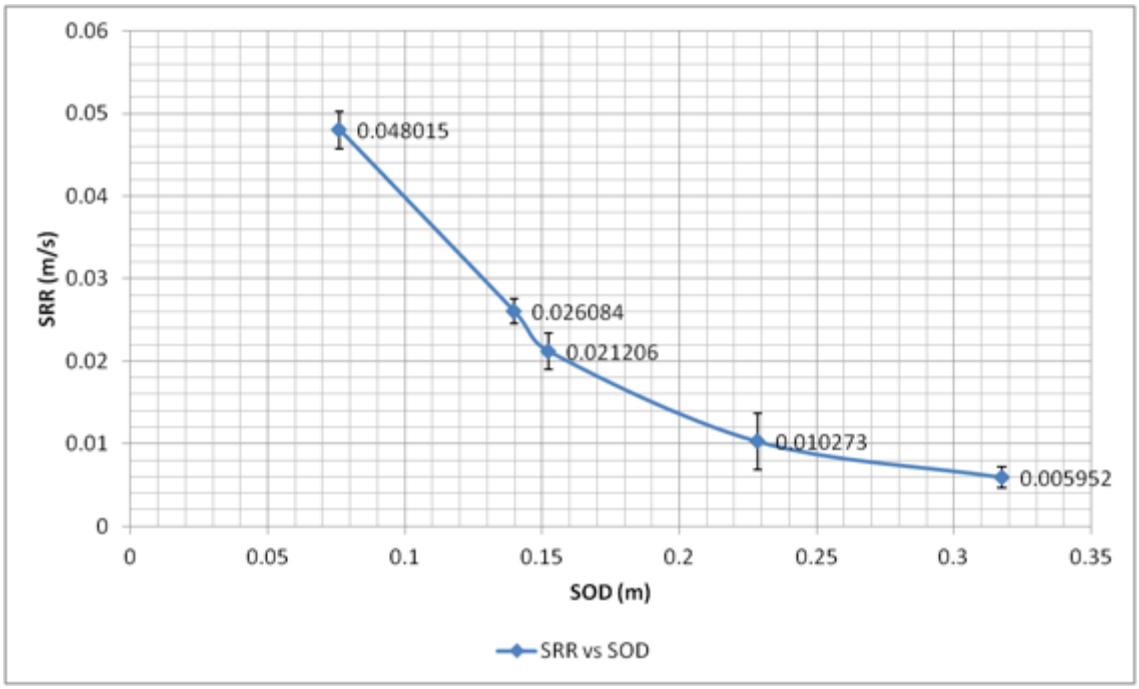

Figure 3.6: Effect of SOD on Sand Removal Rate

From Figure 3.6, the exceptionally strong effect of the standoff distance is evident. The sand removal rate gets significantly faster with lower standoff distances. These result also suggest that using a lower standoff distance is an effective way to increase the jet cutting power, instead of working with high pressures and flow rates, which is more costly. Table 3.2 shows the sand removal rate results of the various standoff distances including the standard deviation of calculated from the repeated tests.

Table 3.2: Results of the 'SRR vs SOD' Tests

SOD (m)	SRR (m/s)	StDev	Variation
0.0762	0.048015	0.002228	4.64%
0.1397	0.026084	0.001516	5.81%
0.1524	0.021206	0.002188	10.32%
0.2286	0.010273	0.003435	33.44%
0.3175	0.005952	0.001305	21.92%

It can be noticed from Table 3.2 that greater variation values in between repetitions were found for the larger standoff distances. This suggests that incoherent flow patterns caused by large standoff distances affect the rate of sand removal.

3.5 EFFECT OF WATERJET MOMENTUM

The momentum of the waterjet is a critically important parameter as it promotes faster penetration through the sand mould and increases the rate of sand removal. Lower waterjet momentums will increase the time of sand removal due to low impinging energy at the mold surface. Waterjet velocity and mass flow rate directly affect the momentum of the waterjet. The orifice size determines the maximum mass flow rate and maximum velocity that the waterjet can reach at a given pressure. Equation 3.1 shows the formula of pressure and flow rate provided by the nozzle manufacturer and equation 3.2 shows how waterjet momentum is calculated.

$$\frac{\dot{Q}_1}{\dot{Q}_2} = \left(\frac{P_1}{P_2}\right)^{0.5} \qquad \textbf{(3.1)}$$

Where $\dot{Q}_1$ *and* $\dot{Q}_2$ *are the Volumetric Flow Rate (m³/s)* and P_1 *and* P_2 *are the Waterjet Pressure (Pa).*

$$WJM = \rho \times \dot{Q} \times V = \dot{m} \times V \qquad \textbf{(3.2)}$$

Where *WJM* is the *Waterjet Momentum (kg.m/s²)*, ρ is the *Density of the water (kg/m³)*, $\dot{Q}$ is the *Volumetric Flow Rate (m³/s)*, $\dot{m}$ is the *Mass Flow Rate (kg/s)*, and V is the *Waterjet Velocity (m/s).*

Typically, in this type of material removal studies, the effects of all these four parameters are investigated. However, the interaction of these parameters always results in a momentum value. In this study, it was assumed that the waterjet momentum determines the rate of sand removal no matter what the interaction between pressure, nozzle orifice size, mass flow rate and velocity is. An experiment was conducted to confirm this assumption. An equivalent waterjet momentum value was

obtained using two different values of pressures, nozzle sizes, flow rates and velocities. Table 3.3 shows the used test conditions. The rate of sand removal of these two cases was compared.

Table 3.3: Equivalent waterjet momentum of two different cases

Nozzle Type	Pressure (kPa)	Spray Angle (°)	Diameter (mm)	Flow Rate (m^3/s)	Orifice Area (m^2)	Velocity (m/s)	Momentum ($kg.m/s^2$)	Flow Type
F5008	544.7	55	1.803	7.07E-05	2.55E-06	27.677	1.956	Turbulent
F5020	210.3	47	2.845	1.12E-04	6.35E-06	17.548	1.956	Turbulent

Each test was repeated three times and then the average was taken. The sand removal data is plotted in Figure 3.7.

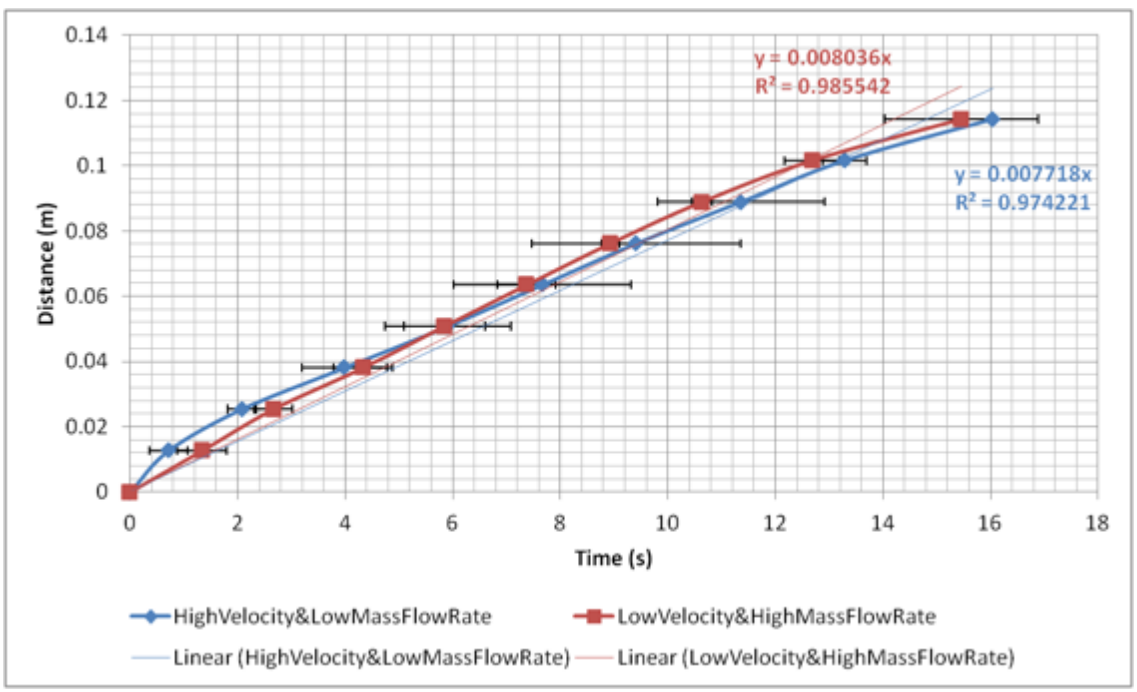

Figure 3.7: Equivalent Waterjet Momentum Sand Removal Rates

It is apparent from Figure 3.7 that the sand removal rate of a 'LowVelocity-HighMassFlowRate' jet is about 4% faster. This was expected because the spray angle at 210 kPa is narrower which results in a smaller coverage area on the sand mold. It is evident that the two cases of equivalent waterjet momentum resulted in almost the

same removal rate. Although, the effect of pressure, nozzle size, flow rate and velocity could be investigated individually, this result confirmed that as long as these four parameters correspond to the same momentum value, the sand removal rate will be almost the same.

In order to investigate the effect of waterjet momentum, tests were conducted with a wide range of waterjet momentum, between 1.336 kg.m/s² and 16.460 kg.m/s², with eleven data points. The standoff distance was kept constant at 13.97cm during these tests and the water at ambient conditions was used. A single nozzle was used and the nozzle type was changed after each set of experiment in order to alter the waterjet momentum. Each set of experiments was repeated three times and the average was taken. The details of parameters used in each experiments are provided in Table 2.2. Figure 3.6 illustrates the distance travelled by the waterjet through the sand over time.

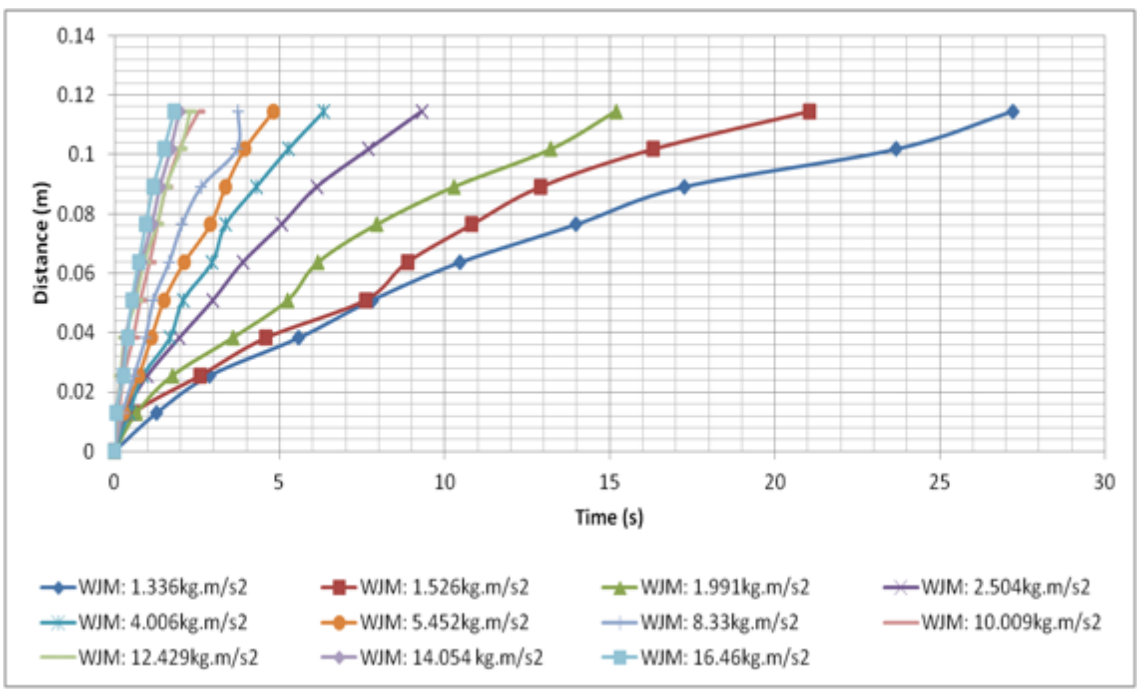

Figure 3.8: Effect of WJM on sand removal time

It is evident from Figure 3.8 that the waterjet momentum has a significant effect on the sand removal time and the removal behaviour. The time of removal of a 12.7 cm thick

sand mould varied between 2 second and 27 second, depending on the waterjet momentum. For the waterjet momentums lower than 4.006 kg.m/s² the removal behaviour seemed non-linear. As the distance away from the nozzle exit gets larger the waterjet loses its impact energy. Considering the fact that the initial momentum was already low for these cases, the penetration starts to decelerate resulting in ineffective removal. The relationship between the waterjet momentum and the rate of sand removal is illustrated in Figure 3.9.

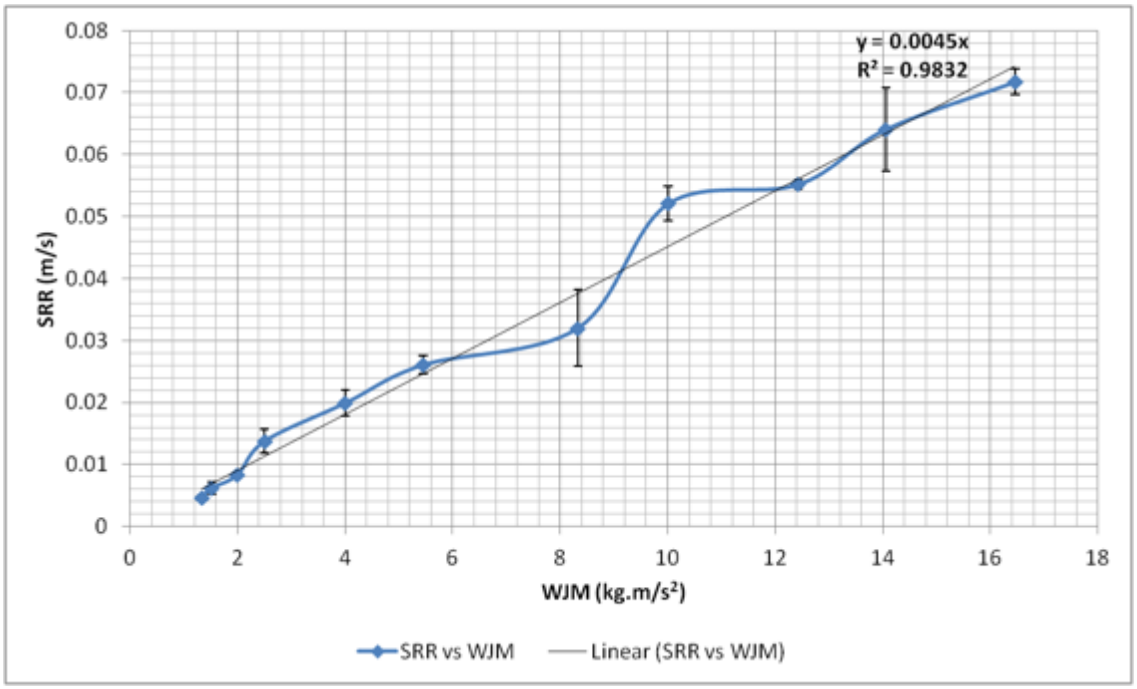

Figure 3.9: Effect of WJM on Sand Removal

In the sand removal process, increasing the waterjet momentum is an effective method of increasing the rate of removal. Figure 3.9 shows a typical trend of the effect of the waterjet momentum on the rate of sand removal. The trend is almost linear and results with an R^2 value of 0.98. It is obvious that the capability of the waterjet to achieve a higher rate of sand removal increases with an increase in its momentum. Table 3.4 shows the sand removal rate results of various waterjet momentums including standard deviation of repetitions.

Table 3.4: Results of 'SRR vs. WJM' Tests

WJM (kg.m/s²)	SRR (m/s)	StDev	Variation
1.336	0.004729	0.0003316	7.01%
1.526	0.006251	0.0010241	16.38%
1.991	0.008305	0.0003878	4.67%
2.504	0.013792	0.0019805	14.36%
4.006	0.019941	0.0021049	10.56%
5.452	0.026084	0.0015157	5.81%
8.33	0.032033	0.0062267	19.44%
10.009	0.052125	0.0028110	5.39%
12.429	0.055212	0.0007904	1.43%
14.054	0.064108	0.0066857	10.43%
16.46	0.071764	0.0020470	2.85%

According to Table 3.4 the maximum variation between repetitions is within 19.4%.

3.6 Effect of Overlapping of Multijets

Flat fan shape nozzles produce a non-uniform spray pattern. The velocity of the waterjet is maximum at the center of the pattern and it gradually decreases towards the edges. Employing multijets and having them overlapped can compensate this difference. The objective of this section is to determine the correct percentage of overlapping where this velocity difference between the centerline of the waterjet and the edge disappears. Multijets were utilized in order to produce a uniform sand removal pattern along the mould surface and it is not expected for their overlapping percentage to have a significant effect on the rate of sand removal. The locations at which the sand removal rate was calculated in this experiments, is shown in Figure 3.10

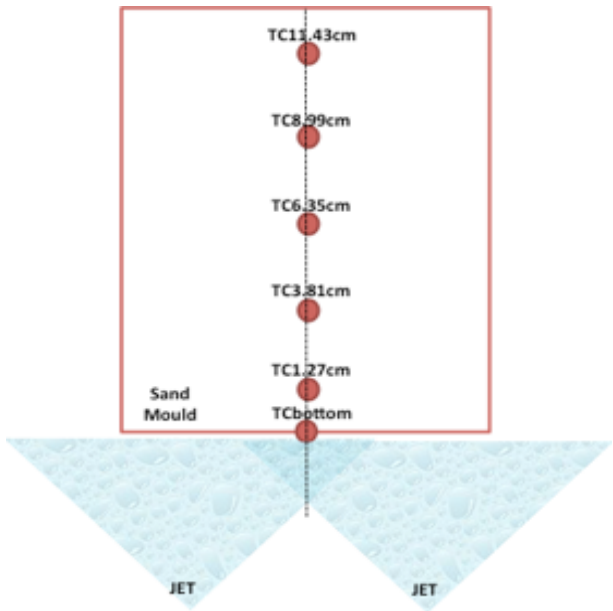

Figure 3.10: Schematic to show at what location the sand removal rate is calculated

An experiment was conducted to examine the difference in the rate of sand removal at various locations along the spray pattern. In addition to the embedded thermocouples at the centerline, two more rows of thermocouples were added at to the right 2.54cm right and to the left from the nozzle centerline. Figure 3.11 shows the basic schematic of this experiment.

A F5020 type nozzle providing 5.018 kg.m/s^2 waterjet momentum at 15.24cm standoff distance was used in this experiment. The water temperature was kept at ambient conditions. The experiment was repeated twice and the average was taken.

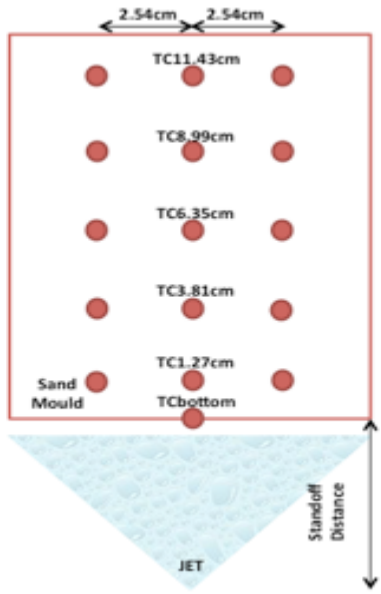

Figure 3.11: Locations of the thermocouples used to examine the difference in sand removal rate along the spray pattern of one nozzle

Figure 3.12 shows the rate of sand removal at various locations in the mould over time at different locations in the sand mould.

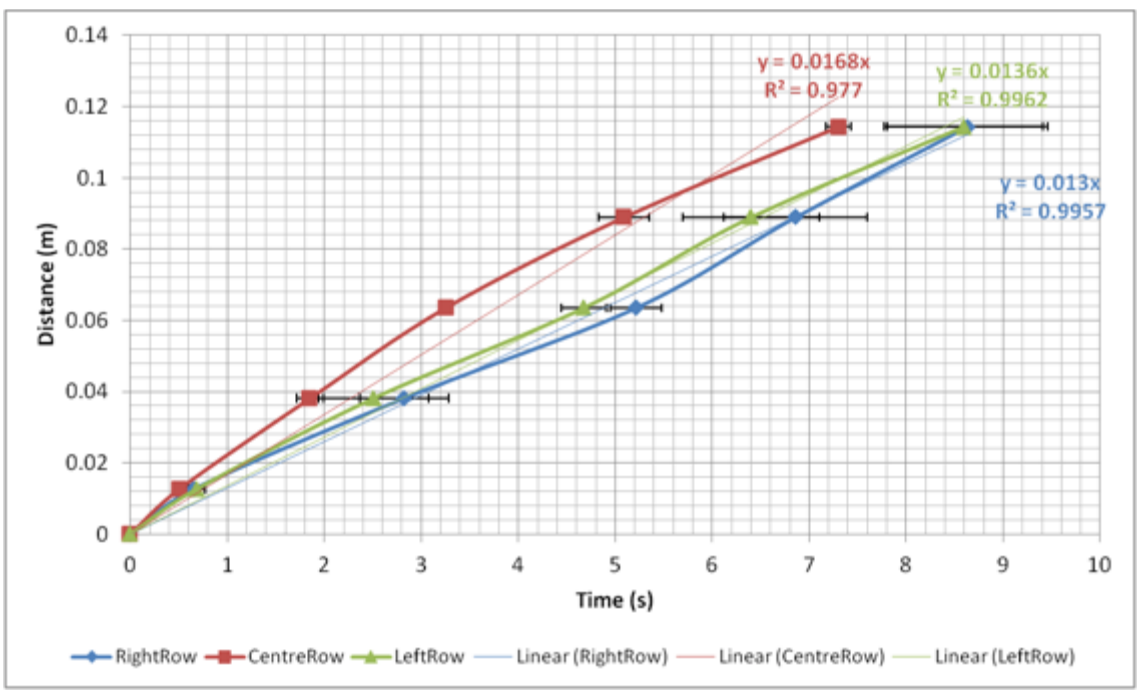

Figure 3.12: The rate of sand removal at various locations in the sand mould

It is evident from Figure 3.12 that the rate of sand removal at the centre of the spray pattern is about 30% higher than at the edges. The thermocouples, which were

embedded on the right and the left rows, gave the same rate of sand removal, as expected. These results show how much the velocity difference within the spray pattern affects the sand removal rate. The need for multijets overlapping to compensate for this difference is clear.

The overlapping percentage was defined as the ratio between the coverage of the overlapping area to the full coverage of a single jet as shown in Figure 2.7.b. In this study, it was assumed that compensating the sand removal rate difference between the overlap area of the two jets and center portion of a single jet would increase the uniformity of the removal process along the length of the sand mould. Tests were carried out to identify the required overlapping percentage to create this uniform removal pattern. Two nozzles (F5020) providing 5.018 kg.m/s^2 momentum each were used. The overlapping was varied between 0% and 30%, with 5% increments. Water temperature was ambient and the standoff distance was fixed at 13.97cm. Each test was repeated two times and the average was taken.

Figure 3.13 shows the effect of the overlapping ratio (OP) on the sand removal time.

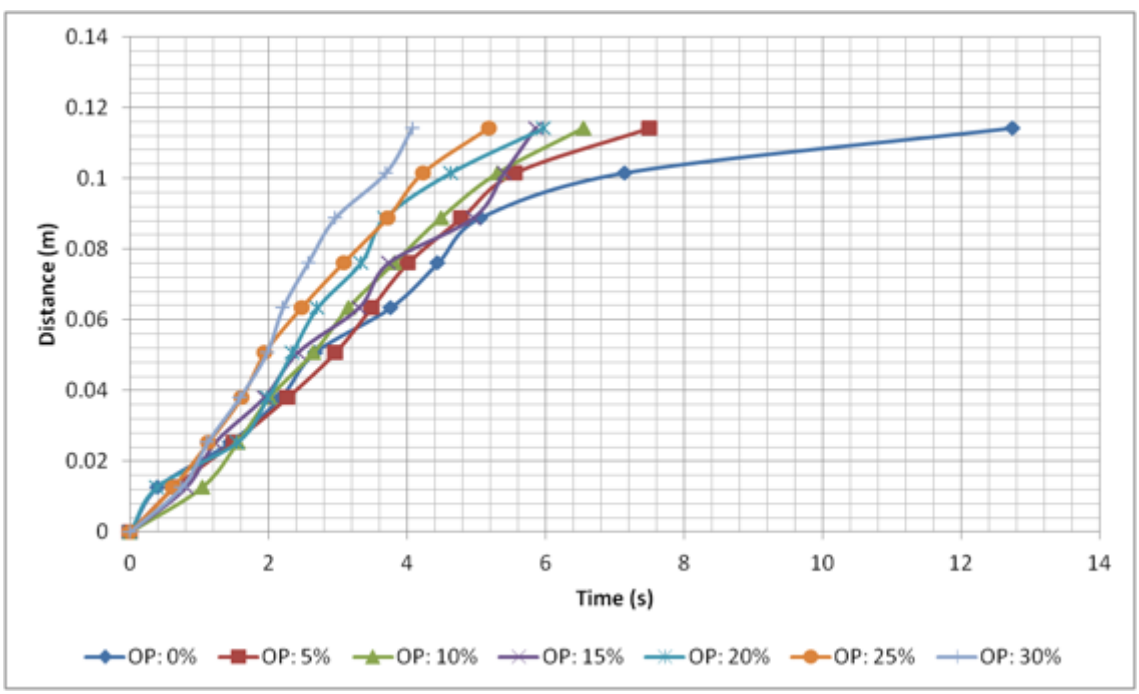

Figure 3.13: Effect of overlapping ratio on time of sand removal

From

Figure 3.13 it can be noticed that increasing the overlapping ratio reduces the time taken to penetrate through the 12.7cm thickness. The effect of overlapping percentage on the rate of sand removal is presented in

Figure 3.14.

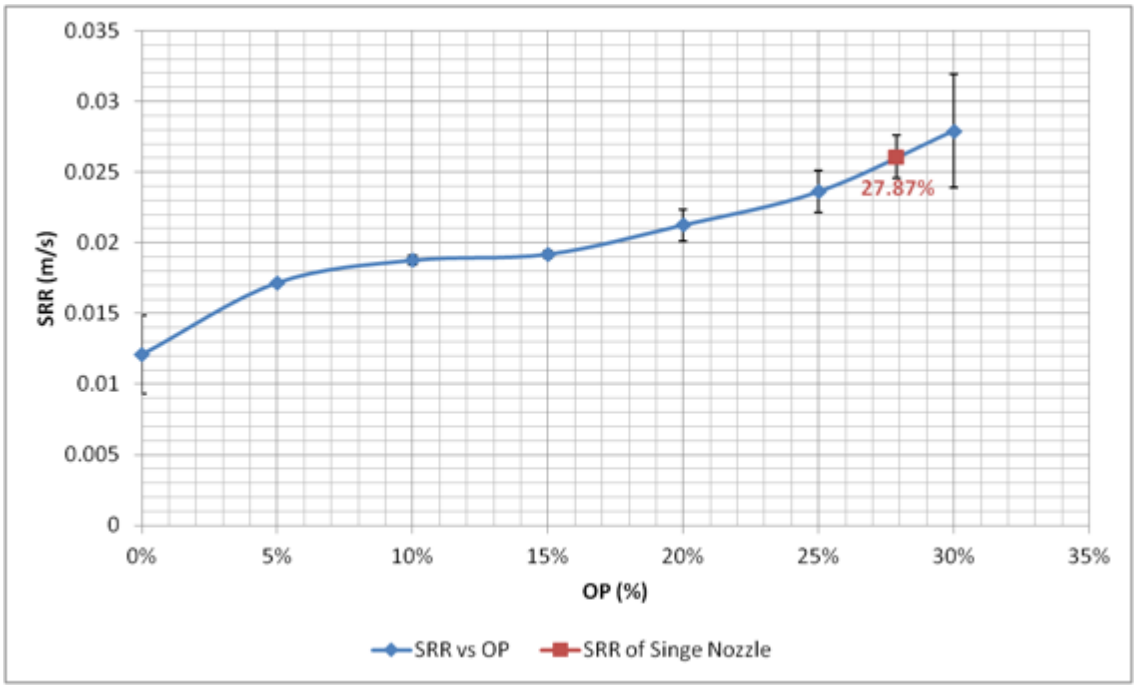

Figure 3.14: Effect of overlapping ratio on sand removal rate

Based on the results shown in

Figure 3.14, the trend is clear as anticipated the impact of overlapping increases as the percentage increases. The sand removal rate of the identical single nozzle (F5020) at the centerline of the spray pattern was calculated in the previous section. The rate of sand removal achieved using multijets equals to the removal rate of a single jet at 27.87% overlapping. Considering that the single nozzle (F5020) had 5.81% variation in sand removal rate, the overlapping percentage that gives the same rate is 26.11% minimum and 29.63% maximum. The overlapping percentage of multijets in this range will

provide uniform removal along the sand mould. Table 3.5 shows the results of the sand removal rate obtained at various overlapping ratios including the standard deviation of the repetitions.

Table 3.5: Results of 'SRR vs. OP' Tests

OP (%)	SRR (m/s)	StDev	Variation (%)
0%	0.012095	0.002766	22.87%
5%	0.017165	0.000148	0.86%
10%	0.018753	0.000332	1.77%
15%	0.019179	0.000258	1.35%
20%	0.021245	0.001107	5.21%
25%	0.02361	0.001491	6.32%
30%	0.02792	0.003987	14.28%

According to Table 3.5 two extreme data points, 0% overlapping and 30% overlapping, have 22.87% and 14.28% variation respectively. The repetitions of the other data points spread out close to each other and resulted in small variances.

3.7 Empirical Model of Sand Removal Rate

After investigating the effect of waterjet parameters on the rate of sand removal, these results were correlated and through a linear regression analysis an empirical model that is able to estimate the time of removal for given sand mould thickness was developed. The process input variables for this model are: The Standoff Distance (SOD), The Waterjet Momentum (WJM), and The Overlapping Percentage of Multijets (OP). The output of the model is the Sand Removal Rate (SRR). The statistics of the regression analysis is listed in Table 3.6.

Table 3.6: Statistics of the Linear Regression Analysis

Regression Statistics	
Multiple R	0.984661192
R Square	0.969557663

Adjusted R Square	0.964185486
Standard Error	0.149059561
Observations	21

The regression analysis resulted in a multiple correlation coefficient and R^2 value of 0.98 and 0.97 respectively. A standard error value of 0.15 was obtained through 21 observations (5 standoff distances, 10 waterjet momentums, 6 overlapping percentages). The predictive model correlating the rate of sand removal with waterjet process parameters is given by the Equation (3.3).

$$SRR = 0.0002 \times SOD^{-1.516} \times WJM^{1.036} \times (1 - OP)^{-0.327} \qquad \textbf{(3.3)}$$

The sand removal time can be calculated from Equation (3.4).

$$t = 4989.6 \times \Delta MT \times SOD^{1.516} \times WJM^{-1.036} \times (1 - OP)^{0.327} \qquad \textbf{(3.4)}$$

Where *SRR* is the *Sand Removal Rate (m/s)*, *SOD* is the *Standoff Distance (m)*, *WJM* is the *Waterjet Momentum (kg.m/s²)*, *OP* is the *Overlapping Percentage of Multijets (%)*, *t* is the *Time (s)*, and *ΔMT* is the *Sand Mould Thickness (m).*

According to equation (3.3), the standoff distance has the highest exponent and it is clearly the most significant parameter. The effect of waterjet momentum on the rate of removal was found almost linear. The exponent of the overlapping percentage shows that its effect is the least.

Using equation (3.3) and equation (3.4), the waterjet input variables can be configured to achieve the desired time of removal for a given sand mould thickness or the time of removal for given operating conditions can be estimated. This will allow adjusting the spraying system prior to the impingement of the waterjet on solidifying metal surface

and surface defects can be avoided while maximizing the effect of cooling on the microstructure.

The test cases for the experimental results were used as the input variable conditions and with the aid of Equation (3.3) the rate of sand removal for each case was calculated. Figure 3.15 illustrates the comparison of the predicted values to the experimental results.

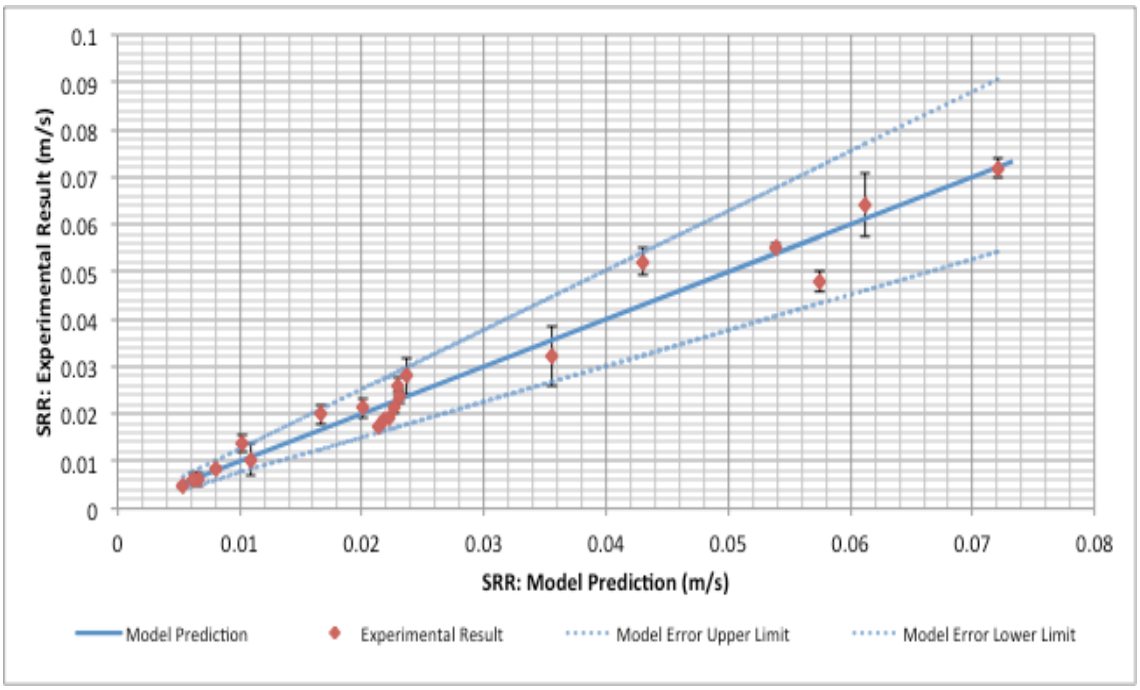

Figure 3.15: SRR: Experimental Results vs. Model Prediction

The maximum difference between the predicted and measured SRR was within +25.7% and –24.7%. These values were used to identify the upper and lower limits of the model prediction. It is evident from

Figure 3.15 the experimental results are nicely spread out around the model prediction and model error limits. In subsection (3.9.5), the effect of instrumental measurement errors on SRR is presented and according to Table 3.11, the maximum error in measuring SRR is within ±14.51%. This could be an explanation of the overshooting and undershooting numbers of +25.7% and –24.7%. In addition to that, even though the sand moulds were prepared with the same exact procedure, one cannot expect for the

sand moulds to be identically the same. This should be also taken into consideration when evaluating the overshoot and undershoot limits of the developed model.

The range of the model validity is as follows:

Standoff Distance: from 7.62cm to 31.75cm
Waterjet momentum: from 1.336 kg.m/s^2 to 16.46 kg.m/s^2
Overlapping Percentage of Multijets: from 5% to 30%.
Sand Mould Thickness: up to 11.43cm
Sand Mould Properties after curing: Density: 1432 kg/m^3 ± 45
Green Hardness: 94.1 ± 3.8 (B Scale)

Other than the range of model validity, it should be noted that this model was developed with waterjets positioned underneath the sand mould providing upward flow. The model would not be valid for downward removal as the water accumulates on the sand mould during the removal process. In the case of downward removal, the accumulation would affect the rate of sand removal and hence the model prediction might be incorrect.

The one and only problem with the developed model is the fact that it is limited to a specific sand type and a water-soluble binder system. If the sand moulds are not prepared with the explained procedure the model might not be able to predict time of removal correctly. In the next section an alternative mechanistic model to overcome this issue is explained.

3.8 A Mechanistic Model of Sand Removal Using an Impinging Waterjet

In machining processes the specific energy is defined, as the required energy input to machine the desired amount of material and it is assumed proportional to the energy

imput of the machining application. In the case of using a waterjet the energy input is the kinetic energy of the waterjet. Equation (3.5) shows a mechanistic relationship between the material removal rate, the specific energy of the material and the kinetic energy of the waterjet.

$$MRR = \frac{1}{u} \times \frac{1}{2} \dot{m} V^2 \qquad \textbf{(3.5)}$$

Where MRR is the *Material Removal Rate (m³/s)*, u is the *specific energy requirement of the material (m³/J)*, $\dot{m}$ is the *Mass Flow Rate (kg/s)*, and V is the *Waterjet Velocity (m/s)*.

Using equation (3.5) the specific energy of the sand mould can be found by inserting the waterjet parameters and the measured material removal rate. However it is worth noting here that the MRR is the volumetric material removal rate. Determining the exact volume of sand removal based on the thermocouple readings is not possible. The best way to calculate the amount of sand volume removed is by monitoring the removal process using a high-speed camera. However in this study the exact depth of cut was obtained using thermocouple readings explained before. In order to obtain the volumetric rate the following assumptions were made. A uniform cut pattern was assumed along the length of the sand mould. The second assumption was in the width of the cutting kerf. The entrance width of 3.175cm and the exit width of 1.905cm were observed. The kerf ratio, which is defined as the entrance width divided by the exit width, in this case is, 1.667. However, it is known that depending on the standoff distance and the size of the nozzle orifice, the entrance and exit widths change and the ratio might change as well. Two cases where evaluated before making an assumption on the width of the cutting kerf. In the first case it was assumed that the cutting kerf had a constant width along the height of the mould and the dimension of it was assumed equal to the average of the width at the bottom and the top (2.54cm). In the second case, a gradual decrease from 3.175cm to 1.905cm in the width along the height of the sand mould was assumed. These two assumptions are illustrated in Figure 3.16.

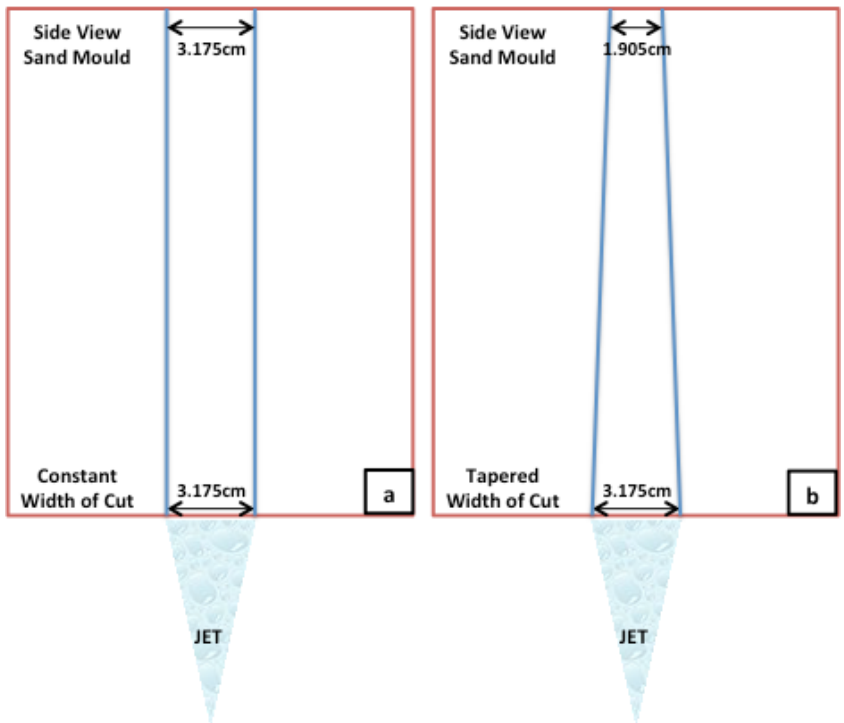

Figure 3.16: a. Constant width of cut, b. Tapered width of cut.

The comparison of these assumptions is illustrated in

Figure 3.17.

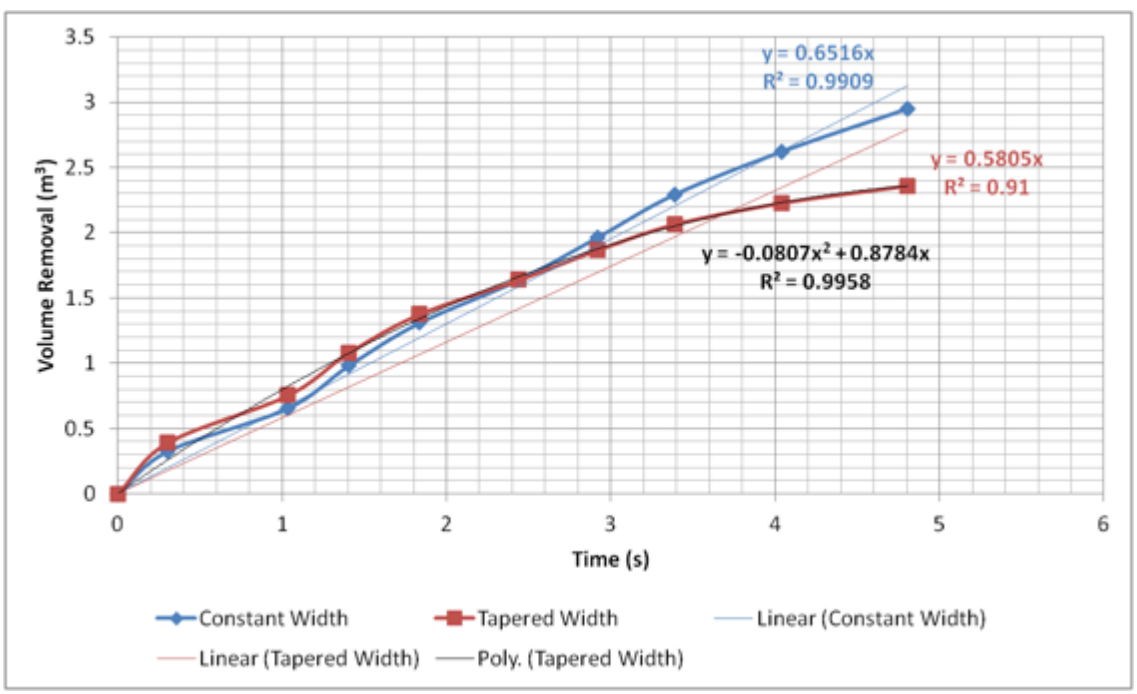

Figure 3.17: Volumetric removal rate calculated based on the constant width vs. the tapered width assumptions

According to
Figure 3.17, if a constant width is assumed the material removal rate will be 12.25% faster than the rate of the case where tapered width is assumed. It is clear that assuming constant removal would not only be contradicting with reality but also would reveal misleading results. This result is in agreement with what was reported in literature by Paul et. al.[34] as opposed to Hashish's work[32]. If a model is based on the assumption that the cutting width does not have any variation, the accuracy of that model in predicting the material removal rate will be negatively affected.

For this reason in this study the tapered width assumption (entrance: 3.715cm, exit: 1.905cm) was used for each and every experiment. Additionally it is apparent from
Figure 3.17 that the removal behaviour in tapered width case gives a much better fit for a polynomial curve. Nonetheless, in order to simplify the study, the rate of removal was taken from the linear curve fit.

A dimensionless standoff distance factor was introduced to Equation (3.5) in order to take the effect of standoff distance into account. With the aid of the data plotted in Figure 3.18, the exponent of this factor was determined and the formula took the form presented in Equation (3.6).

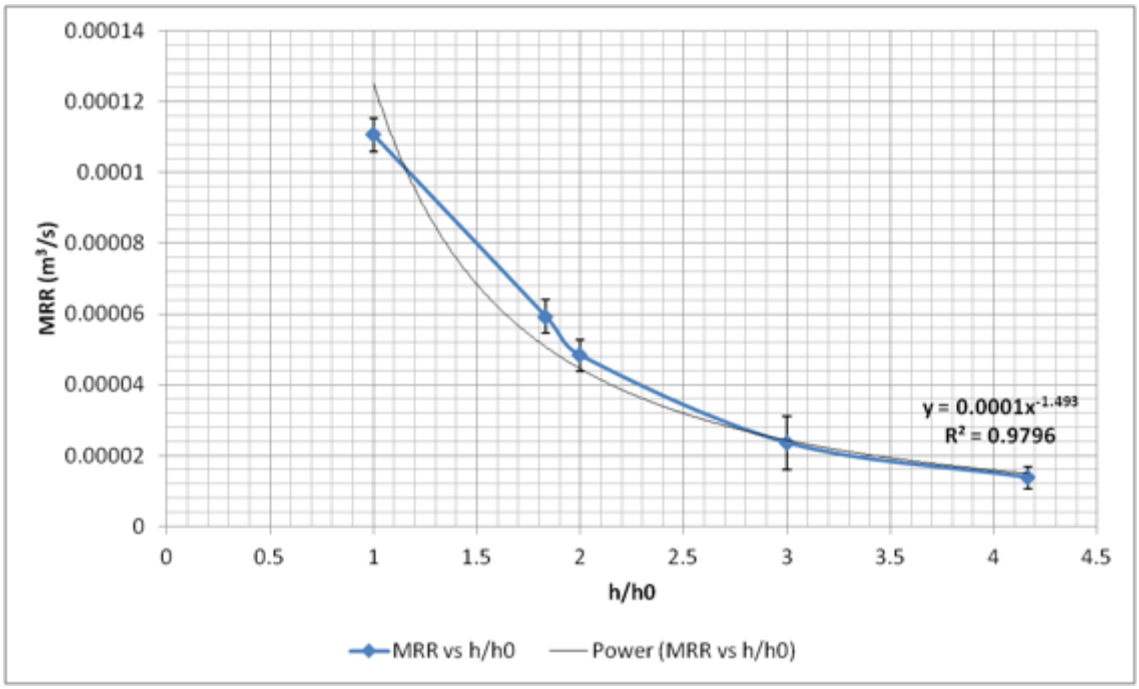

Figure 3.18: Material Removal Rate vs. Dimensionless Standoff Distance Factor

Power function curve fit of the data revealed the exponent value of the dimensionless standoff distance factor and the equation took the following form:

$$MRR = \frac{1}{u} \times \left(\frac{h}{h_0}\right)^{-1.493} \times \frac{1}{2}\rho A V^3 \qquad \textbf{(3.6)}$$

Where MRR is the Material Removal Rate (m^3/s), u is the specific energy requirement of the material (m^3/J), h is the Standoff Distance (m), h_0 is the lowest tested standoff distance (m), ρ is the density of the water (kg/m^3), A is the area of the nozzle orifice (m^2), and V is the Waterjet Velocity (m/s).

The specific energy of the sand mould was calculated by using Equation (3.6). The conditions of the waterjet momentum tests presented in the previous section were used. After inputting the process variables as the energy term on the right hand side and the

corresponding results on the left hand side of the equation, the slope of the linear curve fit was taken to reveal the $\frac{1}{u}$ term. The plotted data is illustrated in

Figure 3.19.

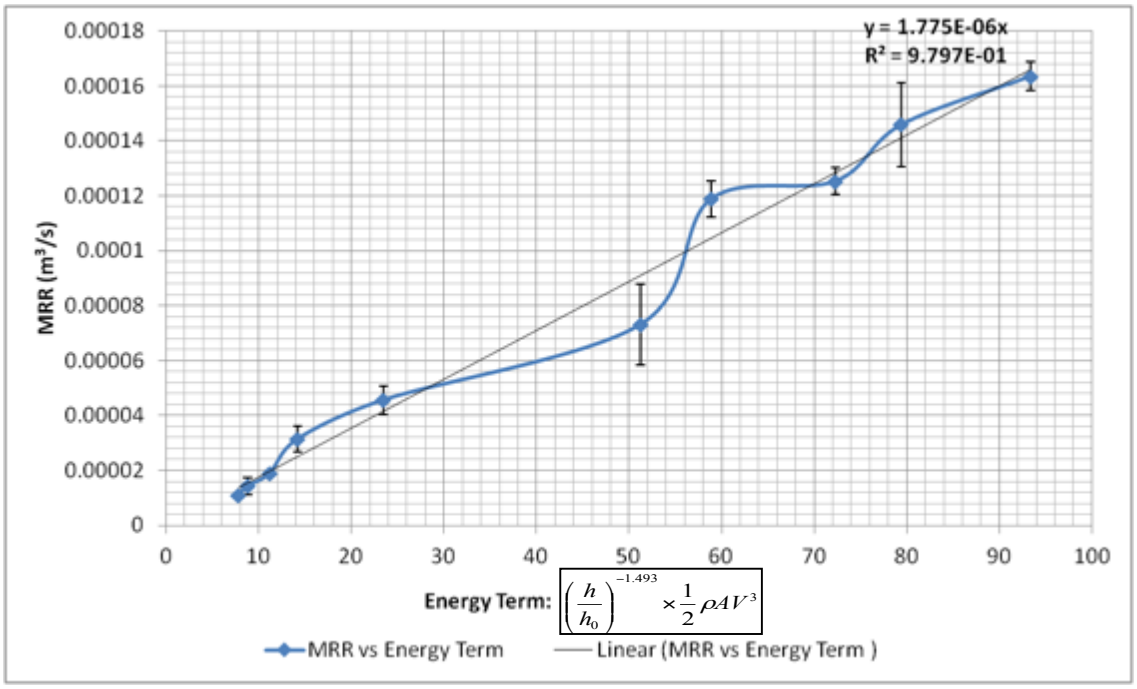

Figure 3.19: Slope of the graph reveals the specific energy value

From

Figure 3.19 the u value was found as $\frac{1}{1.775E-06} = 563349 m^3/J$. It is clear that this value is not the same for every set of experiments. In order to find the range of the specific energy, the slope was recalculated for the lowest three and the highest three energy inputs. As expected for the three lowest energy inputs, a higher specific energy of $625900 m^3/J$ was found. However for the three highest energy inputs it stayed close to the original value and was found as $564270 m^3/J$.

It should be noted that the specific energy used in this study differs from the specific energy used in machining operations, due to the fact that the sand mould includes a

water-soluble binding agent. For this reason, the removal is not purely mechanical as in machining operations. In this study, the specific energy depends on the chemical bonds and the breaking of these bonds by water at the microscopic level. This makes the specific energy a more complex function in terms of the initiation of penetration through the material.

After obtaining the value of the specific energy for the sand mould, as the final step the entire experimental data was used in Equation (3.6) along with the corresponding material removal rates in order to predict the material removal rate. Figure 3.20 illustrates the comparison of the predicted values and the experimental results.

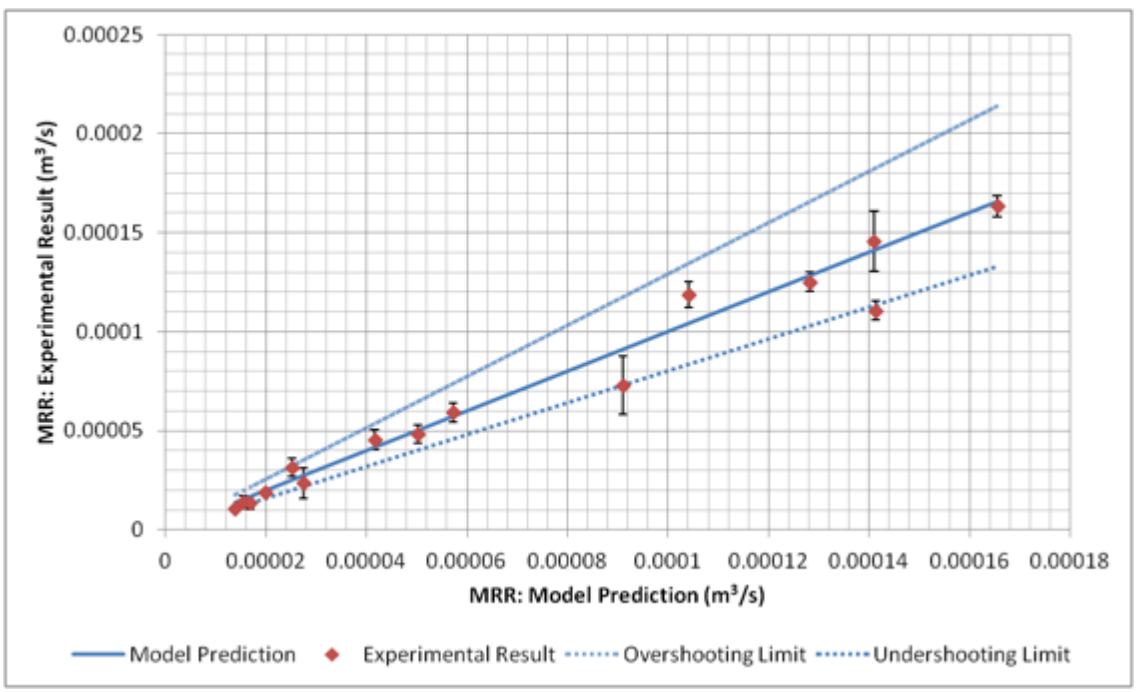

Figure 3.20: MRR: Experimental Results vs. Model Prediction

It is apparent from Figure 3.20 that the experimental data is nicely spread out around the model prediction. The prediction of the model has a maximum overshooting and undershooting values of 29.1% and 19.7% respectively. The overshooting and undershooting limits were determined by calculating the difference between the model prediction and the experimental results. In Table 3.7 the details of each test condition

and both experimental and model prediction results are presented including the variation of the experiments and the difference between the prediction and the experimental result.

Table 3.7: Details of the Tests Conditions and Material Removal Rate Results

Nozzle Type	Orifice Area (m^2)	Velocity (m/s)	h/h_0	MRR: Experimental (m^3/s)	Variation of Tests (%)	MRR: Model (m^3/s)	Difference (%)
F5005	1.588E-06	28.998	1.833	1.074E-05	6.57%	1.387E-05	29.09%
F5006	1.885E-06	28.457	1.833	1.426E-05	21.24%	1.555E-05	9.01%
F5008	2.553E-06	27.924	1.833	1.893E-05	6.17%	1.990E-05	5.13%
F5010	3.161E-06	28.144	1.833	3.142E-05	14.67%	2.523E-05	-19.71%*
F5015	4.765E-06	28.995	1.833	4.559E-05	11.26%	4.159E-05	-8.78%
F5030	8.959E-06	30.494	1.833	7.308E-05	20.21%	9.096E-05	24.47%
F5040	1.186E-05	29.056	1.833	1.188E-04	5.44%	1.041E-04	-12.32%*
F5050	1.498E-05	28.802	1.833	1.252E-04	3.88%	1.282E-04	2.37%
F5060	1.790E-05	28.02	1.833	1.458E-04	10.49%	1.410E-04	-3.29%*
F5070	2.087E-05	28.083	1.833	1.634E-04	3.17%	1.655E-04	1.30%
F5020	6.353E-06	29.296	1.000	1.107E-04	4.35%	1.413E-04	27.74%
F5020	6.353E-06	29.296	1.833	5.926E-05	7.93%	5.719E-05	-3.49%*
F5020	6.353E-06	29.296	2.000	4.831E-05	9.36%	5.023E-05	3.98%
F5020	6.353E-06	29.296	3.000	2.356E-05	32.23%	2.742E-05	16.41%
F5020	6.353E-06	29.296	4.167	1.372E-05	22.76%	1.679E-05	22.39%

*Minus sign indicates the undershooting

From Table 10 it can be noticed that the model is tend to overshoot. Two extremes of the dimensionless standoff distance factor, 1 and 4.167 resulted in the high overshooting numbers (27.74% and 22.39% respectively) along with the lowest extreme of the energy term (29.09%). This can be explained by the change in specific energy depending on the operating conditions. As mentioned earlier, there is a range for the specific energy. Therefore, the occurrence of the maximum overshoot and undershoot of the model at extreme points is expected. The undershooting seems to occur rather randomly and since its value is not greater than 20%, it is considered satisfactory. In subsection (3.9.4), the effect of instrumental measurement errors on MRR was presented and according to Table 3.10, the maximum error in measuring MRR is within ±5.85%. This is also a

contributor to undershoot and overshoot limits of the model along with the possible inconsistencies in the sand moulds used in the experiments.

After introducing the material property of specific energy and correlated to the waterjet process parameters to the removal rate of the material, the developed mechanistic model is capable of predicting the time for various water soluble sand binder systems. If someone wants to use the proposed model to estimate the time of sand removal all he needs to do is to carry out a single set of experiments and calculate the specific energy for the specific sand and water-soluble binder system he is using. Once this value is determined the developed model can be used to estimate the rate of material removal for a given set of process input variables.

3.9 Instrument Measurement Error Analysis

In this section, the effect of instrumental error on the calculated variables (Flow Rate, Waterjet Momentum, Sand Removal Rate, Material Removal Rate) is analyzed in order to determine the amount of error contributed by the instrument.

3.9.1 Effect of Thermocouple Measurement Error on the Sand Removal Rate

In this study, thermocouples were used to measure the sand removal rate by finding the time at which a rapid change in temperature occurs. However the measured temperature itself was not used in any calculations. Therefore the error involved in temperature readings was not relevant to this error analysis. The response time of thermocouples however was important. Takrouri [45] in his PhD thesis reported the response time of the thermocouples, which were identical to the ones used in this study, was found by to be 0.21 seconds in ambient temperature measurement conditions. Since all the thermocouples are delayed with this same response time, the rate of sand

removal is not affected by it. The two cases (measured and actual) are shown in Figure 3.21.

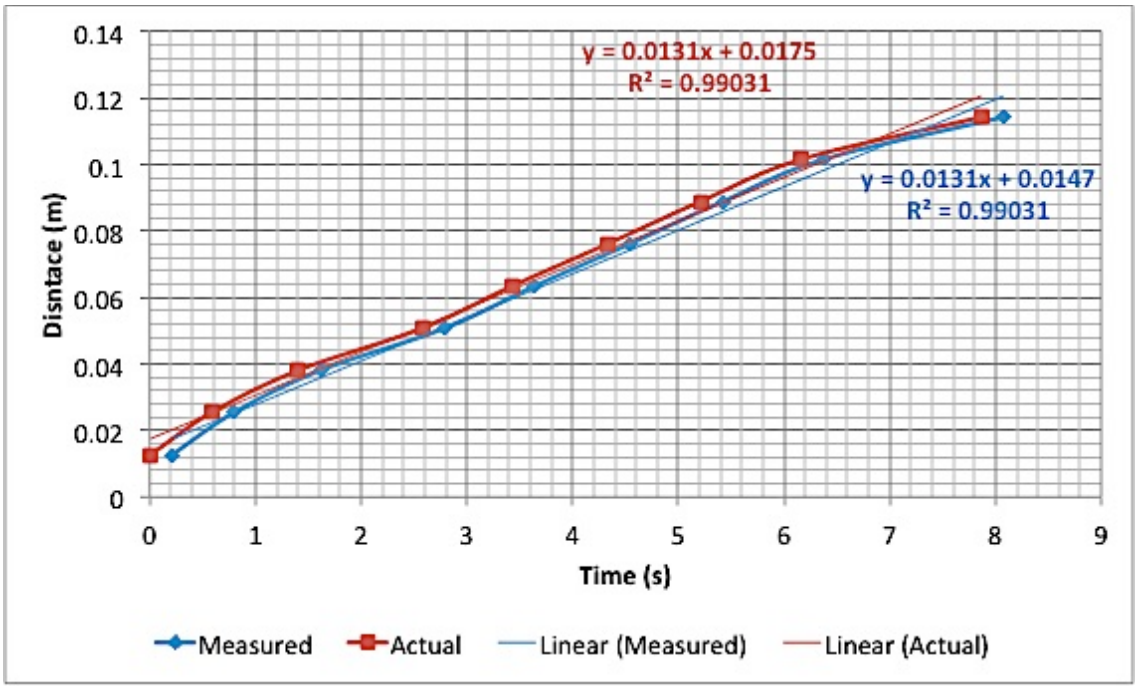

Figure 3.21: The rate of sand removal with (Measured) and without (Actual) thermocouple delay

It is evident from Figure 3.21, in the actual case, all points are just shifted by the response time and the sand removal times are parallel to the measured case. Therefore, the slopes of these two curves result in the same value, which is the same sand removal rate. For this reason the delay of thermocouples in response time can be ignored when calculating the rate of sand removal.

3.9.2. Effect of Pressure Measurement Error on Waterjet Momentum

Throughout this study, waterjet momentum is calculated through pressure readings. The pressure transducer used in the experiments has ±2% error as it is listed in Table 2.1.

The equation (3.7) shows how the error in the dependent variable (y) is calculated based on the error in the independent variables (x_1, $x_{2,..}$ x_n).

$$\Delta y = \sqrt{\left(\frac{\partial y}{\partial x_1}\right)^2 \times (\Delta x_1)^2 + \left(\frac{\partial y}{\partial x_2}\right)^2 \times (\Delta x_2)^2 ..... + \left(\frac{\partial y}{\partial x_n}\right)^2 \times (\Delta x_n)^2} \qquad \textbf{(3.7)}$$

In this subsection, the effect of the error in the pressure measurements (x_1) on the calculated waterjet momentum (y) is analyzed. The relationship between flow rate and pressure, and the relationship between flow rate and waterjet momentum were provided by the Equation (3.1) and (3.2), respectively.

From Equation (3.1), the relationship between flow rate and pressure can be expressed as follows:

$$\dot{Q} = \kappa \times \mathrm{P}^{0.5} \qquad \textbf{(3.8)}$$

Where: κ is a constant.

Substituting Equation (3.8) in Equation (3.2) results in Equation (3.9):

$$WJM(\mathrm{P}) = \frac{\rho}{A} \times \kappa^2 \times \mathrm{P} \qquad \textbf{(3.9)}$$

Deriving Equation (3.9) with respect to pressure reveals Equation (3.10):

$$\Delta WJM(\mathrm{P}) = \frac{\rho}{A} \times \kappa^2 \times \Delta \mathrm{P} \qquad \textbf{(3.10)}$$

Substituting the values of the parameters in Equation (3.10), gives the error in waterjet momentum, which is shown in Table 3.8.

Table 3.8: Effect of Pressure Measurement Error on Waterjet Momentum

Nozzle	Pressure (P)	Flow Rate (Q)	Orifice Area (A)	Momentum (WJM)	Constant (κ)	ΔWJM	**WJM Error %**

Type	(kPa)	(m^3/s)	(m^2)	($kg.m/s^2$)		($kg.m/s^2$)	
F5005	586.1	4.61E-05	1.59E-06	1.336	1.90E-06	4.57E-03	**0.34%**
F5006	551.6	5.36E-05	1.89E-06	1.526	2.28E-06	5.53E-03	**0.36%**
F5008	551.6	7.13E-05	2.55E-06	1.991	3.04E-06	7.25E-03	**0.36%**
F5010	551.6	8.90E-05	3.16E-06	2.504	3.79E-06	9.12E-03	**0.36%**
F5015	586.1	1.38E-04	4.77E-06	4.006	5.70E-06	1.37E-02	**0.34%**
F5020	586.1	1.86E-04	6.35E-06	5.452	7.68E-06	1.86E-02	**0.34%**
F5030	586.1	2.73E-04	8.96E-06	8.33	1.13E-05	2.85E-02	**0.34%**
F5040	517.1	3.45E-04	1.19E-05	10.009	1.52E-05	3.88E-02	**0.39%**
F5050	517.1	4.32E-04	1.50E-05	12.429	1.90E-05	4.83E-02	**0.39%**
F5060	482.7	5.02E-04	1.79E-05	14.054	2.28E-05	5.85E-02	**0.42%**
F5070	482.7	5.86E-04	2.09E-05	16.46	2.67E-05	6.83E-02	**0.41%**

According to Table 3.8, ±2% error in pressure measurements results in maximum error of ±0.42% in waterjet momentum.

3.9.3. Effect of Pressure Measurement Error on Material Removal Rate (MRR)

Similar to the previous section, the error caused by pressure in MRR is calculated.

Substituting the volumetric flow rate given by Equation (3.8) in Equation (3.6) results in the following:

$$MRR(P) = \frac{1}{2u} \times \left(\frac{h}{h_0}\right) \times \frac{\rho}{A^2} \times \kappa^3 \times P^{1.5} \qquad \textbf{(3.11)}$$

Deriving Equation (3.11) to calculate the error in MRR gives the following equation:

$$\Delta MRR(P) = \frac{1}{2u} \times \left(\frac{h}{h_0}\right) \times \frac{\rho}{A^2} \times \kappa^3 \times 1.5P^{0.5} \times \Delta P \qquad \textbf{(3.12)}$$

From this equation the error in the MRR is calculated and is shown in Table 3.9.

Table 3.9: Effect of pressure measurement error on material removal rate (MRR)

Nozzle Type	1/2u	h/h_0	Orifice Area (A) (m^2)	Constant (κ)	Pressure (P) (kPa)	MRR (m^3/s)	ΔMRR (m^3/s)	**MRR Error %**
F5005	8.88E-07	1.833	1.59E-06	1.90E-06	586.1	1.40E-05	7.16E-08	**0.51%**
F5006	8.88E-07	1.833	1.89E-06	2.28E-06	551.6	1.56E-05	8.49E-08	**0.54%**
F5008	8.88E-07	1.833	2.55E-06	3.04E-06	551.6	2.00E-05	1.09E-07	**0.54%**
F5010	8.88E-07	1.833	3.16E-06	3.79E-06	551.6	2.54E-05	1.38E-07	**0.54%**
F5015	8.88E-07	1.833	4.77E-06	5.70E-06	586.1	4.17E-05	2.13E-07	**0.51%**
F5020	8.88E-07	1.833	6.35E-06	7.68E-06	586.1	5.74E-05	2.94E-07	**0.51%**
F5030	8.88E-07	1.833	8.96E-06	1.13E-05	586.1	9.13E-05	4.67E-07	**0.51%**
F5040	8.88E-07	1.833	1.19E-05	1.52E-05	517.1	1.05E-04	6.10E-07	**0.58%**
F5050	8.88E-07	1.833	1.50E-05	1.90E-05	517.1	1.29E-04	7.51E-07	**0.58%**
F5060	8.88E-07	1.833	1.79E-05	2.28E-05	482.7	1.42E-04	8.84E-07	**0.62%**
F5070	8.88E-07	1.833	2.09E-05	2.67E-05	482.7	1.66E-04	1.03E-06	**0.62%**

According to Table 3.9, the material removal rate is not adversely affected by the error in pressure measurements, and the error is within ±0.62%.

3.9.4 Effect of Pressure and Ruler Measurement Errors on Material Removal Rate (MRR)

According to Equation (3.6), in MRR calculation, there are two variables (waterjet momentum and standoff distance) that can contribute to an error. In the previous subsection, how the pressure error translates to the error in waterjet momentum was discussed.

In this study, a ruler was used to measure the standoff distance. Typically, the error in a ruler measurement can be defined as one half of the smallest increment. The smallest increment of the ruler used in this study was 1/8th of an inch (0.32 cm) thus 1/16th of an inch (0.16 cm) was the estimated error.

Using the Equation (3.7),

Where y can be defined as MRR, x_1 is equal to h, and x_2 is equal to P.

Derivative of the function with respect to x_1 is as follows:

$$\frac{\partial y}{\partial x_1} = \frac{1}{2u} \times \frac{\rho}{A^2} \times \kappa^3 \times P^{1.5} \times \left(\frac{1}{h_0}\right)^{-1.493} \times \left(-1.493\right) \times h^{-2.493} \qquad \textbf{(3.13),}$$

and derivative of the function with respect to x_2 is as follows:

$$\frac{\partial y}{\partial x_2} = \frac{1}{2u} \times \frac{\rho}{A^2} \times \kappa^3 \times 1.5 \times P^{0.5} \qquad \textbf{(3.14)}$$

The error in MRR is calculated and shown in Table 3.10.

Table 3.10: Effect of Pressure Measurement and Standoff Distance Erros on Material Removal Rate (MRR)

Nozzle Type	1/2u	h/h_0	O. Area (A) (m^2)	Constant (κ)	Pressure (P) (kPa)	$\partial y/\partial x_1$	$\partial y/\partial x_2$	MRR m3/s	ΔMRR m3/s	%
F5005	8.9E-07	1.8	1.6E-06	1.9E-06	586	-1.5E-04	3.6E-08	1.4E-05	2.5E-07	**1.78%**
F5006	8.9E-07	1.8	1.9E-06	2.3E-06	552	-1.7E-04	4.2E-08	1.6E-05	2.8E-07	**1.79%**
F5008	8.9E-07	1.8	2.6E-06	3.0E-06	552	-2.1E-04	5.4E-08	2.0E-05	3.6E-07	**1.79%**
F5010	8.9E-07	1.8	3.2E-06	3.8E-06	552	-2.7E-04	6.9E-08	2.5E-05	4.6E-07	**1.79%**
F5015	8.9E-07	1.8	4.8E-06	5.7E-06	586	-4.5E-04	1.1E-07	4.2E-05	7.4E-07	**1.78%**
F5030	8.9E-07	1.8	9.0E-06	1.1E-05	586	-9.8E-04	2.3E-07	9.1E-05	1.6E-06	**1.78%**
F5040	8.9E-07	1.8	1.2E-05	1.5E-05	517	-1.1E-03	3.1E-07	1.1E-04	1.9E-06	**1.81%**
F5050	8.9E-07	1.8	1.5E-05	1.9E-05	517	-1.4E-03	3.8E-07	1.3E-04	2.3E-06	**1.81%**
F5060	8.9E-07	1.8	1.8E-05	2.3E-05	483	-1.5E-03	4.4E-07	1.4E-04	2.6E-06	**1.82%**
F5070	8.9E-07	1.8	2.1E-05	2.7E-05	483	-1.8E-03	5.2E-07	1.7E-04	3.0E-06	**1.82%**
F5020	8.9E-07	1.0	6.4E-06	7.7E-06	586	-6.1E-04	3.6E-07	1.4E-04	1.2E-06	**0.86%**
F5020	8.9E-07	1.8	6.4E-06	7.7E-06	586	-6.1E-04	1.5E-07	5.7E-05	1.0E-06	**1.78%**
F5020	8.9E-07	2.0	6.4E-06	7.7E-06	586	-6.1E-04	1.3E-07	5.0E-05	1.0E-06	**2.01%**
F5020	8.9E-07	3.0	6.4E-06	7.7E-06	586	-6.1E-04	7.0E-08	2.8E-05	9.9E-07	**3.60%**
F5020	8.9E-07	4.2	6.4E-06	7.7E-06	586	-6.1E-04	4.3E-08	1.7E-05	9.9E-07	**5.85%**

As shown in Table 3.10, the maximum error contributed by pressure and ruler measurements to the calculated rate of material removal is ±5.8%.

3.9.5 Effect of Pressure and Ruler Measurement Errors on Sand Removal Rate (SRR)

In this model, there are three independent variables (standoff distance (x_1), waterjet momentum (x_2) and overlapping percentage (x_3). The standoff distance and the overlapping percentage are measured using the ruler. The waterjet momentum is a function of the pressure as shown in Equation (3.9).

Using these three independent variables in Equation (3.7), the error in SRR is calculated and shown in Table 3.11.

Table 3.11: Effect of Pressure and Ruler Measurement Errors on Sand Removal Rate (SRR)

Nozzle Type	WJM (kgm/s²)	SOD (m)	OP'	∂SRR /∂WJM	∂SRR /∂SOD	∂SRR /∂OP	ΔWJM	ΔSOD	ΔOP	SRR (m/s)	ΔSRR (m/s)	**Error %**
F5005	1.34	0.14	1	4.1E-03	-5.8E-02	1.7E-03	1.6E-01	1.6E-03	2.6E-04	5.3E-03	6.5E-04	**12.33 %**
F5006	1.53	0.14	1	4.2E-03	-6.6E-02	2.0E-03	1.8E-01	1.6E-03	2.6E-04	6.1E-03	7.6E-04	**12.56 %**
F5008	1.99	0.14	1	4.2E-03	-8.8E-02	2.6E-03	2.3E-01	1.6E-03	2.6E-04	8.0E-03	9.7E-04	**12.08 %**
F5010	2.50	0.14	1	4.2E-03	-1.1E-01	3.3E-03	3.0E-01	1.6E-03	2.6E-04	1.0E-02	1.3E-03	**12.56 %**
F5015	4.01	0.14	1	4.3E-03	-1.8E-01	5.4E-03	4.7E-01	1.6E-03	2.6E-04	1.7E-02	2.1E-03	**12.15 %**
F5020	5.45	0.14	1	4.4E-03	-2.5E-01	7.5E-03	6.6E-01	1.6E-03	2.6E-04	2.4E-02	2.9E-03	**12.32 %**
F5030	8.33	0.14	1	4.4E-03	-3.9E-01	1.2E-02	1.1E+00	1.6E-03	2.6E-04	3.7E-02	4.8E-03	**12.99 %**
F5040	10.01	0.14	1	4.4E-03	-4.7E-01	1.4E-02	1.3E+00	1.6E-03	2.6E-04	4.5E-02	5.8E-03	**12.79 %**
F5050	12.43	0.14	1	4.5E-03	-5.8E-01	1.8E-02	1.5E+00	1.6E-03	2.6E-04	5.7E-02	7.0E-03	**12.28 %**
F5060	14.05	0.14	1	4.5E-03	-6.6E-01	2.0E-02	1.7E+00	1.6E-03	2.6E-04	6.5E-02	7.7E-03	**11.86 %**
F5070	16.46	0.14	1	4.5E-03	-7.8E-01	2.4E-02	1.8E+00	1.6E-03	2.6E-04	7.7E-02	8.5E-03	**11.05 %**
F5020	5.45	0.08	1	1.1E-02	-1.1E+00	1.9E-02	6.6E-01	1.6E-03	2.6E-04	5.1E-02	7.4E-03	**14.51 %**
F5020	5.45	0.23	1	2.1E-03	-7.2E-02	3.6E-03	6.6E-01	1.6E-03	2.6E-04	1.3E-02	1.4E-03	**10.91 %**
F5020	5.45	0.32	1	1.3E-03	-3.2E-02	2.2E-03	6.6E-01	1.6E-03	2.6E-04	8.2E-03	8.3E-04	**10.09 %**
F5020	5.02	0.14	0.95	4.4E-03	-2.3E-01	7.4E-03	6.1E-01	1.6E-03	2.6E-04	2.2E-02	2.7E-03	**12.45 %**
F5020	5.02	0.14	0.9	4.5E-03	-2.4E-01	7.9E-03	6.1E-01	1.6E-03	2.6E-04	2.2E-02	2.8E-03	**12.56 %**
F5020	5.02	0.14	0.85	4.6E-03	-2.4E-01	8.5E-03	6.1E-01	1.6E-03	2.6E-04	2.2E-02	2.8E-03	**12.67 %**
F5020	5.02	0.14	0.8	4.7E-03	-2.5E-01	9.2E-03	6.1E-01	1.6E-03	2.6E-04	2.2E-02	2.9E-03	**12.80 %**

F5020	5.02	0.14	0.75	4.8E-03	-2.5E-01	1.0E-02	6.1E-01	1.6E-03	2.6E-04	2.3E-02	2.9E-03	**12.93 %**
F5020	5.02	0.14	0.7	4.9E-03	-2.6E-01	1.1E-02	6.1E-01	1.6E-03	2.6E-04	2.3E-02	3.0E-03	**13.07 %**

According to Table 3.11 the maximum error in SRR is within ±14.51%.

CHAPTER 4 : Validation of the Use of the Empirical Model in Casting Applications

In this chapter the validation of the empirical model in casting applications is presented. The main objective of this chapter is to validate the empirical model of sand removal rate in small-scale casting applications. Using this model allows users to alter the waterjet operation conditions prior to accelerated cooling stage and helps to avoid causing a surface defect on the solidifying metal while maximizing the cooling rate during the solidification.

In the first section of this chapter, results of small-scale aluminum 7050 alloy casting experiments are presented. The second section contains several examples of the prescribed sand removal and accelerated cooling water-pressure patterns for casting applications and their comparison with model predictions. In the third section, the threshold limits of the waterjet impingement are investigated for casting of aluminum 6061 alloy.

4.1 SMALE SCALE CASTING EXPERIMENTS

In this section, two aluminum 7050 alloy casting experiments are presented. The main goal of this section is to understand the importance of delay time on the ablation casting process. For this reason two tests were carried out and cooling was provided at different stages of solidification.

The experimental set-up presented in Chapter 2 with a similar procedure was used to conduct the experiments. The following gives the explanation of the methodology followed during the tests:

1. The dimensions of the plate pattern were 0.635cm x 5.08cm x 27.94cm.

2. The sand mould prepared as cope and drag and had the plate pattern shape as the mould cavity. 12.7cm thick drag and 7.62cm thick cope were used and the distance from the edges of the cavity to the ambient was 2.54cm each.
3. The mould cavity was 12.07cm away from the bottom of the drag.
4. The molten metal was prepared at 760 °C and poured around 730 °C.
5. For the removal of the sand 552 kPa waterjet pressure was used which results in 5.018 kg.m/s^2.
6. After 4.2 seconds of sand removal, the waterjet pressure was shifted to 69 kPa (0.627 kg.m/s^2) to slowly approach the semi-solid metal and eventually provide cooling.
7. The solidifying metal was subjected to the waterjet from only one edge of the plate.
8. The water at ambient conditions was send through a single nozzle (F5020) from 13.97cm standoff distance during the experiments.

The locations of the thermocouples and the dimensions of the plate pattern are illustrated in Figure 4.1.

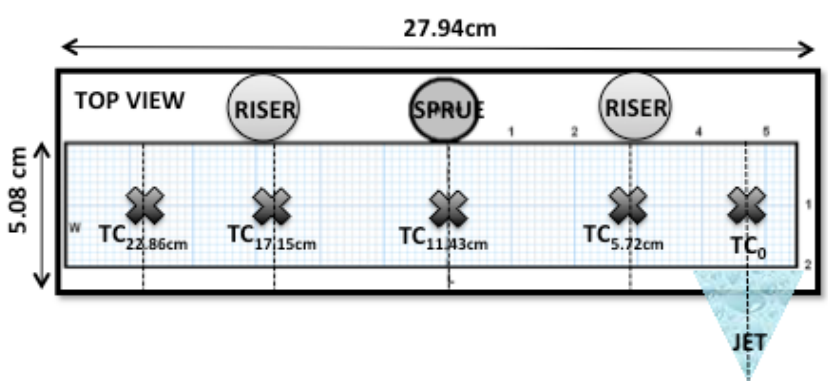

Figure 4.1: Thermocouple Locations in Mould Cavity

The diameter of the sprue and risers was 0.635 cm. TC_0, $TC_{5.72}$, $TC_{11.43}$, $TC_{17.15}$ and $TC_{22.86}$ represent the thermocouple locations in the mould cavity. TC_0 is the thermocouple located at the direct region of impact with the waterjet. The subscripts refer to the

distance away from the T_0 in centimeters. A schematic of the sand mould is presented in Figure 4.2.

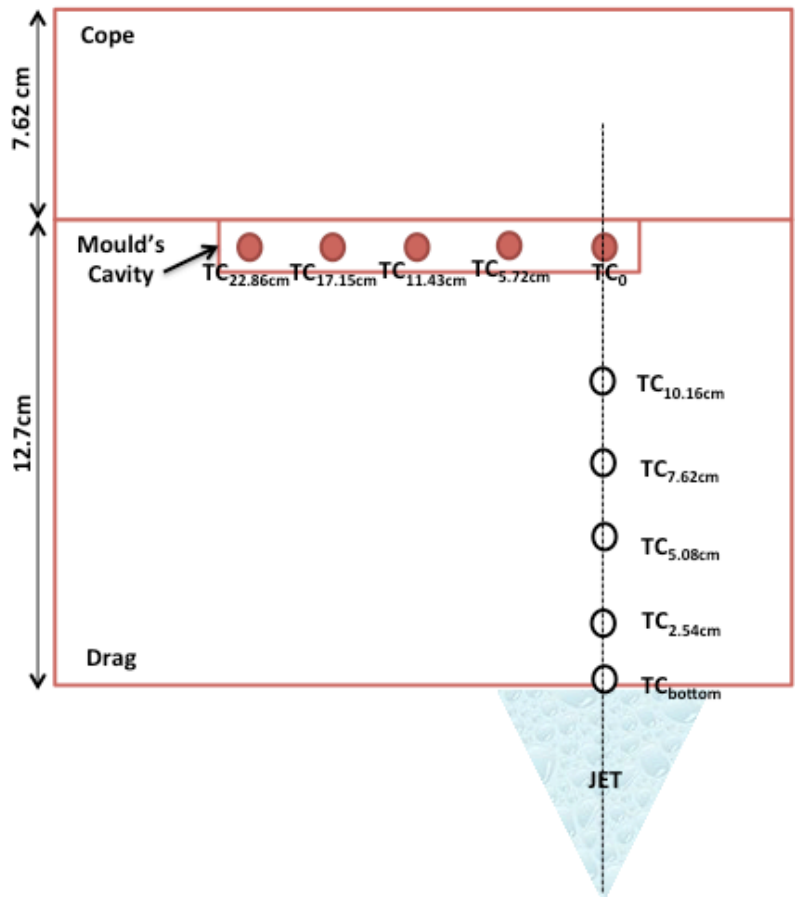

Figure 4.2: Schematic of the Sand Mould used in Plate Casting Experiments

The coverage of the waterjet depends on the operating water pressure. As it is presented in Figure 4.2 five thermocouples were inserted in the sand mould, right above the path of the waterjet in order to record the sand removal data during the experiments and compare with the model prediction.

Figure 4.3 shows the prescribed water pressure pattern along with the sand removal data and the removed distance of the sand predicted by the model. In the first test, the accelerated cooling was provided at relatively an early stage of solidification, the waterjet started to imping on semi-solid metal surface when the thermocouple at the jet

impact region (TC_0) read 608 °C whereas in the second test, the waterjet reached the metal and cooling started at a late stage of solidification when TC_0 read 579 °C. The water pressure pattern shown in Figure 4.3 was used for both tests.

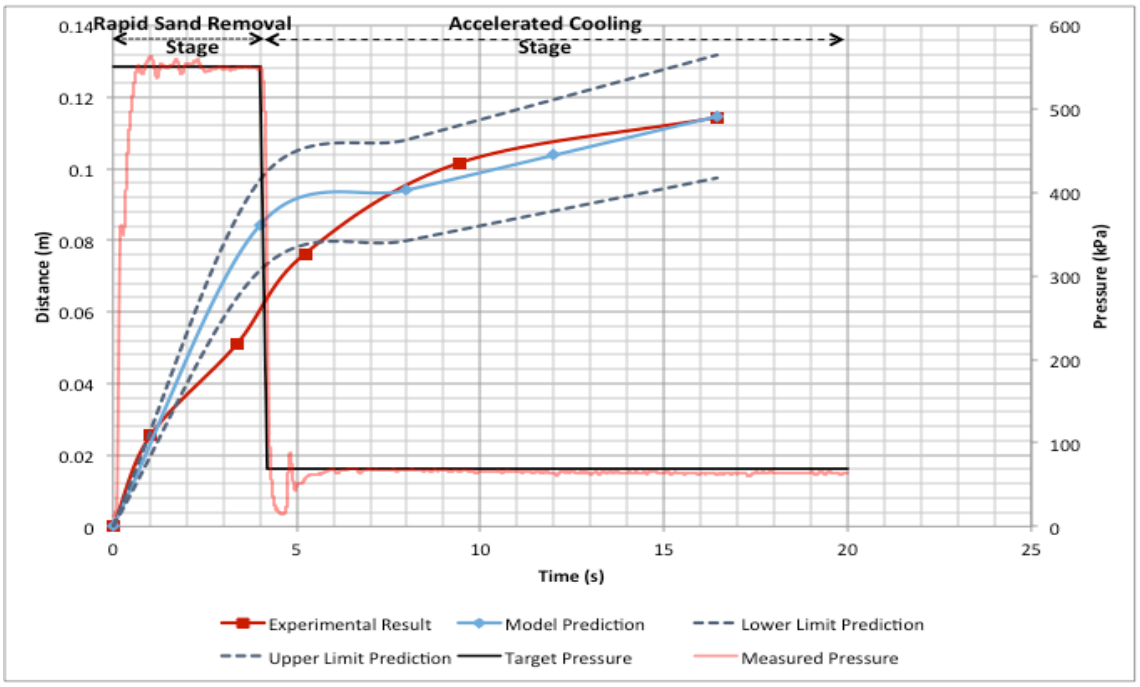

Figure 4.3: Prescribed Water Pressure Pattern for Sand Removal and Cooling, and the Sand Removal Data Recorded in the Experiment and the Model Prediction

As it is apparent from the data presented in Figure 4.3 a high-pressure, around 552 kPa, was chosen for the sand removal process to be fast and then there was a shift in water pressure to a lower value of 69 kPa during the initial impingement of the waterjet. The upper and lower limits of the predicted distance of sand removed are presented along with the actual experimental sand removal data. These limits are determined by using the model error limits of ±15%. It should be kept in mind that the model prediction is calculated based on the target pressure. Based on this pressure the volumetric flow rate and velocity values are calculated. The momentum of the waterjet obtained and inputted in the model along with the standoff distance and the time of sand removal is estimated. It can be noticed in Figure 4.3 that the time of sand removal recorded during the experiment is in good agreement with the model prediction. The waterjet provided

rapid sand removal and after 8.5 cm penetration slowly approached the solidifying metal. The waterjet was about 3 cm away from the solidifying metal when the shift in water pressure occurred in order to avoid any surface defects. The thermal data recorded during this test is presented in Figure 4.4.

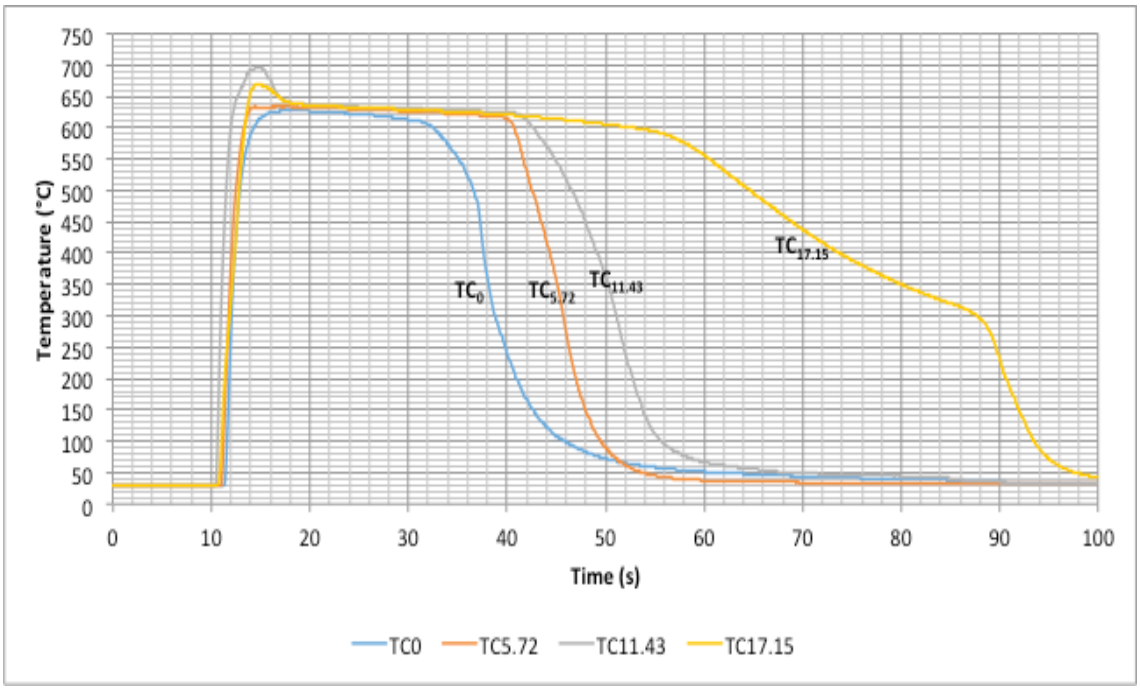

Figure 4.4: Thermal data recorded during test 1 early cooling

According to Figure 4.4, at the time of impingement the temperature at the impact region (T_0) was around 608 °C. Even at such low momentum of 0.627 kg.m/s^2, the impact of the waterjet provided rapid cooling up to 11.43cm away from T_0. Although the effect of the waterjet was not significant at 17.15cm away from T_0, it still accelerated the cooling. Also, it can be noticed that the initial temperature drop becorded by TC_0 is not as sharp as it should be. This could be explained due to the slow approach of the waterjet to the solidifying metal, once the waterjet eventually starts impinging temperature decreases rapidly. Figure 4.5 represents the microstructure images taken throughout the plate. The microstructure samples were taken at the same thermocouple locations.

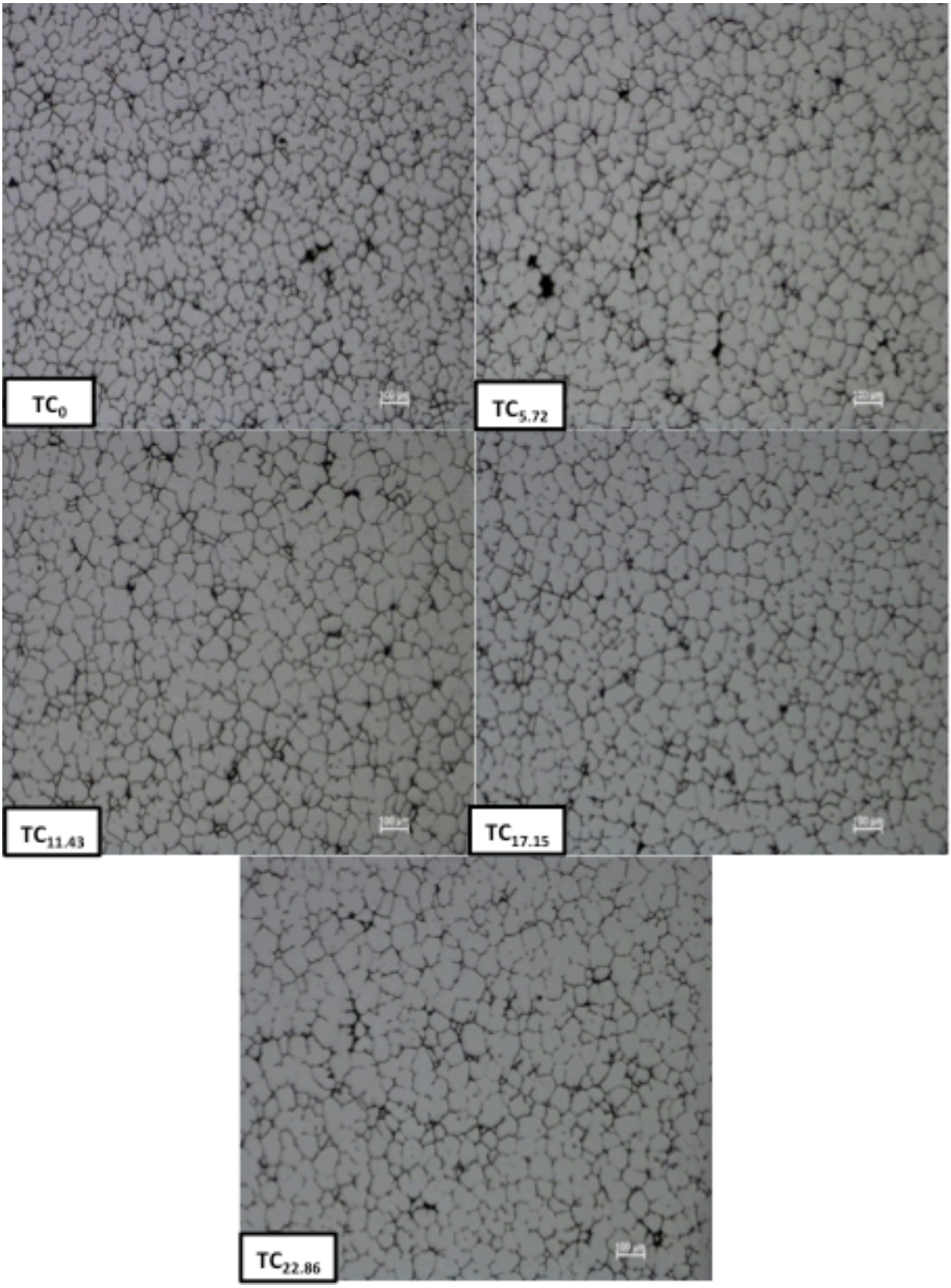

Figure 4.5: Microstructure throughout the plate test 1

ASTM standards [46] were followed while calculating the grain size. Basically, three images of each sample were taken and five diagonal lines were inserted on each image, then the number of intersections were counted and divided by the length of the diagonal. The grain size variation is presented in the following section along with the second test results. In the second test, same prescribed water pressure pattern was applied and when TC_0 read 579 °C, the waterjet came in direct contact with the semi-solid metal and the cooling stage was started. Compared to the first test, the initial impingement temperature is 29 °C lower. The thermal data recorded during the second test is presented in Figure 4.6.

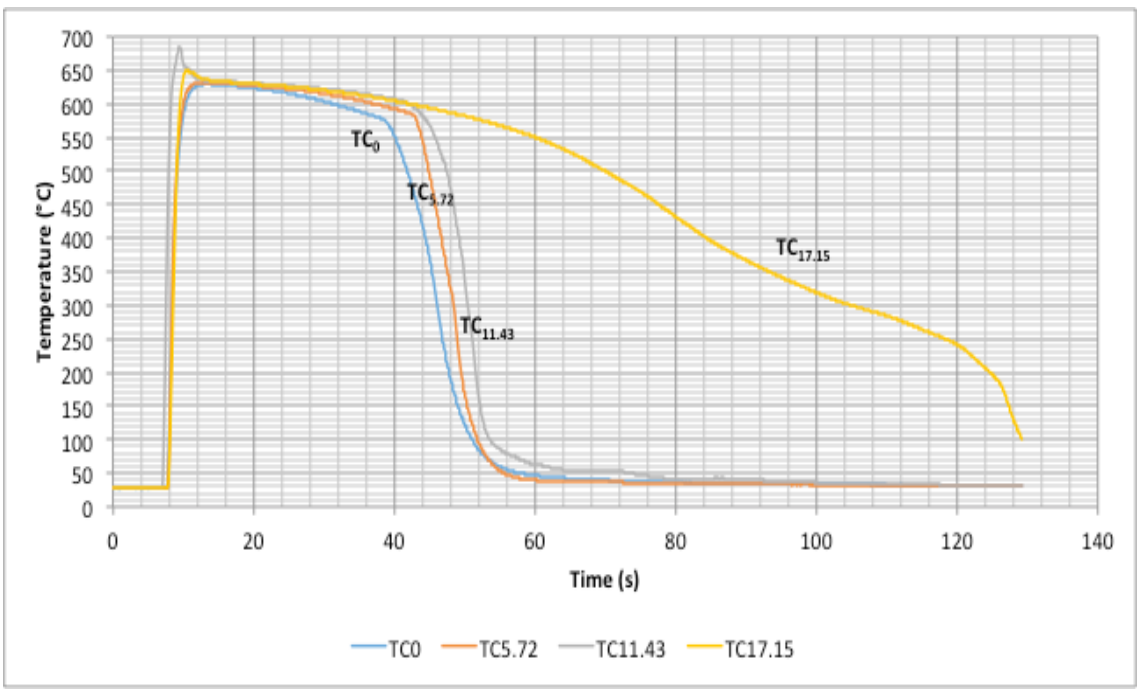

Figure 4.6: Thermal data recorded during test 2 late cooling

It is apparent from Figure 4.6 that waiting for a longer time caused thermocouples to show natural cooling trend at first for about 40 seconds. Due to the longer time of waiting the waterjet started impinging on metal surface when it was at 579 °C (40 °C lower than the first test). The waterjet was effective up to 11.43cm, however at 17.15cm away from nozzle centerline the effect was not significant. Figure 4.7 illustrates the microstructure images taken for the plate after the second test.

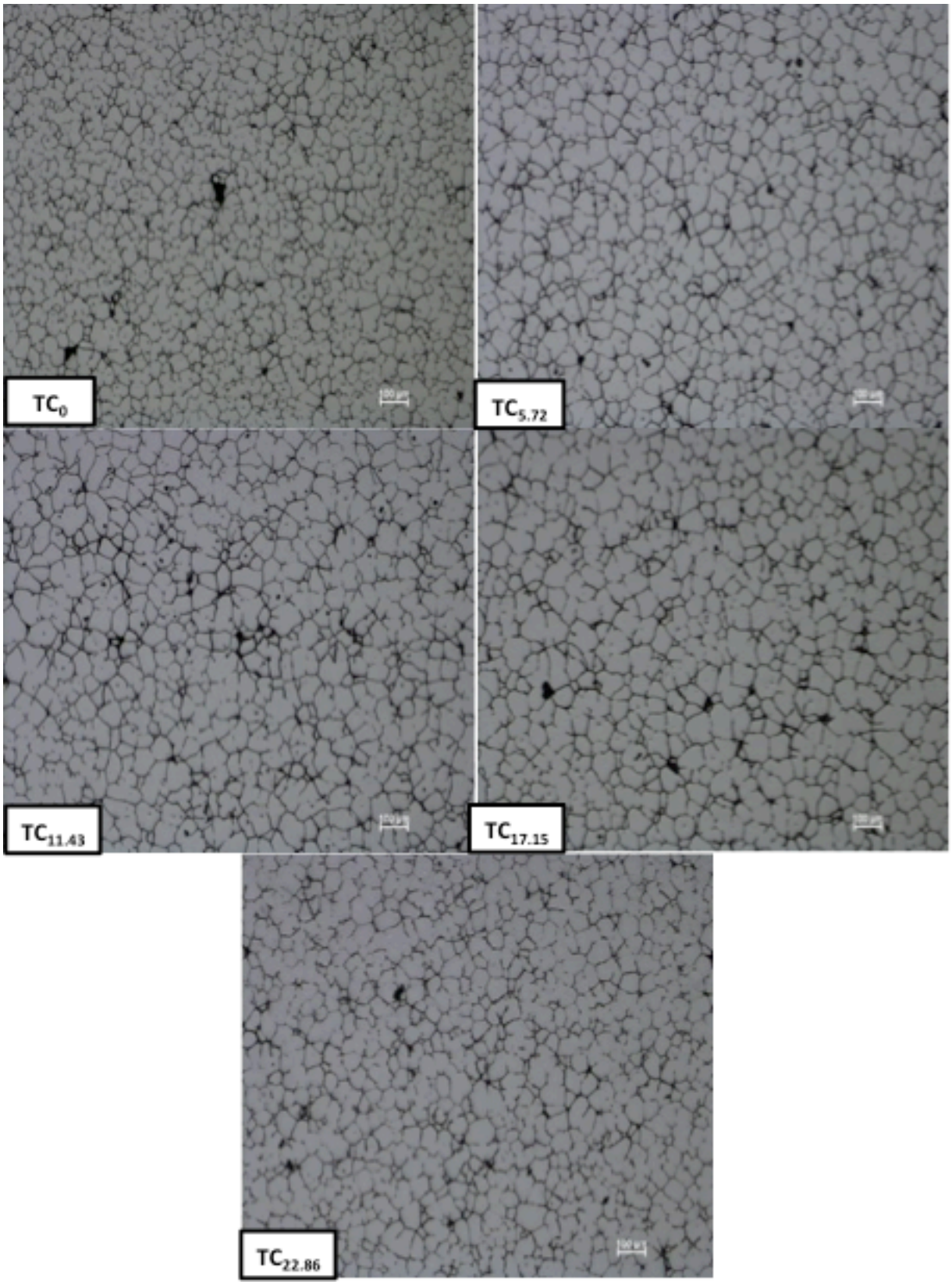

Figure 4.7: Microstructure throughout the plate test 2

The grain size variation throughout the plate for these two tests is illustrated in Figure 4.8.

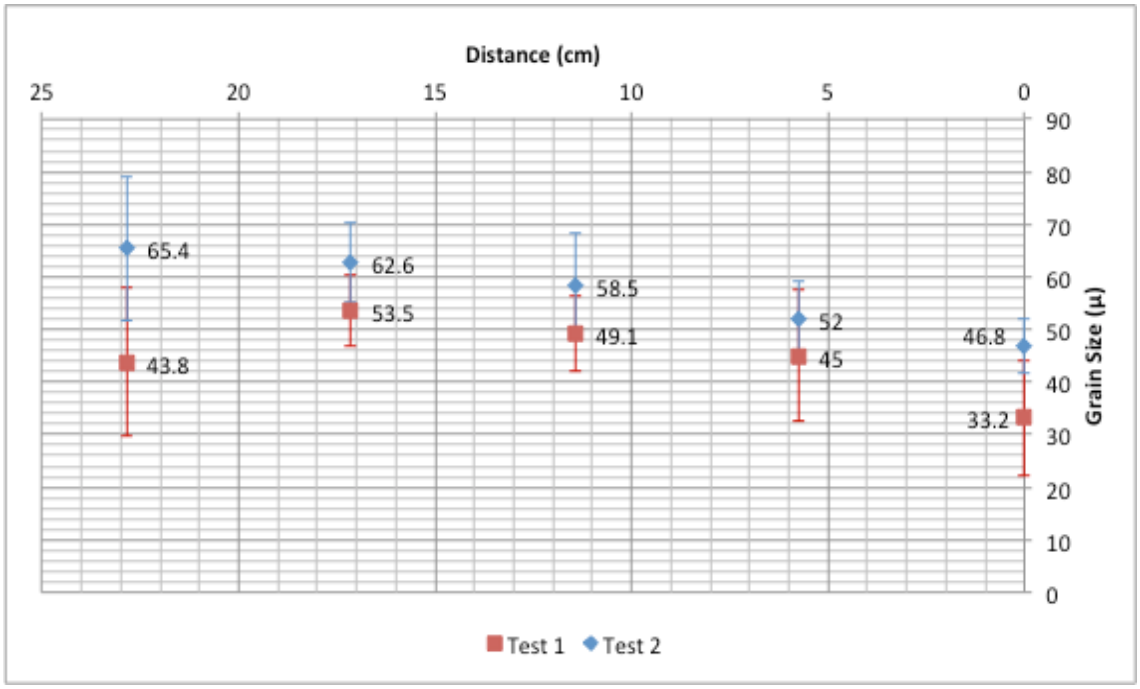

Figure 4.8: Grain size variation throughout the plate

According to Figure 4.8, in test 2, the effect of the intense cooling produced by the waterjet is clear close to the region of impact even in the case of late cooling. Compared with the uncooled edge, the grain size is 18.6 microns smaller.

At the direct impaction zone the grain size is 33.2, and 46.8 microns in test 1 and 2, respectively. It can be concluded that starting the impingement 29 °C earlier reduced the grain size by 13.6 microns at the impaction zone.

In test 2, the grain size increased by ~6 microns in every 5.72 centimetres from the cooled edge until the center of the plate. At 11.43 centimetres, the effect of cooling on the microstructure gradually diminished. The effect of the average cooling rate on the grain size is presented in Figure 4.9.

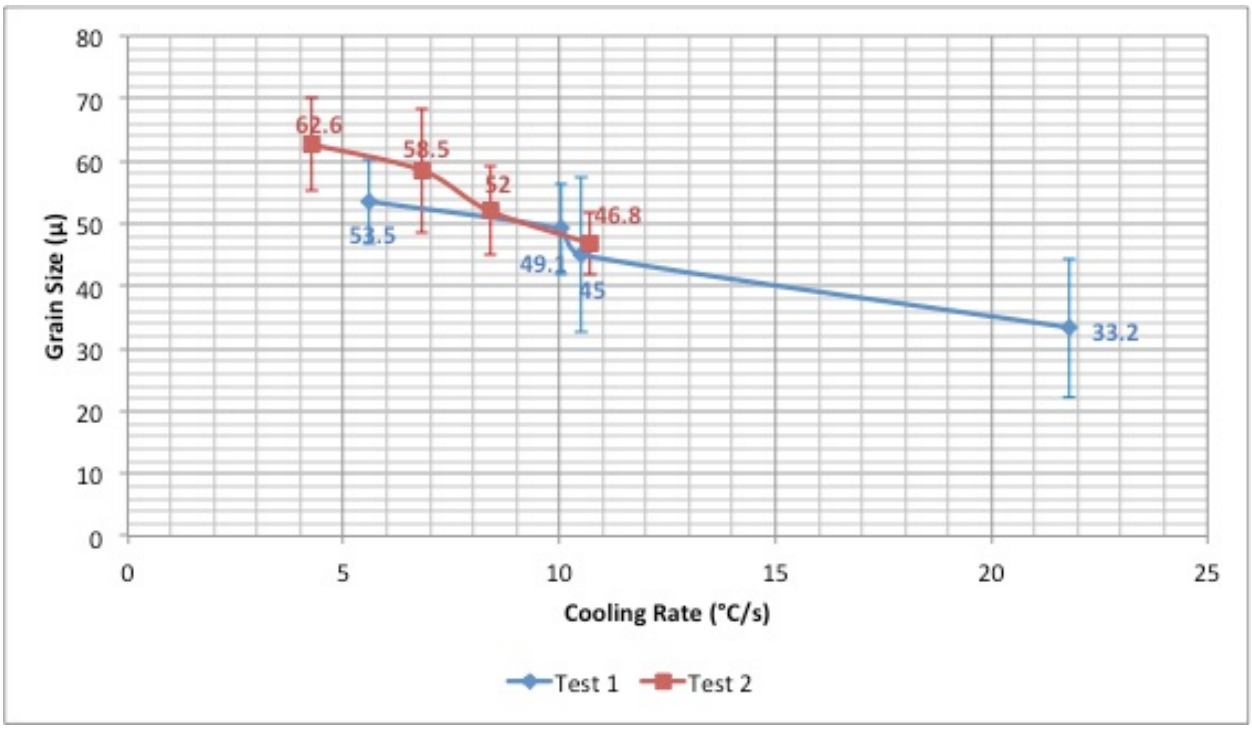

Figure 4.9: Average cooling rate effect on the grain size

The average cooling rate of each thermocouple reading was calculated as follows: The starting point of the cooling was selected as the peak temperature of each thermocouple. The average cooling rate was calculated by the slope of the curve from the peak temperature to 100 °C.

The trend in Figure 4.9 is clear; greater cooling rates result in smaller grain sizes. Considering that test 1 had a head start of 29 °C, the maximum cooling rate was 22 °C per second. Figure 4.10 illustrates a comparison of the cooling rates obtained in these tests with the cooling rates obtained during conventional sand casting.

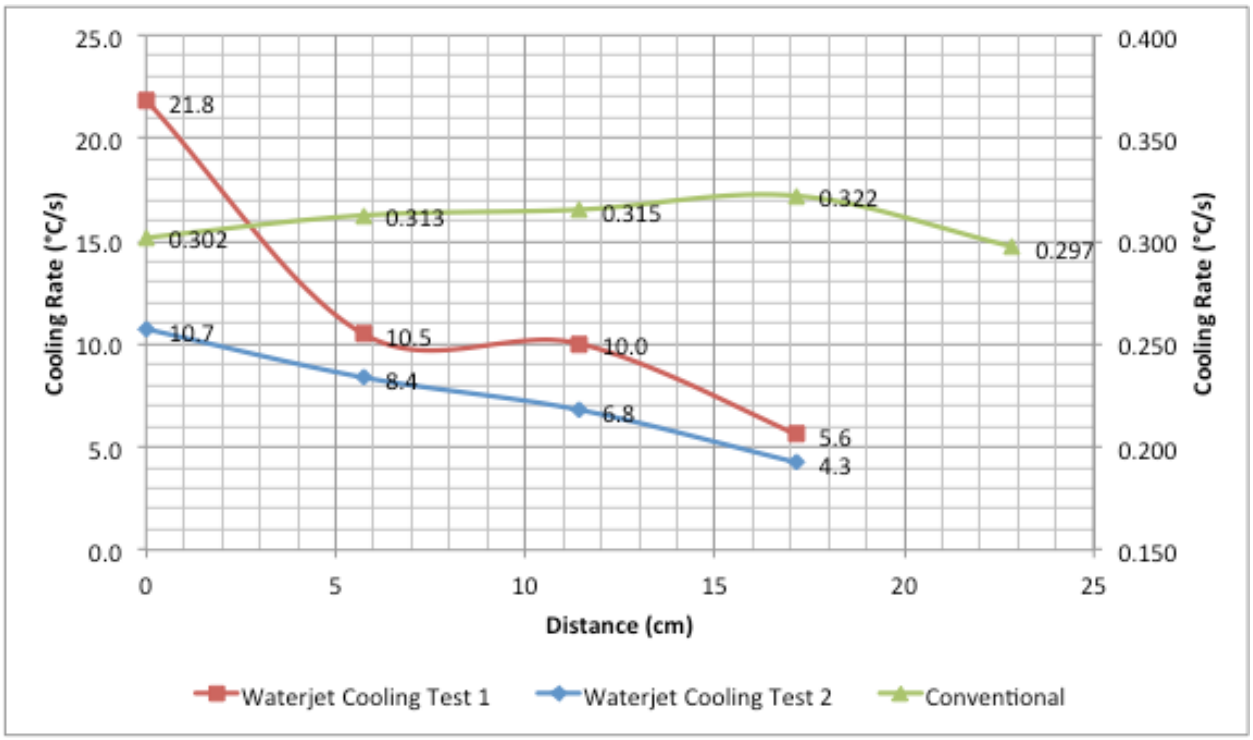

Figure 4.10: Waterjet Cooling vs. Conventional Sand Casting

In Figure 4.10, the y-axis on the right hand side shows the cooling rate of the conventional sand casting case (no waterjet). The distance on x-axis indicates the distance between each thermocouple and TC_0, which was located at the centerline of the waterjet. The difference in the cooling rate between waterjet cooling cases and conventional case is enormous. In Figure 4.9 the importance of high cooling rate on grain size was emphasized. Now bearing in mind that the pressure used for cooling in these tests was only at 69 kPa, much higher cooling rates can be achieved by increasing the water pressure. Consequently, it will promote smaller grain sizes in the microstructure and higher mechanical properties of the casting. Therefore, the use of waterjets in ablation casting is extremely beneficial as it was reported in literature.

4.2 The Use of Empirical Model In Real Castings

Tens of small-scale casting tests were conducted similar to the ones discussed in the previous section. The objective of this section is to use the empirical model developed in Chapter 3 and validate it in 3 sets of experiments in order to confirm its repeatability.

In the first test the water pressure pattern was as follows: waterjet pressure at 650 kPa provided 5.905 kg.m/s^2 waterjet momentum for 3.5 seconds and then dropped down to 207 kPa for 1.5 seconds, then it was increased by 69 kPa every second until it reached 552 kPa. Figure 4.11 shows the water pressure pattern used during the first test.

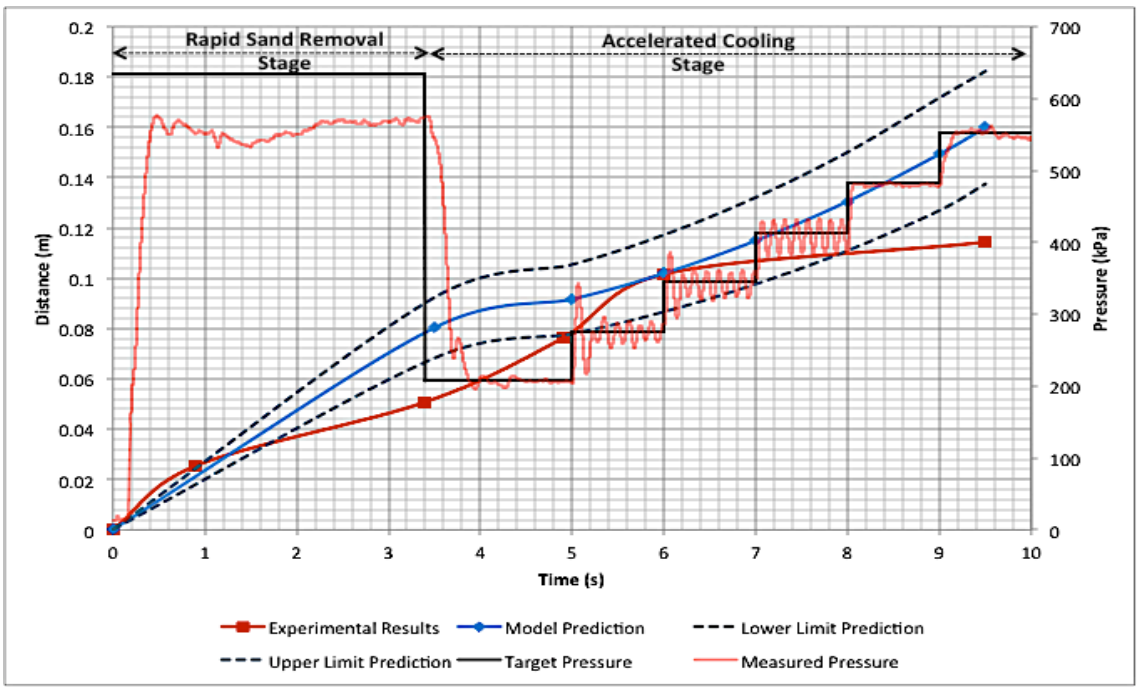

Figure 4.11: Test 1: Comparison of the sand removal data with predicted removal pattern

It is apparent in Figure 4.11 that during the sand removal stage of the test water pressure was lower than the target pressure. This resulted in lesser sand removal than predicted until the shifting point in the water pressure. The late shift of the water pressure caused sand removal to increase towards the expected removal range however the water leaving the nozzle exit was disturbed by the severe fluctuations in water pressure observed after the 5th second. For this reason, the water flow became incoherent.

Consequently, sand removal started to lag behind the expected removal level and reached 11.43 cm penetration depth 3 seconds late compared with empirical model prediction. This was inevitable since the expected removal pattern was based on the target pressure. This test emphasizes the significant effect of water pressure on the rate of sand removal.

Since in the first test, the gap between the target and measured pressure were very high, in the second test, same water pressure pattern was repeated again. Figure 4.12presents the sand removal data and its comparison with the predicted removal.

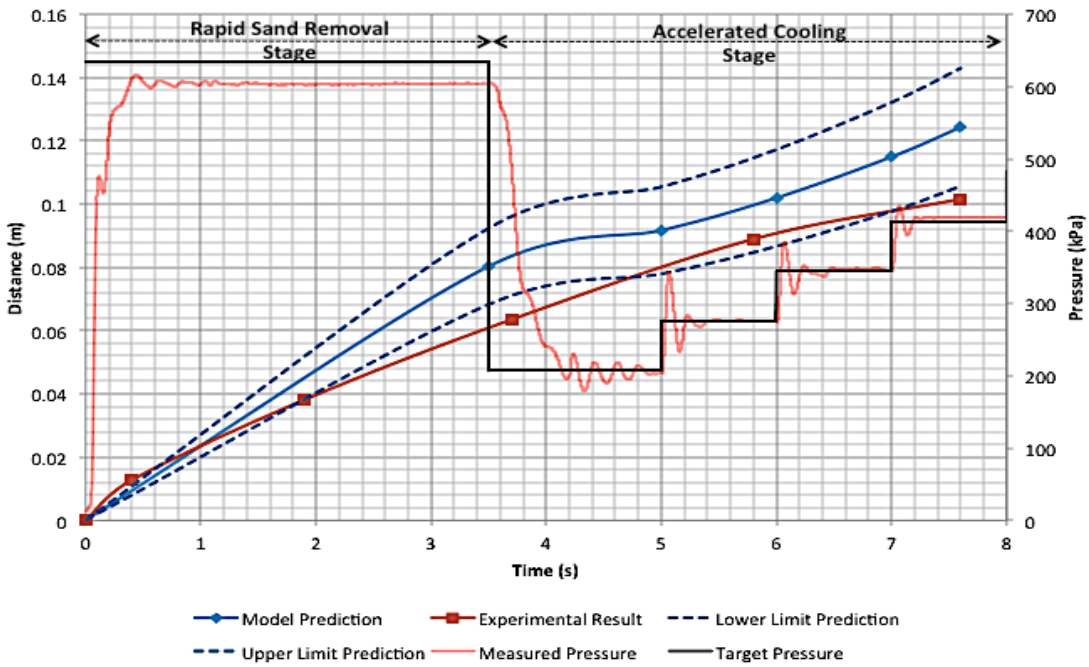

Figure 4.12: Test 2: Comparison of the sand removal data with predicted removal pattern

It can be noticed from Figure 4.12 that the experimental data is in agreement with the lower limit of the prediction. Again water pressure did not reach the target pressure and the removal was out of the predicted range. However, the water pressure at the sudden drop point took half a second more time to reduce to 207 kPa. This put the sand removal rate back on track within the expected range and eventually reached 11.43cm at the same time as the lower limit prediction. The fluctuations in water pressure after

the 5th second was not as severe as in the previous test, which contributed for sand removal to stay within the expected range.

In the third test a simpler water pressure pattern was chosen; the waterjet pressure was kept at 552 kPa, which provided 5.018 kg.m/s² waterjet momentum for 4.5 seconds. It was dropped down to 276 kPa (2.506 kg.m/s²) and was kept there constant throughout the cooling stage. Rather than a sharp drop at the shifting points between the sand removal and accelerated cooling stages, a gradual decrease from 552 kPa to 276 kPa was selected in this test. Figure 4.13 shows the prescribed flow pattern along with the removal data.

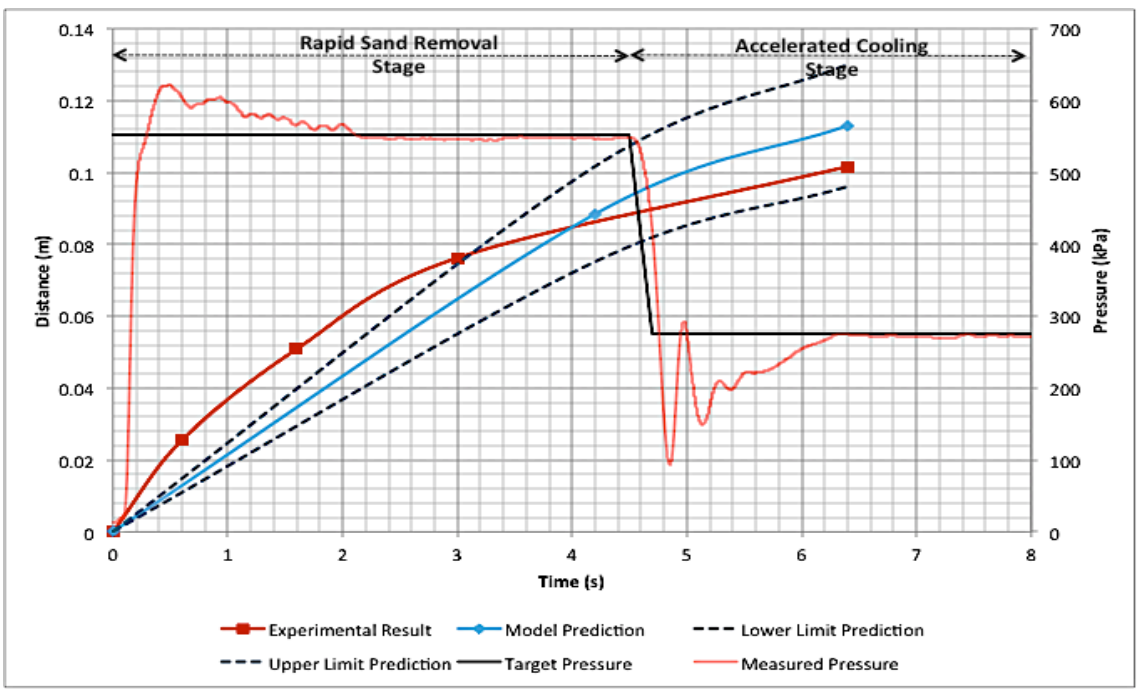

Figure 4.13: Test3: Comparison of the sand removal data with predicted removal pattern

It is apparent from Figure 4.13 that water pressure at first was higher than the target pressure for about 2 seconds and then it stabilized. This higher pressure affected sand removal and caused more sand removal than predicted in the first two and a half seconds. After the shift in pressure, a severe fluctuation from the shifting time 4.5 seconds until the 6th second was observed. As a result, sand removal, which was

initially greater than the model upper limit prediction reached 11.43 cm close to the lower limit prediction.

In all three tests presented in this section, the effect of changes in water pressure on the removal was clear. When the pressure does not follow the prescribed flow pattern, it affects the waterjet momentum and consequently affects the rate of sand removal. However, these differences in target and measured pressure created a great opportunity to understand and analyze the interaction between the waterjet momentum and the removal pattern. The differences can be better controlled however it would be unrealistic to expect 100% match between the target and measured pressure in real applications. It is evident that even a half second shift in pressure or a 69 kPa pressure difference between the target and measured pressure during the process affect sand removal. Considering these differences in order to make sure not to puncture the solidifying metal, the water pressure pattern should be calculated based on the lower limit of the model prediction.

4.3 Threshold Limits of Waterjet Impingement for Aluminum 6061 Alloy

In this section the maximum waterjet momentum that the solidifying metal can withstand without getting punctured is discussed. As it was mentioned before upon completion of the sand mould the waterjet impinges on the semi-solid metal surface to accelerate the solidification rate of the casting. In order to provide the maximum grain refinement throughout the casting this impingement must start at an early stage of the solidification, close to the liquidus temperature. However the waterjet momentum for this impingement process is unknown.

Trial/Error types of casting experiments were carried out in order to map the threshold of the waterjet momentum and the temperature of the metal at the time of impingement. The same procedure explained in the first section of this chapter was

followed and tens of aluminum 6061 alloys were cast. The waterjet pressure for the impingement in these tests varied from 138 kPa to 552 kPa. Figure 4.14 shows the data points obtained in these plate-casting experiments.

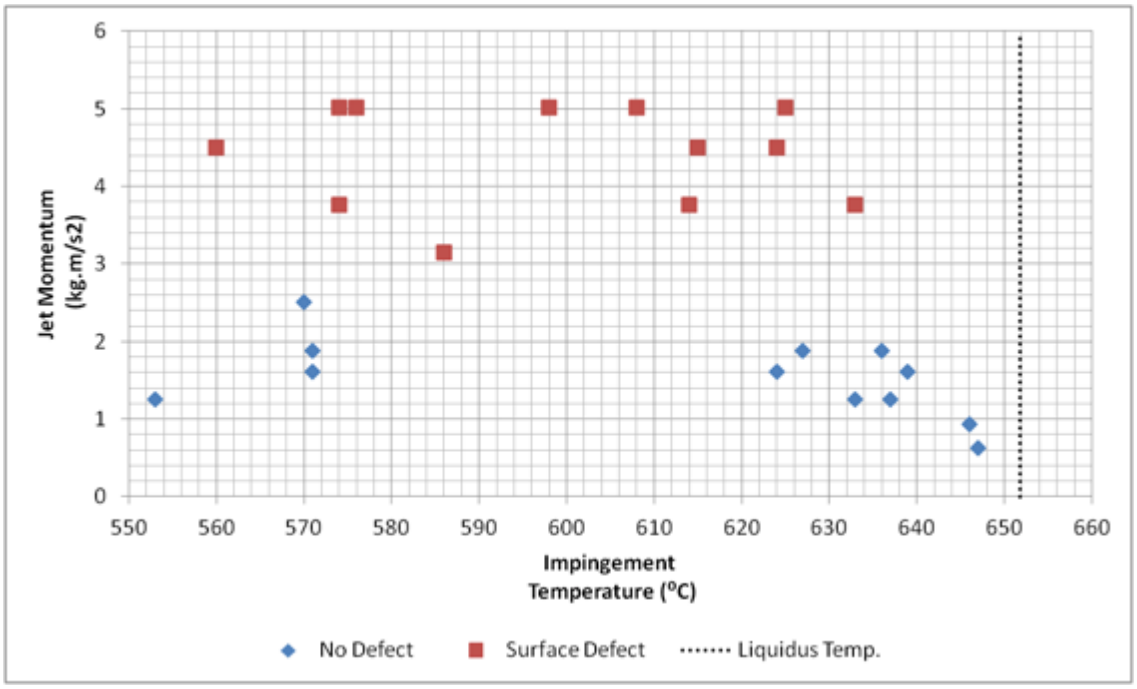

Figure 4.14: Surface defect limits of Al-6061 alloy

It is apparent from Figure 4.14 that the waterjet momentums higher than 3.0 kg.m/s^2 always results in a surface defect regardless of the temperature of impingement and the state of the solidifying metal. The region of interest in this graph is the data points without a defect close to the liquidus temperature. It is evident that within the range from 620 °C to 650 °C waterjet momentum lower than 2.0 kg.m/s^2 is able to successfully cool the part without a defect. However it should be kept in mind that the standoff distance from the sand mould was 13.97cm for all these tests and the molten metal was 12.07cm above from the bottom of the mould. This means the waterjet momentum values that do not cause a defect on the casting are valid from 26.04 cm distance for aluminum 6061 alloy. In case of any change in this distance the momentum of the waterjet must be adjusted accordingly.

CHAPTER 5 : Summary, Conclusion and Future work

5.1 SUMMARY

The objective of this research is to investigate and obtain a proper understanding of the sand removal process for water-soluble sand moulds in ablation casting applications. In order to maximize the benefit of the waterjet cooling in ablation casting method, the waterjet must go through the sand mould in the minimum delay time and start directly impinging on the solidifying metal surface at an early stage of the solidification process. Since it could cause a surface defect in the cooling process the waterjet intensity must be adjusted at the end of the sand removal stage. The main problem with this technique is to estimate the time at which waterjet impingement starts and adjust the process parameters accordingly. This study proposes a predictive empirical model that can estimate the time of sand removal for given operation conditions and sand mould thickness. The effect of standoff distance, waterjet momentum and the overlapping percentage of multijets on the rate of sand removal has been qualitatively investigated and correlated. Ablation casting applications can utilize this empirical model to calculating the time of sand removal for given sand mould thickness and the time at which the waterjet impingement will come in direct contact with the solidifying metal. Also a mechanistic model that includes the specific energy of the sand mould is developed. This model can be implemented and used to predict the volumetric flow rate in other water-soluble sand binder systems.

5.2 CONCLUSION

The major conclusions of this study are as follows:

1. The standoff distance is the most influential waterjet process parameter and is the most effective way of increasing the rate of sand removal using impinging jets.
2. The effect of water temperature on the rate of sand removal is insignificant.
3. In the sand removal process, the mechanical energy of the jet is dominant over chemical dissolution. The process is too fast for dissolution to have a pronounced effect.
4. As long as the mass flow rate and the waterjet velocity result in the same momentum, the rate of sand removal will be the same. This creates an opportunity to work with a wide range of water pressures and nozzle orifice sizes and maintain the sand removal rate.
5. The effect of waterjet momentum on the rate of sand removal was found to be linear. Any change in the momentum directly effects the sand removal time.
6. Using a set of flat fan shape nozzles, with an overlapping percentage of 28% resulted into a uniform sand removal along the length of the mould.
7. A predictive empirical model was established with R^2 value of 0.97 and standard error of ±15%. This model is able to estimate the time of sand removal for given sand mould thickness and process input variables.
8. A mechanistic model that included the specific energy of the sand mould has been proposed, which can be used for other sand binder systems.
9. The developed empirical model was validated in tens of small-scale casting experiments and it is able to predict the time of sand removal correctly.

5.3 FUTURE WORK

In this study many details were provided regarding the interaction between waterjet parameters and water-soluble sand mould. Additionally some aspects of the removal mechanism of the water-soluble sand moulds were discussed. This work can be classified as a primary foundation for the ongoing and future ablation casting studies. In the final section of this thesis, some directions for the future work are suggested.

1. Study the mechanical effect of the waterjet alone, with water-insoluble sand mould that has the same mechanical properties as the sand mould used in this study.
2. Employ a high-speed camera and study the volumetric removal rate in order to increase the accuracy of the mechanistic model.
3. Investigate the dynamic change in the specific energy of the sand mould as penetration occurs.
4. Study the chemical aspects of the dissolution in more detail.
5. Conduct a permeability test for the current sand and binder system.
6. Integrate feedback from sand removal to a controller in order to modify controller behaviour based on the rate of sand removal that needs to be achieved.
7. Examine the mechanistic model's validity with other nozzle/jet types.
8. Explore the mechanistic model's validity with other water-soluble sand and binder systems.
9. Study the mechanistic model's validity in the case of using reclaimed sand.
10. Investigate the effect of sand particle size and geometry of sand grains.
11. Test the validity of the developed models in downward sand removal.
12. Investigate how the age (shelf life) of sand moulds alter the sand removal rate.

CHAPTER 6 References

[1] D. Paxton, J. Carpenter, P. Sklad, M. Smith. "Overview of Lightweighting Materials R&D in the United States Freedomcar and Fuel Partnership." Materials Science Forum Vols 618-619 p395-404 (2009).

[2] A. P. Druschitz, D. C. Fitzgerald. "Lightweight Iron and Steel Castings for Automotive Applications." Intermet Corp. 2000-01-0679 SAE Technical Paper Series (2000).

[3] "Effectiveness and Impact of Corporate Average Fuel Economy (CAFÉ) Standards", National Research Council, National Academies Press, Washington, DC, (2002).

[4] E. Ghassemieh, M. Chiaberge "Materials in Automotive Application, State of the Art and Prospects, New Trends and Developments in Automotive Industry" (2011).

[5] United States Automotive Materials Partnership. Magnesium Vision 2020: A North American Automotive Strategic Vision For Magnesium. (2010).

[6] U.S. Department of Energy | Energy Efficiency of Renewable Energy, Advanced Manufacturing Office, "Development of Integrated Die Casting Process for Large Thin-Wall Magnesium Applications" DOE/EE-0873 October, (2013).

[7] J. Grassi, J. Campbell, M. Hartlieb, F. Major. "Ablation Casting" Aluminum Alloys: Fabrication, Characterization and Applications (2008).

[8] I. Ostrovsky, Y. Henn. "Present State and Future of Magnesium Application in Aerospace Industry." International Conference: New challenges in Aeronautics, Astec'07, August 19-22, (2007).

[9] J. Grassi, J. Campbell, F. Mayor, "Solidification Microstructure of Aggregate Molded Shaped Castings" US. Patent No. 2008/004149A1 Feb 21, (2008).

[10] A. A. Luo. "Magnesium casting technology for structural applications" Journal of Magnesium and Alloys 1 2 – 22. (2013).

[11] B. Cox, J. Zindel, M. Maj, L. Ouimet, A. Luo, D. Osborne, M. Osborne, R. Beals, E. McCarty, S. Robison, D. Weiss, D. Penrod, "High Integrity Magnesium Automotive Components (HIMAC)", in: Presentation at the 111th American Foundry Society Metalcasting Congress, Houston, TX, USA, May 15-18, (2007).

[12] K. Beckius, E. Flodberg, S. Forslund "Olivine sand used in Swedish steel foundries" Mod. Cast, (1962).

[13] "Casting in Action" Engineered Casting Solutions Magazine, , July/August p40 (2008).

[14] J. Grassi, J. Campbell, M. Hartlieb, F. Major. "The Ablation Casting Process" Materials Science Forum, vols. 618-619, pp. 591-594 (2009).

[15] J. Grassi, J. Campbell, M. Hartlieb, F. Major. Technical paper, "Ablation Casting", Foundry Trade Journal, p124-126 May (2010).

[16] D. Weiss, J. Grassi, B. Schultz, P. Rohatgi. "Ablation of Hybrid Metal Matrix Composites" American Foundry Society, pp. 26-29 (Dec. 2011).

[17] D. Weiss, J. Grassi, B. Schultz, and P.Rohatgi. "Discovering Ablation" Metal Casting Design and Purchasing Magazine. Volume 14 Number 1 p37-39 Jan/Feb (2012).

[18] D. Weiss, J. Grassi, B. Schultz, and P.Rohatgi. "Testing the Limits of Ablation" Modern Casting Magazine, p26-29 December (2011).

[19] J. W. Zindel. "Ablation Casting Evaluation for High Volume Structural Castings" USAMP. May (2012) http://energy.gov/sites/prod/files/2014/03/f10/lm055_zindel_2012_o.pdf

[20] M. Tiryakioglu, Paul D. Eason, J. Campbell "Fatigue life of ablation-cast 6061-T6 components" Journal of Material Science and Engineering 2012 A 559 p447-452 (2013).

[21] V. Bohlooli, M. Shabani Mahalli and S. M. A. Boutorabi, "Effect of Ablation Casting on Microstructure and Casting Properties of A356 Aluminium Casting Alloy" Acta Metall. Sin. (Engl. Lett.) Vol.26 No.1 pp. 85—91 February (2013).

[22] T. J. Williams, D. Galles, and C.Beckermann. "Translating Water Spray Cooling of a Steel Bar Sand Casting" Proceedings of the 67th SFSA Technical and Operating Conference, Paper No.5.4, Steel Founders' Society of America, Chicago, IL, (2013).

[23] P. Dudek, A. Fajkiel, T. Regula, T.Bochenak "Research on ablation casting technology for aluminum alloys", Transactions of foundry research institute, Volume LIV, Number 2, (2014).

[24] Prescenzi, A., "Cast Body Nodes for 2016 Acura NSX," SAE Int. J. Mater. Manf. doi:10.4271/2015-01-0512, 8(3): (2015).

[25] OMAX® Abrasive Waterjets, What is Waterjet Cutting?, History of Waterjet. Retrieved May 9th, 2015 from: https://www.omax.com/learn/history-of-waterjet

[26] The John W. Sutherland Research Page, Cyberman, Machining, Non Traditional Machining, Waterjet Cutting. Retrieved May 9th, 2015 from: http://www.mfg.mtu.edu/cyberman/index.html

[27] DeGarmos Materials and Processes in Manufacturing Tenth Edition. Chapter 28 Abrasive Machining Processes. p756 – 789. John Wiley & Sons. (2008).

[28] S. Paul, "Waterjet machining and Abrasive Waterjet Machining", Manufacturing Processes – II, Indian Institute of Technology, Kharagpur. Retrieved May 1st, 2015 from : http://www.nptel.ac.in/courses/112105127/pdf/LM-37.pdf

[29] Finnie I., "Erosion of Surfaces by Solid Particles", Wear, 3/2:87-130. (1960).

[30] J. G. A. Bitter, "A study of erosion phenomena Part I", Wear, Vol.6, pp.5-21, (1953).

[31] J. G. A. Bitter, "A study of erosion phenomena Part II", Wear, Vol.6, pp.5169-190, (1953).

[32] M. Hashish, "A modeling study of metal cutting with abrasive waterjets", J. Eng. Mater. Technol. 106(1), 88-100, (1984).

[33] M. Hashish, "A model for abrasive waterjet machining", J. Eng. Materials Tech., Vol.111, pp.154-162, (1989).

[34] S. Paul, A.M. Hoogstrate, C.A. van Luttervelt, H.J.J. Kals, "Analytical and experimental modeling of abrasive waterjet cutting of ductile materials", J. Mater. Process. Technol. 73 189–199. (1998).

[35] M. Hashish, "Visualization of the Abrasive-Waterjet Cutting Process," Experimental Mechanics, pp. 159-169, June (1988).

[36] R. Kovacevic, "Monitoring The Depth of Abrasive Waterjet Penetration", Int. J. Mach. Tools Manufact. Vol. 32, No. 5, pp.725-736, (1992).

[37] A. Momber, R. Kovacevic. "Fracture of brittle multiphase materials by high energy waterjets", Journal of Materials Science 31 1081-1085 (1996).

[38] J. Zeng, T. J. Kim, "An erosion model of polycrystalline ceramic in abrasive waterjet cutting", Wear, Vol.199(2), pp.275-282, (1996).

[39] S. Paul, A.M. Hoogstrate, C.A. van Luttervelt, H.J.J. Kals, "Analytical modeling of the total depth of cut in abrasive waterjet machining of polycrystalline brittle materials", J. Mater. Process. Technol. 73) 206–212, (1998).

[40] J.M. Fan, C.Y. Wang, J. Wang "Modeling the erosion rate in micro abrasive air jet machining of glasses" Wear 266, 968-974, (2009).

[41] Wu, S.S., Kim, T.J. "An application study of plain waterjet process for coating removal". In: Proc. 8th US Waterjet Conference, Houston, TX, pp. 779–792. (1995).

[42] Retrieved May 26th from:
http://www.spray.com/cat75/hydraulic/files/71.html

[43] N. Karwa, P. Stephan. "Jet Impingement Quenching: Effect of Coolant Accumulation" Journal of Physics: Conference Series 395 (2012).

[44] C.D. Goetz , E.C.Hathaway, H.R. Kottke , "Water soluble mold and core binders and method" Patent no: US 3046147 A, (1962).

[45] K. Takrouri, "Quench of Cylindrical Tubes During Transition From Film to Nucleate Boiling Heat Transfer", PhD Thesis; McMaster University, Hamilton, Canada, (2011).

[46] ASTM International, Standard Test Methods for Determining Average Grain Size, Designation E112-13. (2014).